Vibrio harveyi Acyl Carrier Protein Conformation and Interaction with Partner Enzymes

by

Huansheng Gong

Submitted in partial fulfillment of the requirements
for the degree of Doctor of Philosophy

at

Dalhousie University
Halifax, Nova Scotia
December 2006

Your file Votre référence
ISBN: 978-0-494-27195-7
Our file Notre référence
ISBN: 978-0-494-27195-7

DALHOUSIE UNIVERSITY

To comply with the Canadian Privacy Act the National Library of Canada has requested that the following pages be removed from this copy of the thesis:

Preliminary Pages

Examiners Signature Page (pii)

Dalhousie Library Copyright Agreement (piii)

Appendices

Copyright Releases (if applicable)

Dedicated to my grandparents

Table of Contents

List of Figures ix

List of Tables xi

Abstract xii

List of Abbreviations and Symbols Used xiii

Acknowledgements xviii

Chapter I. Introduction 1

A. Functional Roles of ACP 1

1. Overview 1

2. Fatty Acid Synthase ACP 4

i) Type I FAS 4

ii) Type II FAS 6

3. Specialized ACP Functions 13

i) Lipoic Acid Biosynthesis 13

ii) Lipid A Biosynthesis 13

iii) Hemolysin Maturation 14

iv) Quorum Sensing 16

v) Bioluminescence 17

vi) Phospholipid Biosynthesis 18

vii) Fatty Acid Activation 18

viii) Other ACP Functions 19

4. ACP Homologues in Secondary Metabolism 21

i) Peptidyl Carrier Protein 21

ii) Polyketide Synthase ACP 22

iii) Rhizobial ACPs 24

B. Structural Biology of ACP 25

1. Sequence and Structural Conservation 25

2. Stabilization of ACP Conformation 29

i) Divalent Cation Binding 29

ii) Fatty Acylation 31

iii) ACP as a Natively Unfolded Protein 32
C. Specificity of ACP-Enzyme Interactions 33
1. PT 33
2. Type II FAS Component Enzymes 35
i) FabH 36
ii) FabG 36
iii) FabI 37
iv) FabD 38
3. LpxA 39
D. Significance and Objectives 39
Chapter II. Materials and Methods 41
A. Materials 41
1. General Chemicals 41
2. Bacterial Strains 42
3. Radioisotopes 43
4. Solutions 43
5. Bacterial Growth Media 44
B. Molecular Biology 45
1. Site-Directed Mutagenesis 45
2. DNA Sequencing 45
3. Restriction Digestion and Agarose Gel Analysis 47
4. Preparation of SA/SB Double Site Mutant 48
C. Preparation of ACP and Derivatives 49
1. Purification of Native *V. harveyi* ACP 49
2. Purification of Recombinant Holo-ACP 50
3. Purification of Apo-ACP 51
4. Preparation and Purification of Acyl-ACP 51
D. Enzyme Preparation and Assays 52
1. *V. harveyi* Fatty Acid Synthase 52
2. *E. coli* Holo-ACP Synthase 53
3. *V. harveyi* Acyl-ACP Synthetase 54
4. *E. coli* LpxA 54
E. Biophysical Analyses 55

1. Native PAGE 55
2. Circular Dichroism 55
3. Steady-State Fluorescence Spectroscopy 56
i) Emission Spectra 56
ii) Solute Perturbation 56
iii) Determination of Dissociation Constant 57
F. ACP Homology Modelling 57
Chapter III. Identification of a Key Residue in ACP Required for *V. harveyi* Fatty Acid Synthase Activity 59
A. Rationale 59
B. Results 60
1. Conformational Analysis of ACP Mutants 60
2. Effects of ACP Mutations on FAS and AAS Activities 64
C. Discussion 67
Chapter IV. Roles of Divalent Cation Binding Residues in Maintaining ACP Structure and Function 72
A. Rationale 72
B. Results 74
1. Mutant ACP Preparation 74
2. Mg^{2+}-Induced ACP Folding 74
3. Native PAGE Analysis of Mutant ACP Derivatives 76
4. Role of Divalent Cation Binding Residues in Supporting Enzyme Activities 79
C. Discussion 83
1. Importance of Carboxylates in Shaping ACP Conformation 83
2. Distinct Binding Determinants of Various ACP-Dependent Enzymes 85
Chapter V. Probing ACP Microenvironment: Insights from Tryptophan Fluorescence 88
A. Rationale 88
B. Results 89
1. Preparation and Functional Analysis of Mutant ACPs 89
2. Conformational Analyses of ACP Mutants Using Native PAGE and CD 93

3. Steady-State Fluorescence Emission Spectra of Tryptophan Mutants of ACP 95

4. Examination of Tryptophan Exposure by Fluorescence Quenching 103

5. Interaction between LpxA and Holo-ACP 109

C. Discussion 111

1. Introduction of Tryptophan Residues into ACP Using Site-Directed Mutagenesis 111

2. Probing Tryptophan Exposure by Soluble Fluorescence Quenchers 114

3. Effects of Acylation vs Mg^{2+} Binding on ACP Conformation 117

4. ACP Interaction with LpxA 120

Chapter VI. Conclusions 124

References 128

Appendix I. Copyright Permissions 154

List of Figures

Figure 1.	Biological importance of ACP in gram-negative bacteria	2
Figure 2.	Type II fatty acid biosynthetic pathway	8
Figure 3.	The crystal structure of *E. coli* LpxA	15
Figure 4.	Multiple sequence alignment of ACP homologues	26
Figure 5.	The three-helix core structure of ACPs	27
Figure 6.	Surface electrostatic potential of ACP	61
Figure 7.	Effect of Mg^{2+} on secondary structure of wild type and helix II mutant ACPs	62
Figure 8.	Hydrodynamic analysis of ACPs using conformationally sensitive native PAGE	63
Figure 9.	Cross-species activities of FAS with ACPs from *E. coli* and *V. harveyi*	65
Figure 10.	*V. harveyi* FAS assay characterization	66
Figure 11.	Activities of *V. harveyi* FAS and AAS with wild type and mutant ACPs	69
Figure 12.	Divalent cation binding sites of *E. coli* ACP	73
Figure 13.	Effect of Mg^{2+} on the CD of rACP and mutant ACPs	75
Figure 14.	Effects of Mg^{2+}, Ca^{2+}, and Mn^{2+} on the CD of ACPs	77
Figure 15.	Conformationally sensitive native PAGE analysis of wild type and mutant ACPs	78
Figure 16.	Relative activity of *E. coli* ACPS with selected mutant apo-ACPs	80
Figure 17.	SA, SB and SA/SB mutant ACPs as enzyme substrates	81
Figure 18.	Activity of *V. harveyi* AAS with wild type and mutant ACPs	82
Figure 19.	Activity of *V. harveyi* FAS with wild type and mutant ACPs	84
Figure 20.	Ribbon representation of *E. coli* butyryl-ACP	90
Figure 21.	Enzyme activities with wild type and mutant ACPs	91
Figure 22.	Hydrodynamic analysis of holo- and acyl-ACPs using conformationally sensitive native PAGE	92
Figure 23.	Effect of Mg^{2+} on secondary structure of holo- and acyl-ACPs	94
Figure 24.	Effects of acylation and Mg^{2+} on helical content of rACP	96
Figure 25.	Fluorescence emission spectra of wild type and mutant ACPs	97
Figure 26.	Fluorescence emission spectra of holo- and acyl-ACP mutants	99

Figure 27. Fluorescence emission spectra of holo- and acyl-L46W 100

Figure 28. Effects of acylation and Mg^{2+} binding on fluorescence intensities and wavelength maxima of tryptophan mutants of ACP 101

Figure 29. Mg^{2+}-induced ACP structural transition monitored by CD and fluorescence 102

Figure 30. Fluorescence quenching of holo-ACPs in the presence of Mg^{2+} 104

Figure 31. Effects of Mg^{2+} binding and acylation on tyrosyl contribution to intrinsic fluorescence of L46W 108

Figure 32. Fluorescence indicator of LpxA interaction with ACP 110

List of Tables

Table 1.	Oligonucleotides used in site-directed mutagenesis and sequencing	46
Table 2.	Kinetic parameters of FAS and AAS with wild type and mutant ACPs	68
Table 3.	Fluorescence quenching parameters for holo-ACP mutants in the presence of Mg^{2+}	105
Table 4.	Effect of Mg^{2+} on holo-ACP and ACP-LpxA complex	112

Abstract

Acyl carrier protein (ACP) is a small protein that supplies fatty acyl groups to a remarkable diversity of enzymes and pathways, and is thus essential for bacterial growth and pathogenesis. A central acidic ACP helix (helix II) has been implicated in interaction with ACP partner enzymes, but the roles of specific ACP residues in enzyme docking and conformational changes to release the acyl group to the enzyme active site are largely unknown. Using recombinant *Vibrio harveyi* ACP (rACP) as a template for site-directed mutagenesis, I have explored the contributions of residues in and around helix II to ACP conformation and function with a variety of enzyme systems. An acidic residue at position 41 in the middle of helix II was found to be critical for the activity of fatty acid synthase, but not acyl-ACP synthetase. Combined neutralization of acidic residue clusters at either end of helix II (sites A and B) did not prevent stabilization of ACP conformation by divalent cation binding at the unaltered site, but differentially affected ACP function. Holo-ACP synthase was sensitive to mutations in site A, while site B mutations preferentially affected acyl-ACP synthetase and UDP-N-acetylglucosamine acyltransferase (LpxA) activities. Tryptophan mutagenesis to provide site-specific fluorescent probes of local conformation revealed that ACP folds upon interaction with LpxA, and that ACP folding induced by divalent cation binding and by fatty acylation produce distinct environments in the hydrophobic core. Overall, my results reinforce the concept of helix II as the "recognition helix" of ACP, but also provide detailed insights into the relationships between ACP structure and function that are relevant to the regulation of lipid metabolism and the design of novel antibacterial drugs.

List of Abbreviations and Symbols Used

6:0	hexanoyl
8:0	octanoyl
10:0	decanoyl
12:0	lauroyl
14:0	myristoyl
16:0	palmitoyl
18:0	stearoyl
A. aeolicus	*Aquifex aeolicus*
AAS	acyl-ACP synthetase
ACC	acetyl-CoA carboxylase
AccA	caroboxytransferase subunit of ACC
AccB	biotin carboxy carrier protein
AccC	biotin carboxylase
AccD	carboxytransferase subunit
ACP	acyl carrier protein
AcpH	ACP phosphodiesterase
ACPS	holo-ACP synthase
AHL	N-acylhomoserine lactone
AinS	AHL synthase
ArCP	aryl carrier protein
ATP	adenosine 5'-triphosphate
B. brevis	*Bacillus brevis*
B. subtilis	*Bacillus subtilis*
BSA	bovine serum albumin
CD	circular dichroism
CFE	cell-free extract
CoA	coenzyme A
CP	carrier protein
DCP	D-alanyl carrier protein

DEAE	diethylaminoethyl
DH	β-hydroxyacyl dehydrase
DTT	1,4-dithiothreitol
E. coli	*Escherichia coli*
EDTA	ethylene-diaminetetra-acetic acid disodium salt
ER	enoyl reductase
FabA	β-hydroxydecanoyl-ACP dehydratase/trans-2, cis-3-decenoyl-ACP isomerase
FabB	β-ketoacyl-ACP synthase I
FabD	malonyl-CoA:ACP transacylase
FabF	β-ketoacyl-ACP synthase II
FabG	β-ketoacyl-ACP reductase
FabH	β-ketoacyl-ACP synthase III
FabI	enoyl-ACP reductase I
FabK	enoyl-ACP reductase II
FabL	enoyl-ACP reductase III
FabZ	β-hydroxyacyl-ACP dehydratase
FAS	fatty acid synthase
FASF	partially purified fatty acid synthase fraction
GlcNAc	N-acetylglucosamine
GST	glutathione S-transferase
H. pylori	*Helicobacter pylori*
HEPES	N-(2-hydroxyethyl)piperazine-N'-(2-ethanesulfonic acid)
HlyA	hemolysin A toxin
HlyC	acyl-ACP-proHlyA acyltransferase
IPTG	isopropyl β-D-thiogalactopyranoside
IscS	cysteine desulfurase
KAS	β-ketoacyl-ACP synthase
KDO	3-deoxy-D-manno-octulosonate
KR	β-ketoacyl reductase
KS	β-ketosynthase

L. lactis	*Lactococcus lactis*
La. rhamnosus	*Lactobacillus rhamnosus*
Le. interrogans	*Leptospira interrogans*
LB	Miller's Luria-Bertani broth medium
LpxA	UDP-N-acetylglucosamine acyltransferase
LpxB	disaccharide synthase
LpxC	UDP-3-O-(R-3-hydroxymyristoyl)-N-acetylglucosamine deacetylase
LpxD	UDP-3-O-(R-3-hydroxymyristoyl)-glucosamine N-acyltransferase
LpxH	UDP-2,3-diacylglucosamine pyrophosphatase
LpxK	disaccharide kinase
LpxL	lauroyl transferase
LpxM	myristoyl transferase
LpxP	palmitoleoyl transferase
LuxA	α subunit of luciferase
LuxB	β subunit of luciferase
LuxC	fatty acid reductase
LuxD	myristoyl-ACP thioesterase
LuxE	acyl-protein synthetase
LuxI	AHL synthase
LuxM	AHL synthase
M. tuberculosis	*Mycobacterium tuberculosis*
MAT	malonyl/acetyl transferase
Me. loti	*Mesorhizobium loti*
MES	2-(N-morpholino)ethanesulfonic acid
MIANS	2-(4'-maleimidylanilino)naphthalene-6-sulfonic acid, sodium salt
MPT	malonyl/palmitoyl transacylase
MT	malonyl-CoA:ACP transacylase
NADH	β-nicotinamide adenine dinucleotide, reduced form
NADPH	β-nicotinamide adenine dinucleotide phosphate, reduced form
NRPS	nonribosomal peptide synthetase
P. aeruginosa	*Pseudomonas aeruginosa*

P. stewartii	*Pseudomonas stewartii*
PAGE	polyacrylamide gel electrophoresis
PBS	phosphate-buffered saline
PCP	peptidyl carrier protein
Pl. falciparum	*Plasmodium falciparum*
PlsB	sn-glycerol-3-phosphate 1-O-acyltransferase
PlsC	1-acyl-sn-glycerol-3-phosphate 2-O-acyltransferase
PP	4'-phosphopantetheinyl
ppGpp	guanosine tetraphosphate
PT	phosphopantetheinyl transferase
PKS	polyketide synthase
proHlyA	hemolysin A protoxin
R. leguminosarum	*Rhizobium leguminosarum*
Ra. norvegicus	*Rattus norvegicus*
rACP	recombinant *Vibrio harveyi* acyl carrier protein
RelA	ppGpp synthetase I
S. cerevisiae	*Saccharomyces cerevisiae*
SA	D30N/D35N/D38N
SA/SB	D30N/D35N/D38N/ E47Q/D51N/E53Q/D56N
SB	E47Q/D51N/E53Q/D56N
SD	standard deviation
SDR	short-chain dehydrogenase/reductase
SDS	sodium dodecyl sulfate
SEM	standard error of mean
Sp. oleracea	*Spinacia oleracea*
SpoT	ppGpp synthetase
St. coelicolor	*Streptomyces coelicolor*
St. roseofulvus	*Streptomyces roseofulvus*
St. rimosus	*Streptomyces rimosus*
TCA	trichloroacetic acid
TE	thioesterase
TEMED	N,N,N',N'-tetramethylethylenediamine

TLC	thin-layer chromatography
Tris	tris(hydroxymethyl)aminomethane
TROSY	Transverse-Relaxation Optimized Spectroscopy
UDP	uridine diphosphate
UDP-GlcNAc	uridine diphosphate N-acetylglucosamine
V. fisheri	*Vibrio fisheri*
V. harveyi	*Vibrio harveyi*

Acknowledgements

Once upon a time, the prospect of playing with cool glowing bugs all day lured me into the project to study our little ACP. Although it did not prove to be quite like my fantasy, I was hooked nonetheless and the rest is history. It takes a village to accomplish the long and hard process of a dissertation. My village consists of many people who have touched my life in some ways.

My deepest gratitude goes to Dr. David M. Byers, my great mentor and role model, who made a rich and rewarding graduate school experience possible. Not only has he helped me wade through the project in countless ways but, more importantly, he has nurtured my growth with patience and transformed me on many levels, e.g. liberal thinking, communication, and confidence, to name just a few. He never ceased to amaze me with his devotion to science and ebullience towards daily life. He was always able to point out the silver lining in even the darkest cloud. He was a master of the art of making tough jobs seem fun and easy while setting the bar high and bringing out the best of those working with him. So I had the rare luxury of enjoying the priceless freedom in pursuing some of my own research interests with luminous guidance, support, and encouragement from him every step of the way. As it turned out, his approach worked well for us except that I must have caused him a severe hair loss when he painstakingly scrutinized every single word of my writing, in which a's and the's never seemed to appear at the right places.

One is lucky enough to have a fabulous supervisor. I am really blessed to have a whole committee of top-flight professors overseeing my research, which benefited tremendously over the years from the suggestions and challenges by Drs. Christopher R. McMaster, K. Vanya Ewart, and Stephen L. Bearne. I also thank the graduate coordinator Dr. Richard A. Singer for invaluable advice at later stages. Busy scientists as they are, I am deeply moved by their willingness to go the extra mile to help a student reach professional and personal goals.

I am also in the debt of Dr. Christian Blouin for introducing me to the wonderland of homology modelling and Dr. Martin R. St-Maurice for CD know-how. Hats off to folks from the Atlantic Research Centre for putting up with my quirks and making it a great place to work. Special thanks go out to the past and present Byers lab members, particularly Anne Murphy, Gladys M. Keddy, Sarah J. Minielly, Gavin M. Langille, and Elden E. Rowland for excellent technical assistance and inspiring conversations.

Neither my bugs nor I have starved owing to the generous funding supports from Natural Sciences and Engineering Research Council, IWK Health Centre, and Atlantic Innovation Fund.

Behind every goal in life, there is a reason. My family and friends were my guardian angels and the reasons for doing my best. In fact, I might have very well wound up as a high school dropout and simply could not have made it this far had it not been for their unconditional love. My family in particular made a point of fostering in me not only curiosity and creativity but also a sense of resilience as I witnessed the unfolding of the family drama. They remained humble at glorious times and rolled with the punches at moments of turmoil with unflinching strength and grace. The thesis is dedicated to my well-respected grandfather and beloved grandmother who made her sudden exit from this world in the heat of its preparation. Their spirit of building a life against terrible odds lives on.

Just like what Ralph W. Sockman wrote, "Nothing is so strong as gentleness and nothing is so gentle as real strength". Thanks and good luck to all!

Chapter I. Introduction

A. Functional Roles of ACP

1. Overview

Bacterial acyl carrier protein (ACP), as a discrete subunit of type II fatty acid synthase (FAS), is a small, acidic, and highly conserved protein essential for bacterial growth and pathogenesis. It functions as the carrier of various covalently bound fatty acyl groups, delivering the fatty acyl cargo to many enzymes involved in the biosynthesis of lipids (Fig. 1; Rock and Cronan, 1996). ACP is one of the most abundant proteins in *Escherichia coli*, constituting ~ 0.25% of the total soluble protein (Rock and Cronan, 1979). Recent advances in proteomics have suggested that ACP may interact with over three dozen enzymes, making ACP one of the most promiscuous proteins known to date (Butland, et al., 2005).

ACP belongs to a family of carrier proteins (CPs) that are indispensable cofactors of various primary and secondary metabolic pathways, including fatty acid synthesis, nonribosomal peptide synthesis, polyketide synthesis, and lysine biosynthesis. CPs, as either freestanding proteins or domains in a larger multifunctional polypeptide, typically consist of 70-100 amino acids. Most of their biological functions cannot be accomplished without proper post-translational attachment, at a conserved serine residue, of a 4'-phosphopantetheinyl (PP) prosthetic group derived from CoA, which serves as a swinging arm in delivering the covalently bound building blocks and intermediates (i.e. fatty acids and amino acids) to the active sites of their partner enzymes. Rather than being inert carriers, CPs are obligatory donors of bound substrates and actively contribute to the specificity of enzyme interactions. Thus, FAS and other CP dependent enzymes have long been subjects of genetic and biochemical manipulations for development of antimicrobials, anticancer agents, and genetically modified plants. The overall goal of the current project is to understand the structural and functional determinants behind the specific interactions between the multifunctional ACP and its multiple enzyme partners.

Figure 1. Biological importance of ACP in gram-negative bacteria. Protein names used are: AcpS, holo-ACP synthase; AasS, *Vibrio harveyi* acyl-ACP synthetase; FabA, β-hydroxydecanoyl-ACP dehydratase/trans-2, cis-3-decenoyl-ACP isomerase; FabB, β-ketoacyl-ACP synthase I; FabD, malonyl-CoA:ACP transacylase; FabF, β-ketoacyl-ACP synthase II; FabG, β-ketoacyl-ACP reductase; FabH, β-ketoacyl-ACP synthase III; FabI, enoyl-ACP reductase; FabZ, β-hydroxyacyl-ACP dehydratase; LpxA, UDP-GlcNAc acyltransferase; LpxB, disaccharide synthase; LpxC, UDP-3-O-(R-3-hydroxymyristoyl)-N-acetylglucosamine deacetylase; LpxD, UDP-3-O-(R-3-hydroxymyristoyl)-glucosamine N-acyltransferase; LpxH, UDP-2,3-diacylglucosamine pyrophosphatase; LpxK, disaccharide kinase; LpxL, lauroyl transferase; LpxM, myristoyl transferase; LpxP, palmitoleoyl transferase; LuxA, α subunit of luciferase; LuxB, β subunit of luciferase; LuxC, fatty acid reductase; LuxD, myristoyl-ACP thioesterase; LuxI, acylhomoserine lactone synthase; AinS, acylhomoserine lactone synthase; HlyC, acyl-ACP-proHlyA acyltransferase; PlsB, sn-glycerol-3-phosphate 1-O-acyltransferase; PlsC, 1-acyl-sn-glycerol-3-phosphate 2-O-acyltransferase.

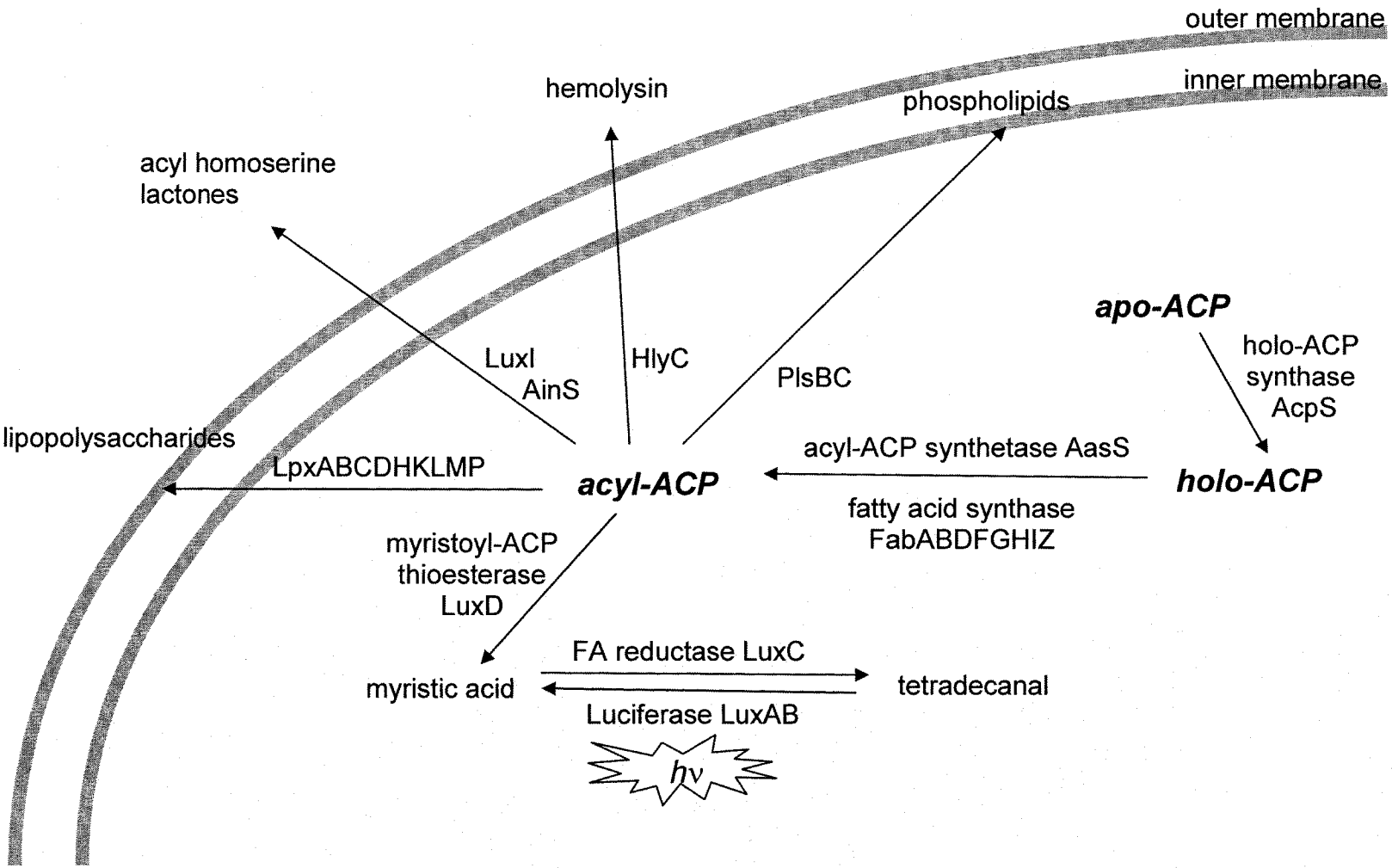
outer membrane
inner membrane
hemolysin
phospholipids
acyl homoserine
lactones
apo-ACP
holo-ACP
synthase
AcpS
LuxI
AinS
HlyC
PlsBC
lipopolysaccharides
LpxABCDHKLMP
acyl-ACP
acyl-ACP synthetase AasS
holo-ACP
fatty acid synthase
FabABDFGHIZ
myristoyl-ACP
thioesterase
LuxD
FA reductase LuxC
myristic acid
tetradecanal
Luciferase LuxAB
hν

2. Fatty Acid Synthase ACP

i) *Type I FAS*

Type I FAS found in metazoans and some microorganisms is a multifunctional protein responsible for de novo biosynthesis of long chain fatty acids from malonyl-CoA. Mammalian cytosolic FAS is a single homodimeric protein of functional domains organized in the order of β-ketoacyl synthase (KS), malonyl/acetyl transferase (MAT), β-hydroxyacyl dehydrase (DH), enoyl reductase (ER), β-ketoacyl reductase (KR), ACP, and thioesterase (TE) (Smith et al., 2003). In humans, the PP moiety is post-translationally transferred from CoA to a conserved Ser residue in the ACP domain by a 30-kDa cytosolic monomeric phosphopantetheinyl transferase (PT) in a mechanism analogous to the widely studied serine phosphorylation (Joshi et al., 2003). Human PT modifies a broad range of substrates including mitochondrial and prokaryotic type II ACP, prokaryotic type II peptidyl carrier protein (PCP), and the yeast PCP domain of α-aminoadipate semialdehyde dehydrogenase involved in lysine metabolism (Praphanphorj et al, 2001).

Biosynthesis of a long chain saturated fatty acid, usually palmitate, involves loading of one acetyl primer and seven malonyl extender moieties from CoA thioesters to the PP thiol of the ACP domain, which is accomplished by MAT. KS-mediated condensation entails transfer of a saturated acyl moiety from ACP to the active site Cys of KS, decarboxylation of malonyl-ACP to yield a reactive carbanion, and nucleophilic attack of the acyl group by the carbanion to form a new C-C bond (Witkowski et al., 1997). The condensed product, now attached to the ACP domain, undergoes a series of β-carbon processing steps under iterative actions of KR, DH, ER, and KS, and is released by the TE domain once the saturated fatty acyl chain length reaches 16 carbons (Naggert et al., 1991). Structural determination has proven to be very difficult for the animal FAS dimer: each subunit contains about 2500 residues (Schweizer and Hofmann, 2004), and was originally proposed to possess a head-to-tail fully extended antiparallel configuration (Wakil, 1989). Mutant complementation (Rangan et al., 2001), cross-linking (Witkowski et al., 1997), and electron micrographic (Kitamoto et al., 1988) studies have led to a revised head-to-head model, which places KS and MAT in the centre with free access to the ACP domains from both subunits and TE at opposite poles of the FAS dimer (Witkowski et al., 2004). Consistent with the revised model, the X-ray

crystallographic map of porcine type I FAS has recently revealed an intertwined dimer architecture with two nonidentical lateral semicircular reaction chambers, each containing a full set of catalytic domains required for fatty acid elongation (Maier et al., 2006). It was not possible to place the ACP and TE domains or to trace the interdomain linking regions, probably because of their inherent flexibility. Cross-linking (Tian et al., 1985), electron microscopic (Asturias et al., 2005), and crystallographic (Maier et al., 2006) studies have suggested the existence of multiple conformations of FAS and their dependence on the presence of substrates.

Saccharomyces cerevisiae type I FAS contains six copies each of two nonidentical subunits as suggested by early electron microscopic investigations (Stoops et al., 1978). The *FAS1*-encoded 1887-residue β subunit contains domains in the order of MAT, ER, DH, and malonyl/palmitoyl transacylase (MPT). The *FAS2*-encoded 1845-residue α subunit contains the remaining FAS domains in the order of ACP, KR, KS, and PT (Kolodziej et al., 1996). Yeast utilizes separate PTs for phosphopantetheinylation of the ACP domain of the cytosolic type I FAS and the mitochondrial type II ACP. The former is capable of self-phosphopantetheinylation since PT is a constituent domain of the α subunit (Fichtlscherer et al., 2000); the latter is modified by a discrete enzyme Ppt2p (Stuible et al., 1998). Recent X-ray crystallographic electron density map of type I FAS from the filamentous fungus *Thermomyces lanuginosus* supports the compartmentalization of fatty acid synthesis for high efficiency (Jenni et al., 2006). The $\alpha_6\beta_6$ heterododecamer assembles into a hollow rotational ellipsoid with two separate interior reaction chambers, where ACP functions as a swinging domain with the PP prosthetic group delivering the acyl substrates into the deep hydrophobic clefts of the enzyme active sites. The palmitoyl end product of fatty acid synthesis is transferred back from ACP domain to CoA by MPT (Stoops et al., 1978).

Type I FAS is also found in certain bacteria, such as *Mycobacterium tuberculosis*, where mycolic acids are the predominant and characteristic lipid components of the cell envelopes (Brennan and Nikaido, 1995). Type II or dissociated FAS systems also present in these bacteria are incapable of de novo biosynthesis of fatty acids and are only used to elongate the products of type I systems (C12 to C16) to very long chain (C50 to C60) fatty acids (Kolattukudy et al., 1997; Schweizer and Hofmann, 2004).

ii) *Type II FAS*

Type II FAS found in most bacteria, plants, and eukaryotic mitochondria is the principle executor of de novo synthesis of fatty acids with each catalytic centre residing in a discrete soluble protein (Rock and Cronan, 1996). Distinct from type I FAS, intermediates in the type II pathway are always covalently attached to the ACP thiol and shuttled between the component enzymes: the latter are believed to function in a noncovalent complex but little information on stoichiometry and organization is available (Roughan and Ohlrogge, 1996). The three-dimensional crystal structure determination of all components of the prototypical *E. coli* type II system has recently been completed (White et al., 2005).

Plant type II fatty acid biosynthetic enzymes are of bacterial origin and reside in plastids such as chloroplasts, though most of the encoding genes are located in the plant nuclear genome. Both plants and bacteria share a similar biosynthesis pathway, commonly involving ACP-mediated elongation (Nagai and Bloch, 1967). It has been recognized that the quality and quantity of seed oils as well as resistance of crops to temperature could be manipulated by overexpressing or altering enzymes that participate in the type II fatty acid biosynthetic pathway (Broun et al., 1998; Tokuhisa and Browse, 1999).

In the extensively characterized bacterial type II system, apo-ACP is phosphopantetheinylated by holo-ACP synthase (ACPS, encoded by the *acpS* gene in *E. coli*) to give holo-ACP containing the nucleophilic thiol group. Despite low sequence similarity (20-30% identity), ACPS homologues have been identified in all sequenced bacterial and Mycoplasma genomes (McAllister et al., 2006), and belong to the PT superfamily (Walsh et al., 1997) that also includes human and yeast PTs despite limited sequence similarities of these enzymes to *E. coli* ACPS (Miller and Bhattacharjee, 1996; Joshi et al., 2003). ACPS is functional as a homodimer in gram-negative bacteria such as the 28 kDa enzyme in *E. coli* (Lambalot and Walsh, 1995), a homotrimer in gram-positive bacteria including *Streptococcus pneumoniae* (Chirgadze et al., 2000) and *Bacillus subtilis* (Parris et al., 2000), and a homodimer in atypical bacteria, e.g. *Mycoplasma pneumoniae* (McAllister et al., 2006). *E. coli* ACPS is not only active with its cognate substrate apo-ACP (with a K_m of about 1 μM), but also recognizes and modifies to significant degrees type II polyketide synthase (PKS) ACPs both in vitro (Gehring et al., 1997) and in vivo (Cox et al., 1997). Although *E. coli* ACPS is active with some remotely related ACP homologues, including *Lactobacillus* D-alanyl carrier protein (DCP) involved in D-alanine activation for cell wall lipoteichoic acid biosynthesis (Debabov

et al., 1996), and *Rhizobium* NodF involved in the biosynthesis of nodulation signalling molecules for plant cell infection (Ritsema et al., 1998), it does not act on PCP (Lambalot et al., 1996). A similar substrate specificity pattern has been observed with *B. subtilis* ACPS (Mootz et al., 2001). Because of its crucial role in ACP activation and bacterial survival, ACPS is considered as a valid target in many drug discovery efforts (Chu et al., 2003; Gilbert et al., 2004; Joseph-McCarthy et al., 2005).

A second PT in *E. coli*, AcpT, modifies two putative CPs that are not recognized by AcpS; they are encoded in O-island 138, a gene cluster located adjacent to *acpT* in the genome of the pathogenic *E. coli* strain O157:H7 but absent in several other sequenced *E. coli* strains (De Lay and Cronan, 2006). AcpT gives barely detectable modification of ACP in vitro (Lambalot et al., 1996), and can not functionally replace AcpS in vivo, but partially complements AcpS by allowing a very slow growth of *E. coli acpS* mutant strain (Flugel et al., 2000).

The reverse reaction of ACP phosphopantetheinylation is catalyzed by a divalent cation-dependent ACP phosphodiesterase (AcpH) to produce apo-ACP and PP (Vagelos and Larrabes, 1967). *E. coli* AcpH is required for PP turnover in vivo but is not essential for bacterial growth (Thomas and Cronan, 2005) and does not likely regulate fatty acid synthesis (Fischl and Kennedy, 1990). This enzyme is not only active on holo-ACP but also on acyl-ACPs with up to 16 carbon acyl chains (Vagelos and Larrabes, 1967; Thomas and Cronan, 2005). Besides its cognate substrate type II ACP from *E. coli*, it is also active with some native FAS ACPs from other species, including *Aquifex aeolicus* and *B. subtilis*, but is not active with peptide fragments of *E. coli* ACP (Vagelos and Larrabes, 1967), *Rhizobium leguminosarum* nodulation protein NodF (Geiger et al., 1991), type II FAS ACP from *Lactococcus lactis*, or the mitochondrial ACP from *Bos taurus* (Thomas and Cronan, 2005), suggesting that a native ACP conformation is required for optimal AcpH activity.

The first committed step of fatty acid biosynthesis (Fig. 2) is accomplished by acetyl-CoA carboxylase (ACC; Cronan and Waldrop, 2002). This heterotetrameric enzyme catalyzes biotin-dependent carboxylation of acetyl-CoA to form malonyl-CoA, the only known metabolic destiny of which is to form fatty acids. Increased ACC expression has been demonstrated to result in elevated rates of fatty acid production (Davis et al., 2000). *E. coli* ACC is in turn a target for feedback inhibition by acyl-ACP from the same source, while

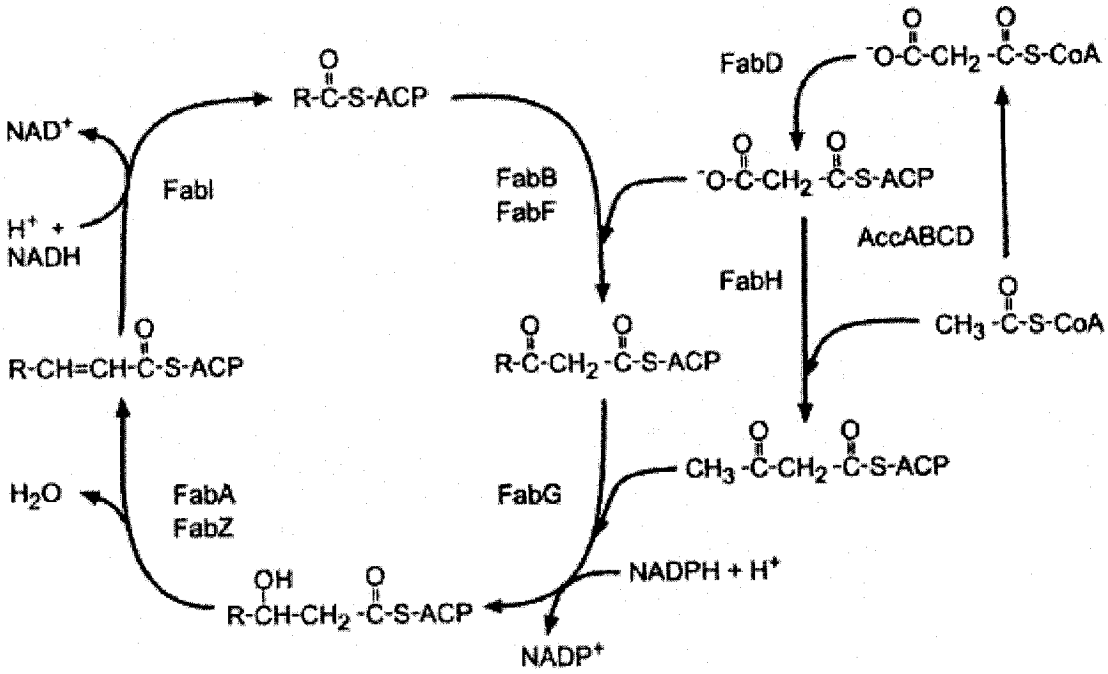

Figure 2. Type II fatty acid biosynthetic pathway. Adapted from Rock and Jackowski, 2002. Protein names used are: AccA, carboxytransferase subunit of acetyl-CoA carboxylase; AccB, biotin carboxy carrier protein; AccC, biotin carboxylase; AccD, carboxytransferase subunit; FabA, β-hydroxydecanoyl-ACP dehydratase/trans-2, cis-3-decenoyl-ACP isomerase; FabB, β-ketoacyl-ACP synthase I; FabD, malonyl-CoA:ACP transacylase; FabF, β-ketoacyl-ACP synthase II; FabG, β-ketoacyl-ACP reductase; FabH, β-ketoacyl-ACP synthase III; FabI, enoyl-ACP reductase; FabZ, β-hydroxyacyl-ACP dehydratase; LpxA, UDP-GlcNAc acyltransferase.

spinach type II ACP thioesters are inactive in this role (Davis and Cronan, 2001). Thus, ACC is thought to be an important regulator of FAS and a subject of cognate acyl-ACP regulation.

The monomeric 32-kDa malonyl-CoA:ACP transacylase (FabD) prepares malonyl-CoA for fatty acid production by accepting the malonyl moiety to form a stable acyl enzyme intermediate at a Ser residue and converting it to malonyl-ACP using a ping-pong kinetic mechanism (Prescott and Vagelos, 1972; Serre et al., 1995). FabD is essential for the operation of FAS with only a single known isoform, making FabD a potential antimicrobial drug target (Harder et al., 1974). However, the FabD reaction is readily reversible and appears to rapidly adjust the level of malonyl-ACP to the supply of malonyl-CoA with no apparent regulatory roles. There are no established inhibitors for this enzyme (Lu et al., 2005).

KAS III (FabH) catalyzes the initial decarboxylative condensation reaction by converting acetyl-CoA and malonyl-ACP to β-hydroxybutyryl-ACP in *E. coli* (Jackowski and Rock, 1987). The catalytic centre is characterized by a conserved Cys-His-Asn triad (Davies et al., 2000). A regulatory role for FabH has been suggested because of its position at the beginning of the pathway. FabH is an essential protein (Revill et al., 2001), the overexpression of which leads to an overall shortening of fatty acid chain lengths (Jackowski and Rock, 1987). FabH is also subject to feedback inhibition by long chain acyl-ACP, the potency of which increases with increasing chain length (Heath and Rock, 1996a,b). FabH substrate specificity dictates membrane fatty acid composition. Only straight-chain fatty acids are produced in *E. coli*. By contrast, FabH in many gram-positive bacteria such as *B. subtilis* is highly selective for branched-chain acyl-CoA derived from amino acid catabolism, leading to the production of branched-chain fatty acids (Butterworth and Bloch, 1970). The *M. tuberculosis* type I pathway is followed downstream by a type II FAS to produce very long chain mycolic acids, the FabH of which prefers long chain acyl-CoA accordingly (Choi et al., 2000). The crystal structures of FabH proteins from *E. coli* (Qiu et al., 1999) and *M. tuberculosis* (Scarsdale et al., 2001) have been determined, paving the way for the synthesis of a number of FabH-specific indole analogues as part of a structure-based drug design effort (Daines et al., 2003).

Although little sequence similarity is observed between the initiation FabH proteins and the elongation condensing enzymes of the FabB/F class, all share a common structural

fold of the thiolase family and a similar overall catalytic mechanism (Mathieu et al., 1997). Unlike FabH, KAS I (FabB) and KAS II (FabF) contain a Cys-His-His configuration in the active site and only condense acyl-ACP primers with malonyl-ACP (Olsen et al., 1999; Moche et al., 2001). In addition to their role in chain elongation, both enzymes are capable of initiating fatty acid biosynthesis by producing an acetyl-ACP primer through malonyl-ACP decarboxylation (Alberts et al., 1969). FabB is important for the biosynthesis of unsaturated fatty acids (Cronan et al., 1969; Rosenfeld et al., 1973), while FabF is responsible for production of cis-vaccenic acid (18:1Δ11) in response to decreased temperature (Garwin et al., 1980). However, only a FabF isoform is present in many pathogens, including those that contain unsaturated fatty acids, such as *Streptococcus pneumoniae* (Lu and Rock, 2006). The structure and distribution of fatty acid products are governed by the substrate specificities and expression levels of FabB/F, which are important determinants of product chain length, competing with glycerol-phosphate acyltransferase (PlsB) (Cronan et al., 1975). FabB/F have proven to be popular targets for antimicrobial drug discovery with two well characterized natural product inhibitors: cerulenin (Price et al., 2001a) and thiolactomycin (Tsay et al., 1992).

The NAD(P)H -dependent reductions in the second and fourth steps of fatty acid elongation in *E. coli* are respectively catalysed by β-ketoacyl-ACP reductase (KR, FabG) and enoyl-ACP reductase (ER, FabI). All characterised bacterial KRs and FabI-related ERs are tetrameric and belong to the short-chain dehydrogenase/reductase (SDR) superfamily with similar structures and signature active site Tyr and Lys residues in a YX_NK motif (Oppermann et al., 2003).

FabG is highly conserved, essential for bacterial growth (Zhang and Cronan, 1998), and is a single isozyme known to catalyze the reduction of β-ketoacyl-ACP in coordination with the cofactor NADPH, resulting in a hydroxyl group at the fatty acid C3 position (Rawlings and Cronan, 1992). Structural determination of FabG from *E. coli* (Price et al., 2001b, 2004), *M. tuberculosis* (Cohen-Gonsaud et al., 2002), and the oilseed rape plant *Brassica napus* (Fisher et al., 2000) has yielded virtually identical structures containing a Ser-Lys-Tyr catalytic triad. Comparison of FabG and FabG-$NADP^+$ structures from *E. coli* has revealed conformational changes upon binding of cofactor that occur at four distinct locations within the enzyme including the active site and monomer interfaces, suggesting that the binding of

cofactor occurs before the ACP-bound substrate binding (Price et al., 2004). Furthermore, FabG exhibits negative cooperativity in that binding of cofactor at one site in the tetramer enhances binding of acyl-ACP to the same site but diminishes the affinity for the cofactor at other sites (Price et al., 2001b). FabG appears to be an attractive target for broad-spectrum antibacterial drug development, yet until recently no inhibitors had been reported (Zhang and Rock, 2004; Li et al., 2006; Wickramasinghe et al., 2006).

ER I (FabI) is a single essential NADH-dependent isozyme in *E. coli* that reduces trans unsaturated intermediates for further elongation (Bergler et al., 1994). It is a determinant factor in pulling each elongation cycle to completion due to the fact that the FabA reaction favors the substrate β-ketoacyl-ACP (Heath and Rock, 1995). FabI catalyzes a rate-limiting step and seems to be a significant regulation target of acyl-ACP product inhibition, presumably more so than FabH (Heath and Rock, 1996b). Several widely used compounds have been found to efficiently inhibit bacterial ER, including the antiseptic triclosan (Levy et al., 1999), antibacterial diazaborine (Roujeinikova et al., 1999), and the front-line antituberculosis agents isoniazid (Banerjee et al., 1994) and ethionamide (Campbell and Cronan, 2001). With no significant mammalian homologues, FabI continues to be a point of interest in drug discovery efforts (Moir, 2005). However, the potential of FabI being an excellent target for broad-spectrum antibiotic is dampened by the discovery that many pathogens carry alternative reductases. NAD(P)H-dependent ER III (FabL) discovered in *B. subtilis* is related to FabI with the same spacing between key catalytic residues (YX_6K) (Heath et al., 2000). Unrelated to FabI, ER II (FabK) found in many streptococci in place of FabI is a NADH-dependent FMN-containing flavoprotein, which also oxidizes the cofactor in the absence of acyl-ACP substrate (Heath and Rock, 2000).

The third step of the elongation cycle is the dehydration of the β-hydroxyacyl-ACP to the trans-2-enoyl-ACP. There are two known isoforms of β-hydroxyacyl-ACP dehydratase (HD) with slightly different substrate specificities: FabZ only catalyzes the dehydration reaction to form the trans-2-enoyl-ACP; FabA not only dehydrates but also isomerises the double bond in the 10-carbon intermediate to form cis-3-enoyl-ACP (Heath and Rock, 1996c).

Most of the work in this area has been focused on FabA since it catalyzes the first

step in anaerobic unsaturated fatty acid synthesis (Silbert and Vagelos, 1967). The structure of *E. coli* FabA is known. Distribution of FabA is limited to gram-negative bacteria that produce unsaturated fatty acids and is always found with its partner FabB (Rosenfeld et al., 1973), which is required to elongate one or more of the critical cis unsaturated intermediates (Garwin et al., 1980). The ratio of saturated to unsaturated fatty acids in *E. coli* is determined by the complex interplay between the isomerization, condensation, and enoyl reduction reactions catalyzed by FabA, FabB, and FabI, respectively (Heath and Rock, 1996c), and can be altered by the changes in expression levels of FabA or FabB (Rock and Cronan, 1996) but not FabI (Heath and Rock, 1996c). The homodimeric *E. coli* FabA adopts a hotdog fold (Dillon and Bateman, 2004) with the catalytic dyad His/Asp formed along the dimer interface (Leesong et al., 1996). The active site His resides in an active site tunnel, the shape of which is consistent with the optimal efficiency of FabA with 10-carbon trans-2-acyl chains (Heath and Rock, 1996c). The active site Asp is thought to be responsible for trans/cis isomerase activity (Leesong et al., 1996). The crystal structure of *E. coli* FabA with its classic mechanism-based inhibitor, 3-decynoyl-N-acetylcysteamine (Kass, 1968), is also known, where the active site His is covalently modified (Leesong et al., 1996).

By contrast, FabZ is ubiquitously expressed in FAS II systems and is involved in the biosynthesis of both saturated and unsaturated fatty acids (Heath and Rock, 1996c). It is the only isozyme in gram-positive bacteria that contain only saturated, branched-chain fatty acids (Aguilar et al., 1998). *Pseudomonas aeruginosa* FabZ exists as a hexamer consisting of three dimers (Kimber et al., 2004), each of which is essentially identical to FabA and also adopts a hotdog fold (Dillon and Bateman, 2004). The active site His/Glu are contributed by different monomers and are formed in the same way as FabA with the exception of Glu replacing Asp in FabZ. However, site-directed mutagenesis studies have suggested that differences in the active site residues do not account for the unique ability of FabA to catalyze isomerization. It has been hypothesized that the different shapes of the substrate tunnels control the conformation and positioning of the bound substrate, thus allowing FabA, but not FabZ, to catalyze the isomerization reaction (Kimber et al., 2004). Decades after the discovery of inhibitors of FabA, compounds that specifically inactivate FabZ from *Plasmodium falciparum* have been reported (Sharma et al., 2003).

3. Specialized ACP Functions

i) *Lipoic Acid Biosynthesis*

Besides the type I FAS in cytosol, mitochondrial type II fatty acid biosynthesis is a widely conserved process in mammals (Cronan et al., 2005), fungi (Brody and Mikolajczyk, 1988), and higher plants (Gueguen et al., 2000). It is important for respiratory competence and mitochondrial morphology maintenance, which lends credence to the endosymbiotic origin of mitochondria (Schneider et al., 1997). The sequence of human mitochondrial KS is indeed more similar to the freestanding counterparts found in prokaryotes and chloroplasts than to the KS domain of the human cytosolic FAS (Zhang et al., 2005). Despite lack of identification of the complete set of enzymes involved in fatty acid synthesis (Zhang et al., 2005), the major product of mitochondrial FAS is C8 octanoyl-ACP (Brody et al., 1997), which is converted to lipoyl-ACP by lipoic acid synthase (Morikawa et al., 2001). Disruption of mitochondrial ACP in yeast results in strongly reduced lipoic acid content and a respiratory-deficient phenotype (Harington et al., 1993). Subsequently, ACP donates lipoic acid to the pyruvate dehydrogenase complex in both mitochondria and *E. coli* (Jordan and Cronan, 1997). Consistent with this, all known lipoate-containing proteins in mammals are located in mitochondria, including α-ketoglutarate dehydrogenase and glycine cleavage enzyme (Perham, 2000). The FAS machinery in mitochondria is also linked to the production of long chain fatty acids (C14, C16), which may be utilized for the remodelling of mitochondrial membrane phospholipids (Schneider et al., 1997).

ii) *Lipid A Biosynthesis*

ACP is required for the biosynthesis of lipid A, a unique multiple acylated glucosamine-based phospholipid that makes up the outer monolayer of the outer membrane of gram-negative bacteria (Raetz, 1993). Not only is lipid A essential for bacterial growth (Galloway and Raetz, 1990; Onishi et al., 1996) and membrane integrity (Vaara, 1993), it is also the immunogenic component of gram-negative endotoxins and potently activates animal innate immunity (Ulevitch and Tobias, 1995), leading to gram-negative septic shock (Rietschel et al., 1993; David, 2001). The immunostimulatory activity of lipid A has implications for antitumoral therapies when used alone or as adjuvant in anticancer vaccines (Reisser et al., 2002).

The product of the single *lpxA* gene in *E. coli* catalyzes the first obligatory reaction leading to the biosynthesis of lipid A in the Raetz pathway by transferring a β-hydroxymyristoyl group from the terminal sulfhydryl of ACP prosthetic group to 3-OH position of UDP-GlcNAc to form UDP-3-O-(R-3-hydroxymyristoyl)-GlcNAc (Anderson and Raetz, 1987). This cytoplasmic acyltransferase requires ACP as the obligatory acyl donor, with activity three orders of magnitude higher than with derivatives of CoA, phosphopantetheine, or DTT (Wyckoff and Raetz, 1999). *E. coli* LpxA is also highly selective for β-hydroxymyristoyl group attached to ACP. Its activity with β-hydroxymyristoyl-ACP is 50 times higher than with 12- or 16-carbon acyl-ACPs hydroxylated at the 3 position (Odegaard et al., 1997), leading to the proposal of a "hydrocarbon ruler" on LpxA (Wyckoff et al., 1998). Evidence supporting this proposal also comes from other bacterial species. *P. aeruginosa* LpxA is specific for β-hydroxydecanoyl-ACP (Williamson et al., 1991) whereas *Chlamydia trachomatis* LpxA utilizes myristoyl-ACP (Sweet et al., 2001), consistent with the chemical structure of lipid A from these organisms. LpxA is the only ACP-dependent enzyme involved in lipid A biosynthesis whose X-ray crystal structure has been solved, both from *E. coli* (Raetz and Roderick, 1995) and *Helicobacter pylori* (Lee and Suh, 2003). Multiple contiguous hexad repeats are present in the 262 residues in each subunit, which constitute 10 coils of an unusual left-handed parallel α-helix (Fig. 3A), a fold generally associated with transferase activity in different taxons (Vuorio et al., 1994; Parisi and Echave, 2004). LpxA shares significant sequence similarity with the second acyltransferase in the pathway (LpxD) that is also specific for β-hydroxymyristoyl-ACP (Kelly et al., 1993). Three identical subunits of LpxA form a tripod, containing three identical active centers and proposed ACP binding basic clefts between each two subunits (Fig. 3B). No LpxA-specific inhibitor had been reported until recently (Williams et al., 2006).

iii) *Hemolysin Maturation*

The pore-forming hemolysin secreted by gram-negative bacteria is another ACP-dependent product implicated in pathogenesis (Issartel et al., 1991). HlyC activates co-synthesized hemolysin protoxin (proHlyA) to hemolysin by post-translationally forming amide linkages between acyl groups and the two internal lysine residues of HlyA (Stanley et al., 1994). Unmodified proHlyA is exported by the HlyBD complex (Ludwig et al., 1987).

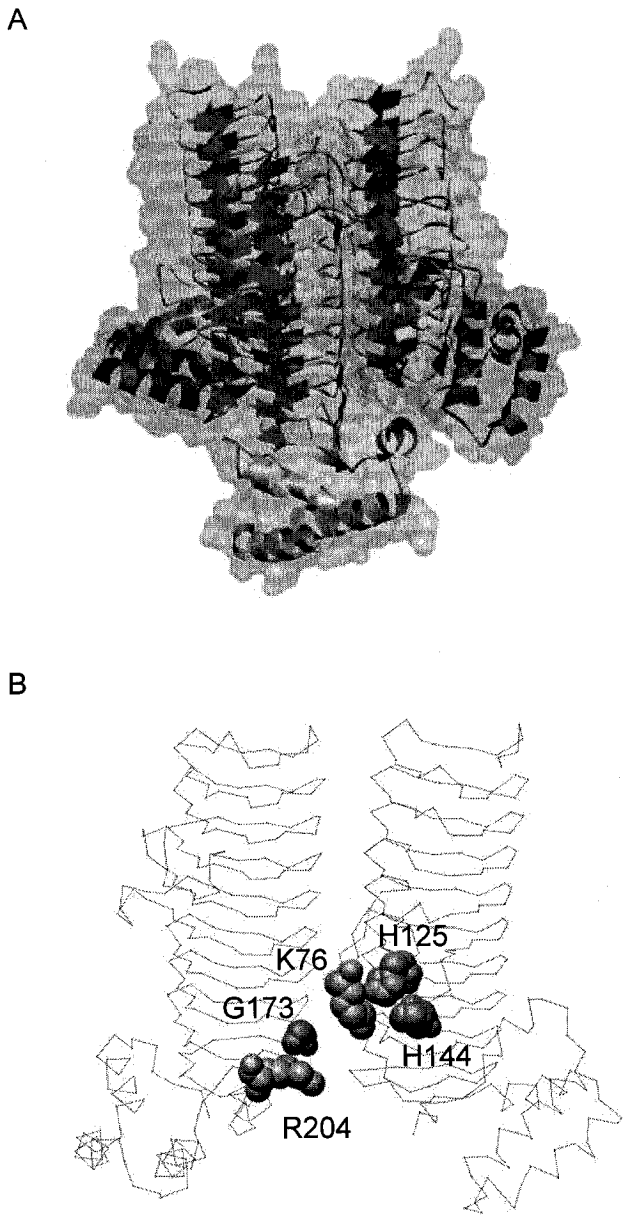

Figure 3. The crystal structure of *E. coli* LpxA. Shown are UCSF-Chimera (Pettersen et al., 2004) representations of A) molecular surface and backbone ribbon of *E. coli* LpxA homotrimer (Protein Data Bank accession code 1LXA; Pfitzner et al., 1995) and B) chain traces of two of the three subunits of *E. coli* LpxA. Conserved residues surrounding the proposed LpxA active site cleft are shown in space-filling representation.

Neither synthesis nor secretion is dependent on acylation. Unlike the eukaryotic protein acylation mechanism that utilizes fatty acyl-CoA thioesters, the homodimeric HlyC requires ACP as the acyl donor but is not specific for the acyl chain length (Issartel et al., 1991). HlyC accepts the fatty acyl group to generate an acylated HlyC intermediate that is depleted in the presence of proHlyA. HlyC is required in vivo at a concentration equimolar to proHlyA, consistent with its low catalytic efficiency (Stanley et al., 1999). No homology has been inferred between HlyC and other bacterial acyltransferases, including those involved in bioluminescence (Lee and Meighen, 1997) or biosynthesis of lipid A (Wyckoff et al., 1998), nodulation factor (Kamst et al., 1998), or phospholipids (Wilkison and Bell, 1997).

iv) *Quorum Sensing*

It has become increasingly recognized that bacteria are colonial organisms that communicate intercellularly, with other bacterial species, or higher organisms. The most common signalling molecules utilized by gram-negative bacteria are N-acylhomoserine lactones (AHLs), which are autoinducers in quorum sensing systems (Fuqua and Greenberg, 1998). AHL modulates expression of genes involved in motility, colonization, biofilm production, virulence, and bioluminescence in a cell density- and growth phase-dependent manner (Meighen, 1991; Lilley and Bassler, 2000; Lupp and Ruby, 2005). AHL is synthesized by at least two distinct families of AHL synthases, which catalyze acylation of S-adenosylmethionine by acyl-ACP and subsequent lactonization of the methionine moiety (Parsek et al., 1999). The LuxI type of enzymes such as *V. fischeri* LuxI and *P. stewartii* EsaR are structurally similar to N-acetyltransferases with a common PP binding fold (Watson et al., 2002). A number of conserved residues in the C-terminal half of LuxI enzymes are implicated in the selection of acyl-ACP intermediates from fatty acid biosynthesis (Val and Cronan, 1998) over CoA derivatives (More et al., 1996; Hanzelka et al., 1997). Acyl chain length selectivity is more complex, possibly requiring structural changes to accommodate acyl-ACPs of different chain lengths (Watson et al., 2002). AHLs produced by different bacterial species vary in acyl chain length (from C4 to C14), oxidation at the C3 position, and saturation (Kuo et al., 1994). A typical LuxI enzyme makes one predominant AHL and one or more minor AHLs, e.g. *P. aeruginosa* LasI makes 3-oxododecanoyl-homoserine lactone as well as 3-oxohexanoyl-homoserine lactone (Pearson et al., 1994). Thus, the specificity for

this system is only moderate, which may be influenced by the enzyme acyl chain specificity and the cellular pool of acyl-ACPs available (Fray et al., 1999). The LuxM type of enzymes such as *V. harveyi* LuxM and *V. fischeri* AinS are functionally similar but not structurally related to LuxI (Cao and Meighen, 1989). AinS can also efficiently use an acyl-CoA thioester as a substrate (Hanzelka et al., 1999). Control of particular bacterial diseases can be obtained by mechanisms that inhibit or misregulate quorum-sensing, such as natural inhibitors of AHL receptors (Manefield et al., 1999) and N-acylhomoserine lactonase that destroys AHL (Dong et al., 2001). Only recently have synthetic inhibitors been developed and a profound understanding of the structural basis of quorum sensing will aid future drug discovery endeavors (Koch et al., 2005; Singh et al., 2006).

v) *Bioluminescence*

The process of visible light emission mediated by luciferase, as observed in many different prokaryotic and eukaryotic organisms, is referred to as bioluminescence (Meighen, 1993). In bioluminescent marine and terrestrial bacteria from genera *Photobacterium* and *Vibrio*, the *lux* operon immediately downstream of *luxI* includes genes coding for the subunits of heterodimeric luciferase (*luxAB*) and the component enzymes of the fatty acid reductase complex (*luxCDE*) responsible for biosynthesis of the long chain aldehyde substrate for luciferase (Engebrecht and Silverman, 1984; Lee et al., 1991). Myristoyl-ACP thioesterase (LuxD) is responsible for generating a fatty acyl group from myristoyl-ACP and myristoyl-CoA thioesters via an acylated enzyme intermediate (Byers and Meighen, 1985), and can also hydrolyze oxyesters (Ferri and Meighen, 1994). The crystal structure of LuxD from *V. harveyi* indicates an overall architecture that resembles α/β hydrolases and a lipase-like Ser-His-Asp catalytic triad (Lawson et al., 1994). The loop containing Ser77 is thought to interact with the acyl-ACP substrate. A structural reorganization at the active site may occur upon substrate binding (Lawson et al., 1994). The acyl group is then transferred to acyl-protein synthetase (LuxE) and subsequently to reductase (LuxC) for NADPH-dependent reduction to aldehyde (Rodriguez et al., 1983; Wall et al., 1986). The products of the *luxCDE* genes have been purified from *Photobacterium phosphoreum* as part of a 500-kDa multienzyme complex composed of a central tetramer of LuxC subunits, each of which interacts with a LuxE subunit that binds weakly to a LuxD subunit (Wall et al., 1986).

vi) *Phospholipid Biosynthesis*

Phospholipid biosynthesis in *E. coli* starts with the transfer of two long chain fatty acyl groups from acyl-ACP to the glycerol-3-phosphate backbone to form phosphatidic acid. The acyltransferases that catalyze these reactions not only utilize acyl-ACP as the physiological acyl donor, but also acyl-CoA in vitro (Murata and Tasaka, 1997; Brown et al., 2002). The structure of plastid glycerol-phosphate acyltransferase indicates hydrophobic and positively charged binding sites for the fatty acyl substrate and the phosphate moiety of the glycerol-3-phosphate, respectively (Turnbull et al., 2001).

The sn-1 position of glycerol-phosphate is acylated by glycerol-3-phosphate acyltransferase (PlsB in *E. coli*; Green et al., 1981). PlsB is an inner membrane protein (Bayan and Therisod, 1989) considered as a possible component affecting dormant cell formation (Spoering et al., 2006). Overexpression of guanosine tetraphosphate (ppGpp) synthetase I (RelA) resulted in accumulation of ppGpp and inhibition of phospholipid biosynthesis. Blockade of PlsB activity led to the accumulation of long chain acyl-ACP and cessation of fatty acid biosynthesis. Thus, PlsB is thought to be the primary site for regulation by ppGpp (Heath et al., 1994). Despite its essential roles in bacterial growth, PlsB homologues are not widely distributed in bacteria (Heath and Rock, 1999).

The product of the PlsB-mediated reaction, lysophosphatidic acid, is subsequently acylated at the sn-2 position by acylglycerol-3-phosphate acyltransferase (PlsC, Coleman, 1990), which is also a membrane protein (Scheideler and Bell, 1986). PlsC selects 18:1 as preferred substrate, and also uses 12:0 and 16:0 at a significant rate (Brown et al., 2002). PlsC and PlsB share common sequences; a conserved histidine is required for acyltransferase activities (Heath and Rock, 1998). Distribution of PlsC is even more restricted among bacteria than that of PlsB, yet homologues of PlsC are found in plants and animals with abilities to functionally complement PlsC in an *E. coli* temperature-sensitive mutant (Hanke et al., 1995; West et al., 1997).

vii) *Fatty Acid Activation*

ACP delivers not only de novo synthesized fatty acids to their destinations, but also free fatty acids through direct activation. In *E. coli*, 2-acyl-glycerophosphatidylethanolamine acyltransferase/acyl-ACP synthetase (encoded by the *aas* gene) is a membrane-associated ACP binding protein responsible for acyl-CoA-independent incorporation of exogenous

fatty acids into the phospholipids (Hsu et al., 1989). Its physiological function in phosphatidylethanolamine remodelling is to regenerate phosphatidylethanolamine from 2-acyl-glycerolphosphatidylethanolamine that is formed by transacylation or phospholipase A1 reactions (Rock, 1984). Acyl-ACP, formed as a reaction intermediate, is neither dissociated in vivo nor exchanged with the biosynthetic acyl-ACP pool (Cooper et al., 1989). A soluble AAS is found in oleaginous yeast *Rhodotorula glutinis* that catalyzes ATP-dependent ligation of free fatty acids with ACP for the biosynthesis of triacylglycerol (Gangar et al., 2001). Antibodies to the yeast AAS cross-reacted with *E. coli* AAS.

By contrast, the recently cloned *V. harveyi* AAS (encoded by the *aasS* gene) is a 60.4-kDa soluble enzyme that is capable of activating exogenous fatty acids for both β-oxidation and phospholipid synthesis (Byers, 1989; Jiang et al., 2006). These acyl-ACP intermediates can also be elongated in a cerulenin-sensitive biosynthetic pathway (Byers, 1989). Further, AAS in bioluminescent bacteria is implicated in ATP-dependent activation of myristate for the formation of the myristyl aldehyde substrate for luciferase (Meighen, 1988). Based on sequence similarity, *V. harveyi* AAS is a member of the medium chain acyl-CoA synthetase family, and less related to the *E. coli* AAS (Jiang et al., 2006). It exhibits weak activity with short chain (C4, C6) and long chain (C16, C18) fatty acids relative to medium chain substrates. It also uses fatty acids of odd chain lengths (from C7 to C15) and unsaturated fatty acids such as cis-3-decenoic acid (Jiang et al., 2006). Its activity profile with noncognate ACP substrates is similar to those of ACPS and AcpH (Thomas and Cronan, 2005). *V. harveyi* AAS is active with type II ACPs from *E. coli*, *A. aeolicus*, and *B. subtilis*; only weak octanoylation of the ACPs from *L. lactis* and *Bos taurus* mitochondria can be achieved (Jiang et al., 2006). The reaction mechanism involves formation of acyl-AMP intermediate (Fice et al., 1993) and resembles that of acyl-AMP ligases in mycobacteria (Trivedi et al., 2004).

viii) *Other ACP Functions*

Besides the extensively characterized roles of ACP in the biosynthesis of a variety of products as described above, ACP is also involved in many biological processes where its function remains to be determined. Membrane-derived oligosaccharides are a class of soluble branched and substituted glucans present in the periplasmic space of bacteria closely related to *E. coli* (Schulman and Kennedy, 1979). They are thought to facilitate the maintenance of osmotic equilibrium in low-osmolarity environments (Kennedy, 1982). The assembly of the

polyglucose backbone of membrane-derived oligosaccharides requires a membrane-bound glucosyltransferase (MdoH; Weissborn and Kennedy, 1984), a periplasmic protein of unknown function (MdoG; Loubens et al., 1993), and ACP (Therisod et al., 1986). Somewhat surprisingly, the PP prosthetic group of ACP is not required for the reaction (Therisod and Kennedy, 1987). Glu4, Gln14, Glu21, Asp51, and a peptide fragment (residues 26-50) of *E. coli* ACP are involved in the interaction with MdoH (Tang et al., 1997).

An ACP distinct from the FAS ACP has been identified as a 10-kDa subunit of citrate lyase from *Klebsiella pneumoniae* (Dimroth and Eggerer, 1975), citramalate lyase from *Clostridium tetanomorphum* (Buckel and Bobi, 1976), and malonate decarboxylase in malonate-degrading bacteria such as *Malonomonas rubra* (Hilbi and Dimroth, 1994). With sequences related to FAS ACP (Walker and Ernst-Fonberg, 1982), the ACP subunits from these enzymes contain 2'-(5"-phosphoribosyl)-3'-dephosphocoenzyme A as a prosthetic group at Ser14 (Dimroth, 1976; Berg et al., 1996). Acetyl-ACP rather than holo-ACP is present in the catalytically active forms of the enzymes (Dimroth and Hilbi, 1997). During catalysis, the acetyl group is exchanged by a malonyl, citryl, or citramalyl group and regenerated upon cleavage of the products (Dimroth et al, 1977a,b).

Tandem affinity purification has identified about three dozen ACP-binding proteins in *E. coli*, many of which are unexpected (Butland et al., 2005). Three of the interactions have been characterized and confirmed to be specific (Gully et al., 2003), including those with cysteine desulfurase (IscS) involved in Fe-S cluster formation (Mihara and Esaki, 2002), MukB involved in chromosome segregation (Graumann, 2001), and ppGpp synthetase (SpoT; Seyfzadeh et al., 1993). IscS (Flint, 1996) and MukB (Niki et al., 1992) were previously shown to copurify with ACP, and both require the functional Ser36 of ACP in the interactions (Gully et al., 2003). Further, the interaction between IscS and ACP involves the formation of a disulfide bond between the thiol group of the ACP prosthetic group and the active site Cys328 of IscS (Gully et al., 2003). ACP has also been found to interact with melittin (Ernst-Fonberg et al., 1990) and stimulate the nicking reaction of transposon Tn3 (Maekawa et al., 1996) and Tn7 (Sharpe and Craig, 1998) in *E. coli.* In porcine liver, an endogenous oligosaccharide-linked ACP has been found to inhibit S-adenosylmethionine dependent methylation reactions (Seo et al., 2000) and, thus, inhibit cell growth (Seo et al., 2002).

4. ACP Homologues in Secondary Metabolism

i) *Peptidyl Carrier Protein*

Peptidyl carrier protein (PCP) is a CP domain of nonribosomal peptide synthetase (NRPS) found mainly in prokaryotes and lower eukaryotes, and participates in the biosynthesis of the vast majority of peptide-based natural products ranging from antibiotic vancomycin, to iron sequestering enterobactin in *E. coli*, or glycopeptidolipids as components of the cell wall (Lautru and Challis, 2004). Unlike the template-directed nucleic-acid-dependent ribosomal mechanism, NRPS is a 100-1700 kDa polyfunctional modular megasynthase organized into repeated functional units in an assembly-line fashion (Marahiel et al., 1997), commonly consisting of an initiation module, a termination module, and elongation module(s), the order of which corresponds to the sequence of the peptide being synthesized. A minimal module is comprised of three core domains structured typically in the order of a 50 kDa condensation (C) domain, a 55 kDa adenylation (A) domain, and a 10 kDa PCP domain (Weber and Marahiel, 2001). The A domain recognizes and activates the amino acid substrate through the formation of an aminoacyl adenylate followed by covalent binding of the activated amino acid as a thioester to the PP of the PCP domain. The C domain catalyzes the peptide-bond formation between two adjacent modules by facilitating the attack of an upstream peptidyl-PCP donor by a downstream chain-elongation unit, an aminoacyl-PCP acceptor nucleophile. In addition to these core domains, modules can contain additional or alternative domains which conduct post-assembly modifications of the incorporated amino acid, e.g. epimerization, N-methylation, oxidation/reduction, or heterocyclization (Cane et al., 1998). The release of the assembled peptide into solution is normally accomplished by a TE domain at the C-terminus of the termination module through hydrolysis or intramolecular cyclization of the peptidyl chain.

In addition to the NRPS systems, PCP is also required in lysine biosynthesis in the yeast *S. cerevisiae*, where α-aminoadipate reductase (Lys2) is a 155-kDa enzyme consisting of adenylation, PCP (14 kDa), and reductase domains (Morris and Jinks-Robertson, 1991). The N-terminal two thirds of the enzyme bears significant sequence similarity to NRPS (Suvarna et al., 1998).

Aryl carrier protein (ArCP) is a specialized CP domain of NRPS that produces iron chelators that are N-capped by a hydroxylated phenyl ring, either 2,3-dihydroxybenzoic acid

or salicylate. The acylated PP-bearing ArCP is formed via a freestanding A domain and is a substrate for the downstream condensation processes programmed for each peptide. Examples of siderophores include *E. coli* enterobactin and *V. cholerae* vibriobactin; these are used by the pathogenic bacteria to compete with their hosts for iron (Neilands, 1976; Griffiths et al., 1984).

Unlike PCP and ArCP, D-alanyl carrier protein (DCP) is a discrete protein required in the formation of D-alanyl-lipoteichoic acid that contributes to the thick peptidoglycan fabric of the cell wall of most gram-positive bacteria (Heaton and Neuhaus, 1994). Lipoteichoic acids consist of polyphosphoglycerol substituted with a D-Ala ester or a glycosyl residue. Because of the anionic nature of lipoteichoic acids, their functions include modulation of cationic autolysin activity, maintenance of cation homeostasis, and definition of the electrochemical properties of the cell wall (Fischer, 1988). An increased negative charge resulting from reduction of D-Ala content in cell wall abolishes biofilm production (Gross et al., 2001) and therefore impairs virulence of the bacterial cells (Collins et al., 2002) and increases their susceptibility to cationic antibiotics (Preschel et al., 2000). In *B. subtilis* and *Staphylococcus aureus*, D-alanylation is accomplished by products of the *dlt* operon, which seems to be widespread among gram-positive bacteria (Neuhaus and Baddiley, 2003). DltA is a 57 kDa protein that resembles the A domain of NRPS except that it is thought to specifically select its cognate amino acid D-Ala instead of the L-amino acids and carboxy acids in NRPS systems. The adenylated D-Ala is transferred to the PP of DCP (DltC) as a thioester and subsequently to lipoteichoic acids, presumably with the aid of DltB and DltD (Kiriukhin and Neuhaus, 2001).

ii) *Polyketide Synthase ACP*

Related to NRPS, the PKS family is found in soil and marine filamentous bacteria as well as in fungi and higher plants. They are responsible for producing a vast variety of polyketides of important therapeutic value, the carbon backbones of which are assembled by the successive condensation of small acyl units (Tsuji et al., 2001). Examples of PKS products include erythromycin from type I or modular PKS (Cortes et al., 1990), aromatic fused-ring polyketide antibiotics actinorhodin and oxytetracycline from type II or heterodimeric iterative PKS (Malpartida and Hopwood, 1984; Butler et al., 1989), plant pigmentation and signalling molecule precursor chalcone from type III or homodimeric

iterative PKS (Reimold et al., 1983), and rapamycin from hybrid PKS/NRPS systems (Aparicio et al., 1996; Dittmann et al., 2001). NRPS functions as a monomer (Sieber et al., 2002) whereas dimerization is required for PKS activity (Staunton et al., 1996).

Type I PKS is a megasynthase organized in much the same way as NRPS, with multiple functional units or modules each comprised of at least a ketosynthase (KS) domain followed by an acyltransferase (AT) domain and an ACP domain (Cane and Walsh, 1999). The AT domain catalyzes the priming of the flanking ACP domain with an appropriate monomeric substrate, usually methylmalonyl- or malonyl-CoA. The KS domain mediates the formation of a C-C bond between an upstream polyketide acyl thioester and a downstream chain-elongation unit by transferring the polyketide acyl chain to an active site Cys, followed by condensation with the extender acyl-ACP. Auxiliary domains conducting modifications of the polyketide chain include ketoreductase (KR), dehydrase (DH), or enoyl reductase (ER) (Cane, 1997). Product off-loading is fulfilled by a TE domain, most often found fused to the C-terminus of the furthest downstream module.

By contrast, type II PKS consists minimally of discrete proteins including KS, chain initiation factor (CIF), and ACP, a complex association of which is likely needed for effective and controlled operation (Shen and Kwon, 2002). The conserved active site Cys essential for KS activity is replaced by Gln in the CIF subunit, which has been shown to possess decarboxylase activity towards malonate, and is implicated in the provision of acetyl starter units for aromatic polyketide assembly (Bisang et al., 1999). Type II PKS complexes lack the AT domains but possess acyltransferase activity, thought to be provided by the malonyl CoA:ACP transacylase (MT) from the host fatty acid biosynthetic machinery (Carreras and Khosla, 1998). However, self-malonylation of ACP from actinorhodin PKS of *Streptomyces coelicolor* has been observed in vitro (Hitchman et al., 1998; Arthur et al., 2005). Little is known about how the chain length of the final product is determined since there is no dedicated TE associated with type II PKS systems (Matharu et al., 1998). The molecular logic of how type II PKS achieves structural diversity in polyketide biosynthesis also remains poorly understood. Nonetheless, the general reaction scheme of a minimal PKS involves transfer of an acetyl starter unit from ACP to KS, followed by sequential decarboxylative condensation between the growing polyketide chain and malonyl-ACP extender thioester, which yields a linear poly-ketoacyl-ACP intermediate (Staunton and Weissman, 2001).

Additional subunits have also been identified for the modification of the polyketide intermediates, such as KR, cyclase, and aromatase (McDaniel et al., 1993).

Type III PKS found predominantly in higher plants and recently in some bacteria (Funa et al., 1999) is the simplest PKS system and is unique in that it lacks ACP (Hopwood, 1997). This chalcone synthase-like PKS is essentially a KS possessing a highly conserved Cys, which first selects an acyl-CoA starter unit and catalyzes sequential decarboxylative condensations with malonyl-CoA directly to synthesize a linear polyketoacyl-CoA intermediate that is eventually cyclized into aromatic products. Other subunits, such as KR and a methylmalonyl-CoA-specific subunit, have been found to contribute additional structural diversity of plant polyketides (Schroder et al., 1998).

PKS is thought to have evolved from FAS ancestors (Hopwood and Sherman, 1990): type I and II PKS emerged via FAS pathway gene duplication and partial loss of function; type III PKS diverged from KAS III (FabH in *E. coli*) ancestors of type II FAS by gain of function (Austin and Noel, 2003). Members of type III PKS share active site residues and structural features with KS of type I and II PKS despite no obvious sequence similarity with the latter two types (Jez et al., 2000).

iii) *Rhizobial ACPs*

Three specialized ACPs have been characterized in rhizobia, i.e. NodF, AcpXL, and RkpF; all are required for the biosynthesis of cell-surface molecules that play a role in establishing the symbiotic relationship between rhizobia and their legume hosts (Geiger and Lopez-Lara, 2002). Nodulation genes (*nodABCEF*) responsible for the biosynthesis of the signalling molecules lipo-chitin oligosaccharides are induced by flavonoids secreted from the plant roots, leading to the onset of the developmental program resulting in nitrogen-fixing root nodules (Spaink, 2000). NodA, NodB, and NodC are thought to mediate the assembly of the lipo-chitin oligosaccharide backbone and subsequent amidation with an α,β-unsaturated fatty acyl group (John et al., 1993). NodE and NodF are homologues of KAS and FAS ACP (Shearman et al., 1986) and are essential for the formation of α,β-unsaturated fatty acid with length ranging from C16 to C20 in different bacteria (Demont et al., 1993). A hybrid ACP consisting of the N-terminal part of *E. coli* FAS ACP and the C-terminal portion of NodF is able to replace NodF in nodulation (Ritsema et al., 1998). AcpXL is required as acyl donor in the biosynthesis of lipid A, which is substituted with a 27-hydroxyoctacosanoic

acid in all members of the *Rhizobiaceae* family (Bhat et al., 1991; Que et al., 2000). In *Sinorhizobium meliloti*, other (ω-1)-hydroxylated fatty acyl groups (C18-C26) carried by AcpXL are incorporated into *nodD3*-dependent lipo-chitin oligosaccharide (Demont et al., 1994; Brozek et al., 1996). RkpF is involved in the production of a capsular polysaccharide (Reuhs et al., 1993).

B. Structural Biology of ACP

1. Sequence and Structural Conservation

Bacterial ACP is a small acidic protein sharing a high degree of identity with over 200 known protein sequences, particularly in the central region corresponding to the second α-helix in *E. coli* ACP (Fig. 4). The prosthetic group attachment site Ser is situated within a DSL signature motif, which is recognized by PTs (Mofid et al., 2002). The DSL motif is not only common to almost all PKS and FAS ACPs but also appears to be positioned in a conserved segment of secondary structure, i.e. at the N-terminus of helix II in a number of ACP 3D structures (Crump et al., 1996). Based on sequence similarity, FAS ACPs are more similar to each other than to PKS ACPs. For example, FAS ACPs from gram-negative bacteria *E. coli* and *V. harveyi* are 86% identical, while *E. coli* ACP shares only about 15% sequence identity with *B. brevis* tyrocidine synthetase PCP domain (Mootz and Marahiel, 1997) and R. *leguminosarum* NodF (Geiger et al., 1991). A slightly higher portion (21-27%) of *E. coli* ACP sequence is in common with *Lactobacillus rhamnosus* DCP (Debabov et al., 1996), rat *Rattus norvegicus* type I ACP domain (Witkowski et al., 1987), and type II PKS ACPs, e.g. actinorhodin ACP from *St. coelicolor* (Fernandez-Moreno et al., 1992) and frenolicin ACP from *St. roseofulvus* (Bibb et al., 1994).

Despite the sequence variations, a common three-helix bundle fold is adopted by ACPs from different species and pathways (Fig. 5), based on the solution structures of *B. subtilis* FAS ACP (Fig. 5B; Xu et al., 2001), *St. coelicolor* PKS ACP (Fig. 5I; Crump et al., 1997), the PCP domain of *B brevis* tyrocidine synthetase 3 encoded by the *tycC* gene (Fig. 5J; Weber et al., 2000), *La. rhamnosus* DCP (Fig. 5K; Volkman et al., 2001), and the ACP domain of rat type I FAS (Fig. 5H; Reed et al., 2003). Superposition of the ACP structures shows that structural homology extends to all three helices with differences in the packing and length of the helices. Major differences are also observed in the loop regions, particularly the

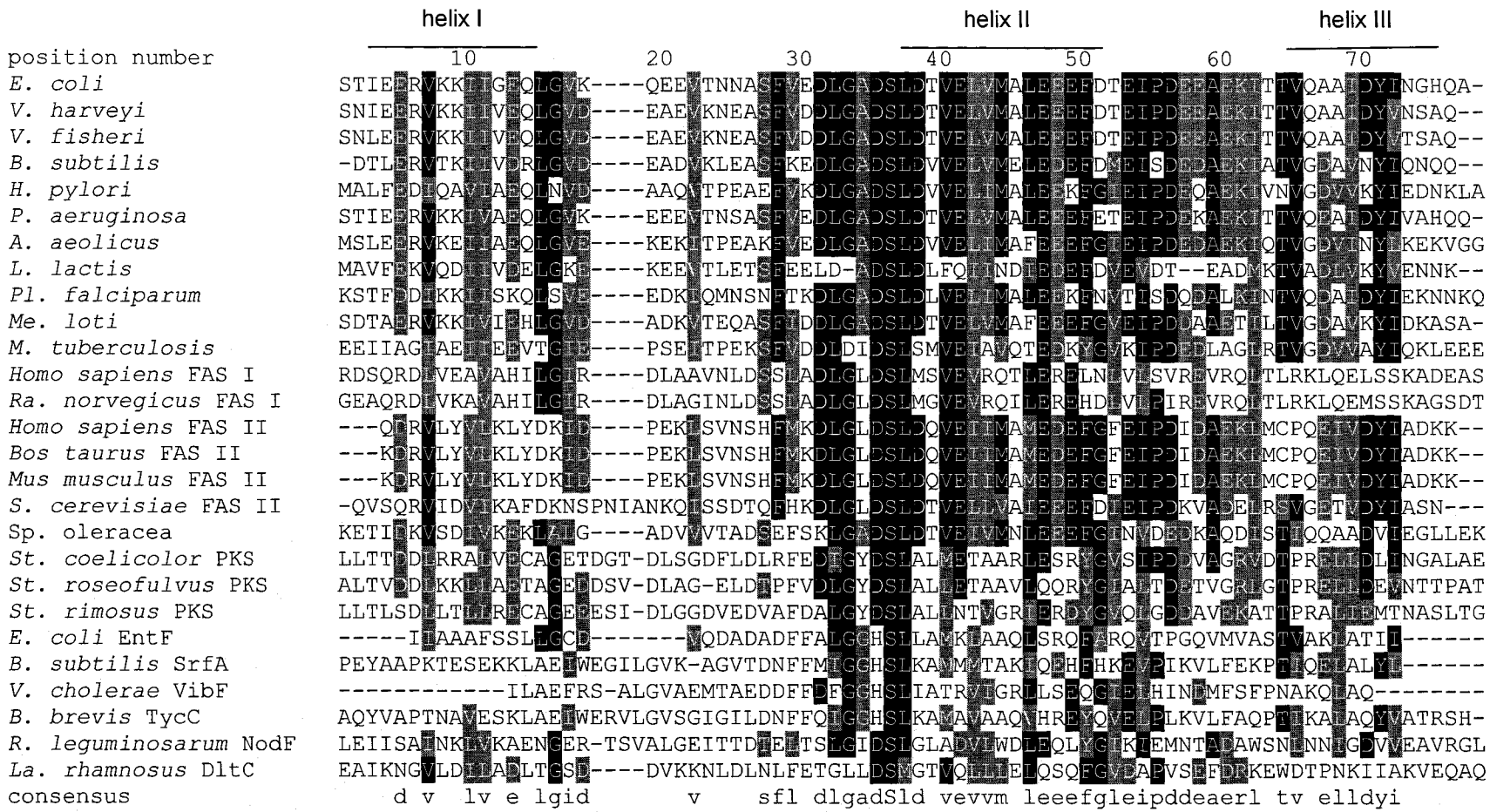

Figure 4. Multiple sequence alignment of ACP homologues. Protein sequences were aligned using Clustal W alignment algorithm (Higgins et al., 1996; http://align.genome.jp) and shaded using BoxShade (http://www.ch.embnet.org/software/BOX_form.html). Identical residues are shaded black. Conserved residues are shaded grey. The three α-helices of *E. coli* ACP are indicated. Position number corresponds to the sequence of *E. coli* ACP. The capitalized S in the consensus sequence stands for the prosthetic group attachment site serine.

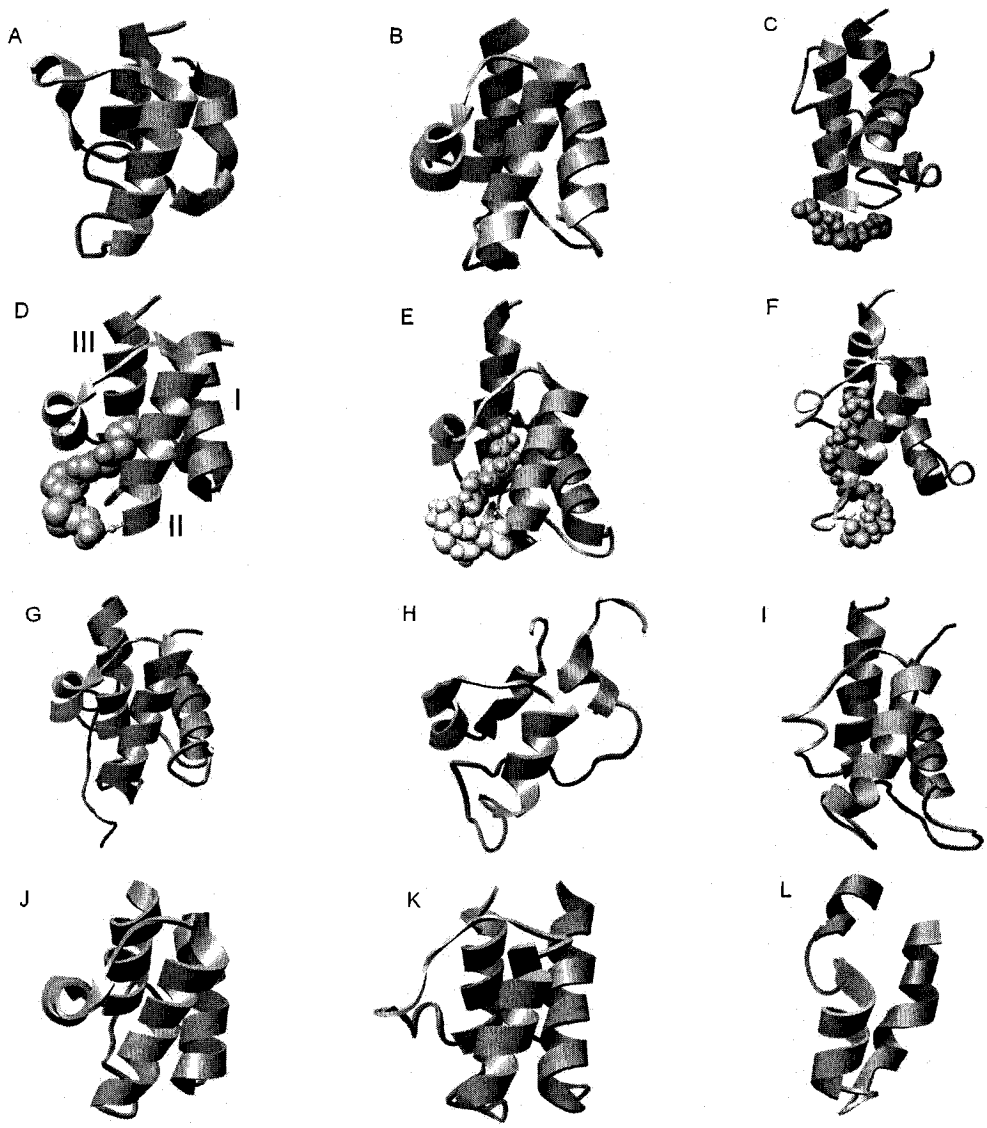

Figure 5. The three-helix core structure of ACPs. Shown are UCSF-Chimera ribbon diagrams of ACP NMR or crystal structures (Pettersen et al., 2004). The prosthetic group and the attached acyl chains are depicted in space-filling representation. A) *E. coli* FAS ACP (Protein Data Bank accession code 1ACP). B) *B. subtilis* FAS ACP (1HY8). C) *Pl. falciparum* FAS ACP major conformation (2FQ0). D) *E. coli* butyryl-ACP (1L0I) with the three α-helices indicated (I-III). E) Spinach *Spinacia oleracea* chloroplast decanoyl-ACP (2FVF). F) Spinach stearoyl-ACP (2FVA). G) *Mycobacterium tuberculosis* ACP (1KLP). H) Rat *Rattus norvegicus* type I FAS ACP domain (1N8L). I) *St. coelicolor* actinorhodin PKS ACP (2AF8). J) *B. brevis* tyrocidine synthetase 3 PCP domain (1DNY). K) *La. rhamnosus* DCP (1HQB). L) *R. leguminosarum* NodF partial backbone fold (1FH1).

long loop I connecting helices I and II (White et al., 2005).

Intrinsic flexibility of ACP is thought to be essential for structural rearrangements to accommodate a growing acyl chain and for specific interactions with functionally distinct enzyme partners. The ACP domain backbone is untraceable in the electron density map of animal and fungal type I FAS, likely resulting from the highly flexible nature of ACP (Maier et al., 2006; Jenni et al., 2006). The most studied *E. coli* ACP is composed of a preponderance of acidic residues grouped into three α-helices (residues 3-15 in helix I, residues 37-51 in helix II, residues 65-75 in helix III), which constitute over 50% of the secondary structure elements (Kim and Prestegard, 1990b). Hydrogen-deuterium exchange experiments at pH 6.0 indicate that helix II of *E. coli* ACP is one of the least stable secondary structural elements in the apo form (Andrec et al., 1995). By contrast, helix II amides of oxytetracycline ACP are more protected from fast amide exchange (Findlow et al., 2003). NMR studies of backbone dynamics have indicated that loop I exhibits the greatest flexibility (Kim et al., 2006), with the N-terminal portion (residues 15-17) more flexible than the C-terminal portion (residues 26-34) (Andrec et al., 1995). Similarly, the N-terminal half of loop I is found to be unstructured in several other ACP structures, including *St. coelicolor* actinorhodin ACP (Crump et al., 1997), *St. rimosus* oxytetracycline ACP (Findlow et al., 2003), rat type I ACP domain (Reed et al., 2003), and *H. pylori* ACP (Park et al., 2004).

ACP must undergo rapid folding and unfolding to allow efficient transfer and release of its acyl cargo. *E. coli* ACP has a low predicted isoelectric point at 4.1, which may contribute to its flexibility due to repulsion between negatively charged residues (Prescott and Vagelos, 1972). Not surprisingly, it readily refolds into its native conformation following denaturation induced by heat, organic solvent, high pH (Rock and Cronan, 1979), or denaturant guanidine hydrochloride (Takagi and Tanford, 1968). Thermodynamic studies of animal type I ACP domain and type II ACP from the bacterium *H. pylori* suggest lack of single stable elements in unfolding, and cooperativity in two-state folding (Reed et al., 2003; Park et al., 2004). The NMR structure of *E. coli* ACP is conformationally averaged between two or more states in fast exchange on the NMR time scale (Kim and Prestegard, 1989). Spinach ACP (Kim and Prestegard, 1990a), *St. roseofulvus* frenolicin ACP (Li et al., 2003), and type II ACP from malaria parasite *Pl. falciparum* (Sharma et al., 2006) are also found to exist in conformational equilibrium between two isomeric forms that are in slow exchange on the NMR time scale. The difference between the two forms of *Pl. falciparum* ACP arises from a

reorientation of the PP prosthetic group, which accounts for a small enthalpy difference implying a critical conformational switch for the activation of holo-ACP (Sharma et al., 2006).

The backbone coordinates of all holo-ACPs studied are essentially identical to that of the apo-counterparts (Holak et al., 1988; Crump et al., 1997; Xu et al., 2001). No interaction between the PP prosthetic group and the ACP polypeptide had been observed until recently, in ACPs from *Pl. falciparum* (Fig. 5C) and *E. coli*, suggesting the characteristic flexibility of the PP arm in solution (Kim et al., 2006; Sharma et al., 2006). In both isomeric forms of *Pl. falciparum* holo-ACP, the approximately 18-Å long PP moiety attached to Ser37 interacts with Val41 in helix II through space and with Ser37, Leu38, and Asp39 through covalent bonds (Sharma et al., 2006). Two alternate conformations of the Ser36 side chain are also observed in the crystal structure of apo-ACP from *E. coli*, with the hydroxyl oxygen atom pointing towards or away from the N-terminus of helix II (Qiu and Janson, 2004). The former conformation is predicted to permit interaction between the prosthetic phosphate group and the helix II dipole; the latter conformation would allow the prosthetic amide nitrogen to interact with the carbonyl of Glu60 and the acyl chain to be buried in the core hydrophobic pocket (Qiu and Janson, 2004). These two conformations are also observed in *M. tuberculosis* type II ACP (Wong et al., 2002). Further, comparison of *E. coli* apo- and holo-ACP structures has identified residues directly or indirectly involved in interactions with the prosthetic group (Kim et al., 2006). Residues from Asp35 to Met44, surrounding the PP attachment site, undergo chemical shift perturbations. Ile54, Glu60, and Ile62, in loop II between helices II and III, also exhibit chemical shift variations between the two structures, and are located in a hydrophobic cleft purported to provide interactions with the prosthetic group. In particular, the mercaptoethylamine moiety in PP is stabilized by a hydrogen bond between its amide nitrogen and the backbone carbonyl group of Glu60 (Kim et al., 2006).

2. Stabilization of ACP Conformation

i) *Divalent Cation Binding*

A prominent feature of ACP is its high negative charge and ability to bind cations. *E. coli* ACP contains 26% acidic residues and a much smaller proportion (8%) of basic residues. The acidic residues are clustered in the central portion of ACP (loop I, helix II, and loop II),

where the ACP backbone is more flexible than the rest of the molecule (Andrec et al., 1995; Kim et al., 2006). The basic residues, however, are found mainly near the N- and C-termini of ACP. Similar ratios and charge distribution are also found in FAS ACPs from other bacterial species but not in ACP domains of type I FAS or CPs from secondary metabolic pathways (Fig. 4). Circular dichroism (CD) measurements indicate that the ordered structure of *E. coli* ACP is lost at high pH or upon acetylation of amino groups, and is restored effectively by addition of divalent cations (Schulz, 1975). These observations suggest that electrostatic repulsion between negatively charged residues on ACP can be reduced by the presence of protonated amino groups or cations, which stabilize the protein against pH- or modification-induced structural perturbations (Schulz, 1975; Tener and Mayo, 1990). Mn(II) electron paramagnetic resonance binding studies suggest the presence of two low-affinity manganese binding sites (average K_d/site ~ 80 μM) at physiological pH. Manganese paramagnetic effects have been used to identify two discrete divalent cation binding sites clustering around Asp35 (site A) and Glu48 (site B) at either end of helix II of *E. coli* ACP (Frederick et al., 1988). Site A employs Glu30, Asp35, and Asp38 in ion coordination, whereas site B involves interactions with Glu47, Asp51, Glu53, and Asp56 near a proline-containing bend (see Chapter IV). The average number of bound metal ions increases above pH 8 with decreased binding affinity, possibly reflecting progressive structural perturbations. This is consistent with the involvement of ACP residues containing carboxylate groups in cation coordination (Tener and Mayo, 1990). Metal ions are thought to regulate ACP flexibility (Park et al., 2004). They have been implicated in reducing ACP conformational heterogeneity for NMR structure determination (Kim and Prestegard, 1989) and improving ACP crystallization by mediating crystal-packing interactions (Qiu and Janson, 2004). ACP follows two-state folding both in the absence and presence of divalent salts (Horvath et al., 1994).

Unlike divalent cations that bind to specific sites present only in the native state of ACP, monovalent ions provide stability to ACP by balancing its intrinsic negative charge nonspecifically in both the native and denatured forms (Horvath et al., 1994). CD (Keating et al., 2002) and thermodynamic studies (Horvath et al., 1994) have indicated that submolar levels of monovalent salts stabilize ACP conformation and raise the denaturation temperature of ACP to the same degree as millimolar concentrations of divalent salts.

ii) ***Fatty Acylation***

The overall secondary structure of *E. coli* ACP is largely conserved upon acylation (Jones et al., 1987b). The covalently attached fatty acyl group is immobilized against helix II through hydrophobic interactions, with an apolar pocket enclosed by the amphipathic helices (Gally et al., 1978). Acylation shifts the conformational equilibrium of ACP from the dynamically disordered states towards the ordered folded form (Zornetzer et al., 2006). ^{19}F-^{1}H Heteronuclear Overhauser studies of difluorohexanoyl-ACP from *E. coli* indicate that ^{19}F at the 5-position of the acyl chain is in close contact with the polypeptide primarily through interactions with Ile54 and Ala59 (Jones et al., 1987a). Analysis of distance restraints of short chain acyl-ACPs demonstrates substantial chemical shift variations for Phe50, Tyr71, and His75 as a function of fatty acyl chain length, reflecting subtle progressive conformational changes throughout the ACP molecule (Mayo and Prestegard, 1985). Acylated ACP retains its capability of binding divalent cations, albeit more weakly (average K_d/site ~ 1 mM). Acylation and metal binding do not appear to produce an identical microenvironment of Tyr71, based on the solvent accessibility of this residue (Tener and Mayo, 1990).

Reorientation of secondary structural elements occurs upon introduction of the acyl chain, with the largest alteration in loop II connecting helices II and III (Jones et al., 1987b). The X-ray crystallographic study of butyryl-ACP from *E. coli* provides more detailed evidence of ACP conformational changes required for successive cycles of chain elongation (Roujeinikova et al., 2002). Butyryl-ACP exists in two conformations with differences in the orientation of the acylated prosthetic group. In the open conformation, the space between loop II and the three-helix bundle allows insertion of the lipophilic acyl group into the hydrophobic pocket. By contrast, loop II is packed against the helices in the closed conformation and prevents the insertion of the acyl group into the protein interior; the prosthetic group is thought to be in a flexible and extended conformation (Roujeinikova et al., 2002). Spinach decanoyl- (Fig. 5E) and stearoyl-ACP (Fig. 5F) solution structures indicate that the C-terminal portion of the loop I region between Phe31 and Thr41 provides entrance to the fatty acid binding pocket (Zornetzer et al., 2006). The presence of an acyl chain pushes helix II away from helix I. Different conformational changes accompany conversion of holo-ACP to 10:0- vs 18:0-ACP with the hydrophobic pocket of the latter 50% larger than the former, supporting the role of ACP in actively accommodating a growing fatty acyl intermediate.

Despite the presence of a larger fatty acid binding pocket, solvent exposure of the acyl group generally increases with the chain length. Hydrophobic interaction chromatography suggests that ACP effectively shields fatty acids with fewer than 10 carbons and that a portion of longer chain fatty acyl moieties is exposed to solvent (Rock and Garwin, 1979; Cronan, 1982). The butyryl group of 4:0-ACP is completely buried in the hydrophobic core of ACP (Fig. 5D; Roujeinikova et al., 2002). By contrast, the PP moiety in 18:0-ACP from spinach chloroplast has more apparent freedom of motion compared to its counterpart in 10:0-ACP, as a consequence of increased solvent accessibility and dynamics of the longer acyl chain (Zornetzer et al., 2006).

iii) *ACP as a Natively Unfolded Protein*

Type II ACPs from some bacterial and mycobacterial species have been found to exist in dramatically different conformations under different conditions, involving local or global structural rearrangement. Unlike *E. coli* ACP, which maintains a native conformation at pH 7 (Schulz, 1975), *H. pylori* (Park et al., 2004) and *V. harveyi* ACP (Keating et al., 2002) are largely unfolded at neutral pH and only adopt an ordered structure in acidic solutions. The C-terminal extension from helix III of the type II ACP from *M. tuberculosis* exists in a random coil, which is proposed to interact with the very long chain intermediates in mycolic acid biosynthesis or to regulate specific protein-protein interactions (Wong et al., 2002). Loop I of *B. subtilis* ACP also appears unstructured in solution (Xu et al., 2001). However, a short α-helix (residues 28-31) is observed in loop I in the crystal structure of ACP-ACPS complex from *B. subtilis* (Parris et al., 2000). In addition, helix III of *B. subtilis* ACP is longer in the free form (residues 65-75) than in the complex (residues 65-71). Thus, ACP may belong to a large family of "natively unfolded proteins", which are functional proteins despite structural disorder under physiological conditions (Wright and Dyson, 1999).

High net charge is thought to be a necessary but not sufficient condition for a protein to be natively unfolded, which is determined by the combination of low hydrophobic interactions and high charge repulsion (Uversky et al., 2000). A sequence signature of intrinsic disorder is the presence of low sequence complexity and amino-acid composition bias, with a low proportion of bulky hydrophobic residues (Val, Leu, Ile, Met, Phe, Trp, and Tyr) and a high content of particular polar and charged amino acids (Gln, Ser, Pro, Glu, and Lys) (Romero et al., 2001). Analysis of sequences from complete genomes indicates that

intrinsically disordered proteins are present in all kingdoms of life, and that the proportion of these proteins increases with the increasing complexity of an organism (Ward et al., 2004). For example, 30% of the proteins from *S. cerevisiae* are predicted to be partially or fully unstructured.

Discovery of an intrinsically unstructured protein family challenges the traditional view that protein function equates with a stable three-dimensional structure. These proteins are often associated with roles in cellular signalling and regulation (Tsai et al., 2001). One of the advantages of inherent plasticity is that proteins like ACP can be induced to interact with a number of different partners with specificity and rapid on and off rates (Dyson and Wright, 2002). In general, proteins with intrinsic disorder can not bury a sufficient hydrophobic core to fold spontaneously (Dyson and Wright, 2005). Binding of a natural partner drives many to fold into an ordered structure by affecting their mean net charge, mean hydrophobicity, or both (Uversky et al., 2000). The entropic cost associated with the disorder-to-order transition is compensated by a favorable enthalpic contribution from target binding. Thus, specific protein-protein interactions are achieved through coupled folding and binding (Tsai et al., 1998).

C. Specificity of ACP-Enzyme Interactions

1. PT

The first structure of type II ACP in complex with a partner enzyme was obtained for ACP and ACPS from *B. subtilis* because of the relatively high affinity of ACP for this enzyme (Parris et al., 2000). Trimerization is required for ACPS activity since the active site is only formed at the molecular interface between two ACPS molecules. The contacts between ACP and ACPS are primarily between helix I of ACPS and helix II of ACP. Comparison of the free and bound forms of ACP indicates that helix II of ACP is pulled away from other helices and closer to ACPS in the complex (Xu et al., 2001). A key electrostatic interaction involves a salt bridge formed between Arg14 of ACPS and Asp35 within the DSL signature motif of ACP (Parris et al., 2000). Arg14, conserved in almost all ACPS-type enzymes, is also implicated in hydrogen bonding with Asp38 of ACP. These interactions serve to correctly orient Ser36 near the β-phosphate of CoA in the active site to

receive PP from CoA. Ser36 is in close contact with Glu58, a conserved residue in ACPS involved in coordination of CoA-bound magnesium ion. The interaction of Asp48 from ACP with Arg24 and Gln22 from ACPS serves to position the other end of helix II against ACPS. In addition to these predominately hydrophilic interactions, there are two significant hydrophobic contacts involving Leu37 and Met44 from helix II of ACP (Parris et al., 2000). The pattern of polar interactions mixed with small hydrophobic patches (1-3 residues) is observed in most protein-protein interfaces studied (Larsen et al., 1998). Not surprisingly, in vitro activity of *E. coli* ACPS is decreased with the less negatively charged *Streptomyces* PKS ACPs (Gehring et al., 1997). *B. subtilis* ACPS is inactive with PCP but activity increases with increasing resemblance of PCP to FAS ACP in helix II (Finking et al., 2004), e.g. ACPS is active with a K47D mutant of PCP (position 38 on ACP). Mutational studies suggest that residues along helix II are also implicated in interaction of the ACP domain of type I erythromycin PKS from *Saccharopolyspora erythraea* with its cognate PT (Weissman et al., 2006). The CoA substrate is proposed to bind ACPS to initiate the formation of a protein assembly before the binding of the apo-ACP substrate (Parris et al., 2000). There is not sufficient space for a CoA molecule to enter the active site if ACP binds first, which explains substrate inhibition of apo-ACP at high concentrations (Flugel et al., 2000). Once the PP moiety has been transferred to ACP, the loss of trimer stability afforded by CoA binding facilitates release of the holo-ACP product.

Unlike the ACPS-type PTs, which have a narrow substrate spectrum, the Sfp-type enzymes are double in size (~ 230 residues) and function as monomers with CP substrates in both primary and secondary metabolism with preference given to the latter (Walsh et al., 1997). The prototypical *B. subtilis* Sfp converts the apo forms of the seven PCP domains of surfactin synthetase (SfrA) for the production of the lipoheptapeptide antibiotic surfactin (Nakano et al., 1992; Lambalot et al., 1996). The structure of Sfp exhibits an intramolecular two-fold pseudosymmetry, suggesting a similar dimerization mode for ACPS with each half representing an ACPS subunit (Reuter et al., 1999). The C-terminal half of Sfp has marginal sequence similarity with ACPS. CoA and presumably a CP substrate are bound in a pocket formed by the interface of the two Sfp halves. Sequence analysis suggests that the region between α-helix V and β-strand VII may be responsible for the broad protein substrate specificity of Sfp by recognizing structural features of the CPs rather than specific residues only (Reuter et al., 1999). Structural and mutational analysis of Sfp has identified the loop

between β-strand IV and α-helix IV (residues Thr111-Ser124) as the PCP-binding region, in which Lys112, Glu117, and Lys120 are proposed to engage in electrostatic and hydrogen bonding interactions with PCP (Mofid et al., 2004). Modelling ACP with Sfp shows a nonoptimal fit and suggests less efficient PP transfer (Parris et al., 2000). The active site for Sfp is wider and more shallow than the active site of ACPS, consistent with the fact that the primary CP substrates for Sfp are domains of a larger protein whereas substrates for ACPS are small discrete proteins like type II ACP. Consequently, the substrate specificities of ACPS and EntD, an Sfp-type PT, are mutually exclusive (Grossman et al., 1993; Lambalot et al., 1996). *P. aeruginosa* PcpS (Barekzi et al., 2004) and *P. syringae* PcpT (Seidle et al., 2006), single PTs present in the pseudomonad species, effectively modify CPs from both primary and secondary metabolism, but the structural information is not yet available.

2. Type II FAS Component Enzymes

Acidic residues have long been known to be important for ACP function, e.g. neutralization of half of the 21 carboxylates on *E. coli* ACP by chemical amidation induces no apparent change in ACP structure but causes the loss of FAS activity (Abita et al., 1971). Similar to ACPS, type II FAS component enzymes do not possess sequence similarity that defines a common ACP-binding motif, but rather are predicted to recognize ACP through a positively charged/hydrophobic patch adjacent to the active site opening (Zhang et al., 2003a). Helix II of ACP, the so called "recognition helix", bears a cluster of electronegative/hydrophobic residues arranged in a fashion that is predicted to match the basic/hydrophobic ACP docking site on its partner enzymes, including FabA, FabB, FabD, FabF, FabG, FabH, FabI, and LpxA (Zhang et al., 2001, 2003b). The distances from the predicted ACP docking sites to the active site openings vary from 10.1 Å for FabH to 14.9 Å for LpxA, suggesting the need for a mobile ACP structure (Zhang et al., 2001). Because of the intrinsic flexibility of ACP and the low affinity of ACP for FAS components (in the micromolar range), no ACP-enzyme complex structure was solved until very recently (Rafi et al., 2006). ACPs are not simply interchangeable between various type II FAS and PKS systems despite their high degree of sequence and structural similarity, suggesting that only a correct arrangement of charged/apolar residues may ensure accurate enzyme recognition (Khosla et al., 1992; Crosby et al., 1998; Florova et al., 2002; Matharu et al., 1998).

i) *FabH*

The crystal structure of *E. coli* FabH reveals two adjacent but non-overlapping basic patches on the generally acidic surface of FabH, one for CoA and the other hypothesized to be for ACP (Davies et al., 2000; Zhang et al., 2001). The region beside the active site is thought to provide the only access to the active site Cys112 and, therefore, the possible binding site for the malonyl-ACP substrate and the feedback inhibitor palmitoyl-ACP (Heath and Rock, 1996a; Qiu et al., 1999). This region includes mainly α-helices C1 and C2, containing highly conserved arginines 36, 40, 235, 249, 256, 257, Lys214, and His222. Among these residues, the invariant Arg249 has been predicted by computational docking analysis to be in close contact with Glu41 in helix II of ACP, and confirmed to be critical for FabH-ACP interaction by mutagenic and surface plasmon resonance direct binding studies (Zhang et al., 2001). Other predicted hydrophilic contacts include those between Arg6, Glu13, Ser36, Glu47, and Glu49 from ACP, and His222, Lys256, Arg36, Lys214, and Lys257, respectively. Modeled hydrophobic interactions involve the unusually exposed Phe213 of FabH with Met44 of ACP and Ala253 of FabH and Ala45 of ACP. Alkylation of Met44 of ACP is known to diminish FAS activity and change the relative contents of β-hydroxy-fatty acids and saturated fatty acids without affecting the conformation or the thermal stability of ACP (Abita et al., 1971). A proposed three-step ACP-FabH interaction mechanism entails recognition for effective alignment of Ser36 near the active site entrance, conformational changes in ACP for injection of substrate into the active site at the base of a 20-Å-deep tunnel, and finally a reversal of the conformational changes for product release (Zhang et al., 2001).

ii) *FabG*

Like ACP-FabH interaction, mutagenesis and binding assays demonstrate that ACP-FabG interaction requires basic residues close to the active site entrance of *E. coli* FabG, including Arg129 and Arg172 (Zhang et al., 2003b). This interaction causes NMR chemical shift perturbations of residues primarily along helix II of ACP, involving most significantly Asp35, Ser36, Asp38, and a loop II residue Ile54. The involvement of Ile54 suggests that FabG binding may alter the fatty acid binding site in ACP to facilitate the release of the acylated prosthetic group during enzyme catalysis. The ACP docking site is adjacent to the active site of a neighboring monomer in the FabG tetramer, and moves towards the active

site by ~1.3 Å upon binding of cofactor NADPH (Price et al., 2004). Structural analysis also indicates that the loop between β-strand V and α-helix V of FabG becomes ordered upon cofactor binding. The location of the loop between the ACP binding site and the active site suggests that the ordered loop and the conserved Asn145 within the loop may play an important role in orienting the PP moiety of ACP. Divalent cations inhibit FabG activity in vitro and bind to FabG near the active site by interacting directly with Asn145, supporting a role for this region in ACP interaction (Price et al., 2004). Thus, movement of the interface and ordering of the βV-αV loop allow substrate delivery to take place across the subunit interface. Small movements in the quaternary structure across the interface can have a large effect on the active site of this allosteric enzyme (Price et al., 2001b). A further conformational change may occur upon ACP binding, which involves a closing of the helix VI/VII subdomain to create a well-defined entrance tunnel to the active site (Price et al., 2004). Analogous tunnels are also observed in condensing enzymes FabH (Davies et al., 2001) and FabF (Price et al., 2003).

The crystal structure of tetrameric KR of type II PKS from *St. coelicolor*, a close relative of FabG and FabI in the SDR superfamily, reveals that KR-ACP interaction rather than cofactor binding is essential in triggering a conformational change in the closed active site of the enzyme, opening the predominantly hydrophobic substrate binding cavity (Hadfield et al., 2004). An ACP docking model using actinorhodin ACP places the prosthetic group attachment site Ser42 near the active site and positions Glu47 in a positively charged pocket lined by the adenine base of $NADP^+$ and the side chains of Arg38, Arg65, and Arg93 of KR, supporting the primary role of helix II of ACP in interaction with this enzyme (Hadfield et al., 2004).

iii) *FabI*

Direct evidence of involvement of ACP helix II in interaction with a FAS enzyme comes from the structure of dodecenoyl-ACP bound to FabI from *E. coli* (Rafi et al., 2006). Two ACP molecules are observed in the complex with the FabI tetramer. Steric conflicts prohibit further docking of ACP molecules onto the complex, suggesting that the lack of 1:1 stoichiometry is biologically relevant. The complex is mainly stabilized through hydrogen bonding interactions between the ACP helix II and a cluster of basic residues in helix VIII of FabI in proximity to the substrate-binding loop (Stewart et al., 1999). Upon complexation

with ACP, the substrate binding loop undergoes a major conformational change, whereas helix VIII is shifted towards helix II of ACP (Rafi et al., 2006). Specifically, Gln14, Asp35, Asp38, Glu41, and Glu48 from ACP are in contact Lys201, Arg204, and Lys205 from FabI. Because of the absence of the electron density for the prosthetic group, a model has been built using the crystal complex structure and a crotonyl-phosphopantetheine group. The model indicates an additional series of hydrogen bonds between polar residues of FabI and the PP moiety of ACP, including that between the PP phosphate oxygen and the side chain amino group of Lys205, between the PP hydroxyl group and the backbone carbonyl of Lys205, between the PP amide nitrogen and the backbone carbonyl of Asp202, and between the PP amide carbonyl oxygen and the side chain hydrogen of His209 (Rafi et al., 2006).

Structural studies of FabI and its homologue in *M. tuberculosis*, InhA, shed light on the mode of inhibition by some established ER inhibitors. The 2,4-dichlorophenoxy ring of triclosan occupies a pocket of FabI anticipated to accommodate the amide group of the PP arm of ACP (Levy et al., 1999). Hydrophobic groups attached to the sulphonyl moiety of diazaborine inhibitors occupy a similar position (Baldock et al., 1996). Indeed, kinetic characterization suggests that enoyl-ACP competes with triclosan for the binding site on FabI (Ward et al., 1999). Acyl-ACP can also prevent isoniazid-dependent inhibition of InhA, suggesting that isoniazid interacts with the substrate binding region of InhA (Johnson et al., 1995; Rozwarski et al., 1998). However, fatty acyl substrate binding seems to occur in the opposite orientation to that indicated by structural studies using inhibitors (Rafi et al., 2006).

iv) *FabD*

Helix II of ACP appears to play a lesser role in interaction with FabD. Different from the prediction by Rock and coworkers (Zhang et al., 2001), a docking simulation using the structures of FabD from *St. coelicolor* and actinorhodin ACP predicts that the DSL motif of ACP forms the primary contact with a helical flap in the larger of the two subdomains of the FabD monomer instead of with the smaller ferredoxin-like subdomain (Keatinge-Clay et al., 2003). The helical flap of FabD, formed of five α-helices (residues 1-75), resembles the ACP-binding motif in ACPS (N-terminal 64 residues), which is also observed in Sfp (Parris et al., 2000; Reuter et al., 1999). Asp41 from actinorhodin ACP forms a salt bridge with Lys298 from *St. coelicolor* FabD, while Leu43 of ACP is in contact with Phe16 of FabD (Keatinge-Clay et al., 2003).

3. LpxA

LpxA catalyzes the S-O transfer of acyl group from a thioester on ACP to a chemically more stable oxygen ester on glucosamine. However, the LpxA reaction equilibrium unexpectedly favors the substrates rather than the products, possibly because of the hydrophobic stabilization of ACP by the attached acyl substrate (Anderson et al., 1993). Crystallographic and mutagenic studies of *E. coli* LpxA have indicated a number of conserved residues important for its catalysis and substrate binding (Fig. 3B; Raetz and Roderick, 1995). His125 acts as a general base in preparing UDP-GlcNAc for nucleophilic attack (Wyckoff and Raetz, 1999). Gly173 is implicated in acyl chain length determination as a "hydrocarbon ruler" (Wyckoff et al., 1998; Sweet et al., 2002). Lys76, His144, and Arg204 are thought to be critical for ACP binding (Wyckoff and Raetz, 1999; Jain et al., 2004). Similar residues have been identified on LpxA from *H. pylori* (Lee and Suh, 2003).

Three identical active centers and substrate binding sites are formed in the cleft between each two LpxA molecules upon trimerization, with the important residues at each site being contributed by different LpxA subunits (Raetz and Roderick, 1995). Salt-bridges between acidic residues on ACP and basic residues on LpxA are thought to be important for ACP binding to LpxA (Wyckoff and Raetz, 1999). Upon complexation with LpxA, residues 35-41 of *E. coli* ACP, particularly the DSL motif, exhibit the largest chemical shift perturbation, suggesting the involvement of this region in ACP-LpxA interaction (Jain et al., 2004). Residual dipole coupling NMR data has been used to build a model of the ACP-LpxA complex, where Ser36 and helix II of ACP are in the proximity of the active site His125 of LpxA, likely forming salt bridges between Asp35 of ACP and Lys76 of LpxA as well as between Asp38 and Glu41 of ACP and Arg204 of LpxA. There is a hydrophobic groove on LpxA between Phe162 and Gly173 that can accommodate the acyl chain during transfer. Leu37 of ACP is positioned to potentially stabilize the interaction of the acyl chain with LpxA (Jain et al., 2004).

D. Significance and Objectives

Insight into CP-enzyme interactions has a great potential for human health and biotechnology. ACP-dependent enzymes like FabI are proven antimicrobial drug targets. Production of desirable fatty acids in plant seeds can be achieved by engineering FAS component enzymes or acyltransferases. PKS and NRPS can be manipulated to synthesize

novel polyketides and nonribosomal peptides (e.g. by domain swapping), promoting the chemical diversity of a growing repertoire of therapeutically valuable secondary metabolites.

The structures and reaction mechanisms of a number of ACP-dependent enzymes have been well-characterized, including FAS, ACPS, and LpxA. Over a dozen X-ray crystal and NMR solution structures of CPs from various organisms and pathways have also been determined. However, we are only beginning to understand the interactions between ACP and its binding partners and the roles of specific residues and regions of ACP in these interactions. Because of its highly dynamic and flexible nature, stability and conformational reorganization of ACP may also be important in the interactions. Thus, *V. harveyi* rACP was used in this work as the template for site-directed mutagenesis to investigate:

i) the role of acidic residues in and around helix II in ACP structure and function;

ii) the effects of divalent cation binding and acylation on ACP conformation;

iii) the effect of LpxA-binding on ACP folding.

Chapter II. Materials and Methods

A. Materials

1. General Chemicals

Acetyl-CoA	Sigma-Aldrich
30% Acrylamide/Bis Solution 37.5:1	Bio-Rad
40% Acrylamide/Bis Solution 29:1	Bio-Rad
ATP	Sigma-Aldrich
BD TALON Metal Affinity Resins	BD Biosciences
Centricon YM-3 concentrators	Millipore
CM-Sepharose CL-6B	GE Healthcare
Coenzyme A	Sigma-Aldrich
DEAE-Sepharose FF	GE Healthcare
Factor Xa restriction protease	GE Healthcare
GelCode Blue Stain	Pierce Biotechnology
GeneEditor Mutagenesis System	Promega
GenElute Plasmid Miniprep Kit	Sigma-Aldrich
Glutathione, reduced	Sigma-Aldrich
Glutathione-Sepharose 4B	GE Healthcare
Hexanoic acid	VWR International
DL-β-hydroxymyristic acid	Sigma-Aldrich
IPTG	Sigma-Aldrich
Lauric acid	Sigma-Aldrich
Low melting point agarose	Invitrogen
Malonyl-CoA	Sigma-Aldrich
Micro BCA Protein Assay	Pierce Biotechnology
MILLEX-GP filter units	Millipore
Myristic acid	Doosan Serdary Research Labs

NADPH	Sigma-Aldrich
NADH	Sigma-Aldrich
Palmitic acid	Fisher Scientific
pGEX-5X-3 vector	GE Healthcare
13 mm PVDF Syringe Filters 0.45 μm	National Scientific Company
QIAfilter Plasmid Midiprep Kit	Qiagen
QIAprep Spin Miniprep Kit	Qiagen
QIAquick Gel Extraction Kit	Qiagen
Restriction enzymes and buffers	New England Biolabs
Sephacryl S-300	GE Healthcare
SOURCE 15Q	GE Healthcare
Superdex 200	GE Healthcare
Surfact-Amps Triton X-100	Pierce Biotechnology
T4 DNA ligase and buffer	New England Biolabs
T7 Sequencing Kit	GE Healthcare
Uniplate Silica Gel G 250 micron TLC plates	Analtech
Vivapure Q Mini M Spin Columns	Vivascience Sartorius Group
Zeba Desalt Spin Columns	Pierce Biotechnology

All other general chemicals were of highest quality available, and were obtained from Boehringer Ingelheim, BC Biosciences, Bio-Rad, Fisher Scientific, Invitrogen, J. T. Baker, Sigma-Aldrich, and VWR International.

2. Bacterial Strains

E. coli BL21	Stratagene
E. coli BMH 71-18 *mutS*	Promega
E. coli DH5α	Invitrogen
E. coli JM109	Promega
V. harveyi MAV	Dr. David Byers, Dalhousie University
V. harveyi M17	Dr. David Byers, Dalhousie University

3. Radioisotopes

[^{3}H]Acetyl-CoA (4.1 Ci/mmol)	GE Healthcare
[α-^{35}S]dATP (1250 Ci/mmol)	NEN/Perkin Elmer
[2-^{14}C]Malonyl-CoA (51 mCi/mmol)	NEN/Perkin Elmer
[9,10-^{3}H]Myristic acid (49 Ci/mmol)	NEN/Perkin Elmer
[^{3}H]Uridine diphosphate N-acetyl-D-glucosamine (39.7 Ci/mmol)	NEN/Perkin Elmer

4. Solutions

Acetyl-CoA	1 mM acetyl-CoA in 10 mM Na^+-acetate, pH 5.0, stored at −20 °C
Buffer BA	10 mM Na^+-MES, pH 6.0
Buffer BB	10 mM Na^+-MES, pH 6.0, 1 M NaCl
Buffer H	50 mM Tris base, 10 mM $MgCl_2$, 2 mM DTT, 4% glycerol, pH adjusted to 8.1 using 1 M MES
Buffer HA	50 mM Na^+-MES, pH 6.5, 10 mM $MgCl_2$, 2 mM DTT, 4% glycerol
Buffer HB	50 mM Na^+-MES, pH 6.5, 10 mM $MgCl_2$, 2 mM DTT, 4% glycerol, 1 M NaCl
Buffer NA	10 mM Na^+-MES, pH 6.0, 10 mM DTT, 1 mM EDTA
Buffer NB	10 mM Na^+-MES, pH 6.0, 10 mM DTT, 1 mM EDTA, 1 M NaCl
Buffer RA	10 mM Na^+-MES, pH 6.0, 2 mM DTT
Buffer RB	10 mM Na^+-MES, pH 6.0, 2 mM DTT, 1 M NaCl
DNA loading buffer (6X)	2.5 mM EDTA, 60% glycerol, 0.25% bromophenol blue in H_2O
Dulbecco's PBS	0.2 g KCl, 0.2 g KH_2PO_4, 0.1 g $MgCl_2 \cdot 6H_2O$, 8.0 g NaCl, 1.14 g Na_2HPO_4 in H_2O to 1 L, pH 7.0
Fatty acid solutions	10 mM or 100 mM in ethanol, stored at −20 °C
High pH regeneration buffer	0.1 M Tris-HCl, pH 8.5, 0.5 M NaCl
Low pH regeneration buffer	0.1 M Na^+-acetate, pH 4.5, 0.5 M NaCl

Malonyl-CoA	1 mM malonyl-CoA in 10 mM Na^+-acetate, pH 5.0, stored at –20 °C
Na^+/K^+-phosphate buffer	68% 1 M K_2HPO_4, 32% 1 M NaH_2PO_4, pH 7.0
Native PAGE running buffer (10X)	30.3 g Tris base, 144 g glycine in H_2O to 1 L , pH 8.3
Native PAGE sample buffer (4X)	0.25 M Tris-HCl, pH 6.8, 25% glycerol, 0.25% bromophenol blue in H_2O
SDS-PAGE running buffer (10X)	30 g Tris base, 144 g glycine, 10 g SDS in H_2O to 1 L, pH 8.3
SDS-PAGE sample buffer (4X)	125 mM Tris base, 5% SDS, 25% glycerol, 0.25% bromophenol blue in H_2O
TAE (50X)	242 g Tris base, 57.1 mL glacial acetic acid, 50 mM EDTA in H_2O to 1 L
TBE (5X)	54 g Tris base, 27.5 g boric acid, 10 mM EDTA in H_2O to 1 L
TCM	10 mM HEPES, pH 7.7, 50 mM $CaCl_2$, 10% glycerol, filter sterilized, stored at –20 °C
TE buffer	10 mM Tris-HCl, pH 8.0, 1 mM EDTA

5. Bacterial Growth Media

1% Complex medium	10 g NaCl, 3.7 g Na_2HPO_4, 0.5 g $(NH_4)H_2PO_4$, 1 g KH_2PO_4, 0.2 g $MgSO_4 \cdot 7H_2O$, 5 g tryptone peptone, 0.5 g yeast extract, 2 mL glycerol in H_2O to 1 L
LB plus ampicillin plate	15 g Bacto agar per litre of LB medium, ampicillin added to 50 μg/mL at 50-60 °C
Miller's LB medium	10 g NaCl, 10 g tryptone peptone, 5 g yeast extract in 1 L H_2O
SOC medium	0.5 g NaCl, 20 g tryptone peptone, 5 g yeast extract, 950 mL H_2O, 10 mL of 250 mM KCl, pH adjusted to 7.5 with NaOH, autoclaved before adding 20 mL of filter sterilized 1 M glucose and 5 mL of filter sterilized 2 M $MgCl_2$

B. Molecular Biology

1. Site-Directed Mutagenesis

The basis for all mutagenesis was the *V. harveyi acpP* open reading frame ligated into pGEX-5X-3 vector for expression of ACP N-terminally fused to GST (Flaman et al., 2001). Mutations were introduced into the coding region of ACP using the GeneEditor in vitro Mutagenesis System. Custom-made mutagenic oligonucleotides purchased from Sigma Genosys or Cortec were designed to provide at least eight bases between either end and the closest mismatch. All primers contained C or G at the 3' end, were 5' phosphorylated, desalted, resuspended in TE buffer to 40-50 μM, and stored at −20 °C (Table 1). Plasmid DNA was extracted from *E. coli* BMH 71-18 *mutS* and JM109 cells using GenElute Plasmid Miniprep Kit or QIAprep Spin Miniprep Kit as indicated by the manufacturers, except that DNA was eluted with TE buffer and stored at −20 °C. Mutations were confirmed by manual DNA sequencing, or by restriction enzyme digestion followed by automated DNA sequencing at Cortec. Plasmids encoding mutant GST-ACP were maintained in *E. coli* DH5α or JM109 strains and expressed in *E. coli* BL21. Glycerol stocks of *E. coli* cells were prepared after incubating cells in 5 mL of LB containing 50 μg/mL ampicillin at 37 °C for 16 h with vigorous aeration (250 rpm). An equal volume of overnight culture was mixed gently in a sterile microfuge tube with 40% glycerol in LB and incubated at room temperature for 5 min. The mixture was quickly frozen in liquid nitrogen before storage at −80 °C.

2. DNA Sequencing

The ACP coding region of mutants was sequenced using T7 Sequencing Kit. Double stranded plasmid DNA template was denatured by mixing 1-2 μg of DNA with 400 mM NaOH in sterile distilled water and incubating at room temperature for 10 min. Denatured DNA was precipitated by adding 7 μL of 3 M Na^+-acetate, pH 4.8, 4 μL of H_2O, and 120 μL of 100% ethanol, and incubation at −80 °C for 5 min followed by centrifugation at 21,000 × g for 15 min at 4 °C. The pellet was washed with 250 μL of cold 70% ethanol followed by centrifugation at 21,000 × g for 10 min at 4 °C. The pellet was dried under

Table 1. Oligonucleotides used in site-directed mutagenesis and sequencing.

Name	Primer sequence
E41D	CACTGTAGA**C**CTAGTAATG
E41K	GACACTGTA**A**AGCTAGTAATG
A45C	AGCTAGTAATG**TG**TCTAGAAGAG
A45G	CTAGTAATGG**G**TCTAGAAGAGG
A45W	GCTAGTAATG**TGG**CTAGAAGAGG
SA	AACGAAGC**C**TCTTTCGTT**A**ACGATCTAGGTGCT**A**ATTCTCTA**A**ACACTGTAG
SB	TGGCTCTA**C**AAGAGGA**G**TTC**A**ACACT**C**AGATTCCT**A**ATGAAGAAG
D30N	AACGAAGC**C**TCTTTCGTT**A**ACGATCTAG
D35N	AACGAAGC**G**TCTTTCGTTGACGATCTAGGTGCT**A**ATTCTCTAG
D38N	AACGAAGC**A**TCTTTCGTTGACTATCTAGGTGCTGATTCTCTA**A**ACACTGTAG
E47Q	TGGCTCTA**C**AAGAGGA**G**TTCGACACTG
E53Q	AGAGGAATT**T**GACACT**C**AGATTCCTG
D56N	AGAGGAATT**T**GACACTGAGATTCCT**A**ATGAAGAAG
E25W	GCTAGGTGTAGACGAAGCAGAAGTTAAAAAC**TGG**GCTTCTTTCGTTGAC
L46W	GTAATGGCT**TGG**GAAGAGGA**G**TTCGACACTG
F50W	GCTCTAGAAGAGGAAT**GG**GACACTGAGATTC
V72W	GCTGCAATCGACTAC**TGG**AACAGCGCTCAG
5pGEX	GGGCTGGCAAGCCACGTTTGGTG

Replaced nucleotides are in bold. Altered restriction sites are underlined.

vacuum, dissolved in 10 μL of H_2O, and stored at -20 °C or used immediately. Forward sequencing primer 5pGEX was diluted in H_2O to 5 μM, which binds near the 3' end of the N-terminal GST. The denatured DNA template was mixed with 2 μL of diluted 5pGEX and 2 μL of annealing buffer. The annealing mixture was incubated at 65 °C for 5 min, 37 °C for 10 min, and then room temperature for at least 5 min. Before the polymerization reaction was started, T7 DNA polymerase was diluted five fold in Dilution Buffer. Microfuge tubes containing 2.5 μL each of A, C, G, and T Mix-Short were incubated at 37 °C. The reaction mixture contained 14 μL of the annealing mixture, 2 μL of Labeling Mix dATP, 1 μL of 0.01 mM [α-^{35}S]dATP (12 mCi/mL), and 2 μL of diluted T7 DNA polymerase, and was incubated at 37 °C for 8 min. One quarter (4.5 μL) of the reaction mixture was added to each of four pre-warmed tubes containing Mix-Short and was incubated at 37 °C for another 8 min before the addition of 5 μL of Stop Solution and removal of tubes to room temperature. A polyacrylamide sequencing gel (17.5 mL of 40% Acrylamide/Bis Solution 29:1, 44 mL of 46% w/v urea, 18 mL of 5X TBE, 8.5 mL H_2O, 100 μL of 10% ammonium persulfate, and 40 μL of TEMED, polymerized overnight) was pre-electrophoresed in 0.5X TBE at 60 W for 1 h. Each sample was mixed with 2 μL of 6X DNA loading solution and heated at 75-80 °C for 5 min; 3 μL of this sample was resolved in the pre-warmed 8% sequencing gel in 0.5X TBE at 60 W for 3 h. After the gel was dried under vacuum with heat for 1 h, Kodak film was exposed to the gel for at least 24 h at -80 °C and developed. In later experiments, plasmids were sent to Cortec for automated DNA sequencing.

3. Restriction Digestion and Agarose Gel Analysis

In order to quickly determine whether mutagenesis was successful, a unique restriction site for either HindIII (site A) or EcoRI (site B) was altered in mutagenic oligonucleotides. Restriction digestion was conducted for initial screening of mutants, where the EcoRI or HindIII site was blocked as a result of mutagenesis. The reaction mixture contained 0.5-3 μg of plasmid DNA, 20 U of restriction endonuclease, 2 μL of 10X restriction enzyme buffer, 2 μL of 10X BSA, and sterile distilled water in a total volume of 20 μL and was incubated at 37 °C for 2 h. HindIII and NEBuffer 2 were used for screening mutations of SA, D30N, D35N, D38N, and E25W. EcoRI and EcoRI Buffer were used for

screening DNA from mutagenic reactions of SB, E47Q, D51N, E53Q, D56N, L46W, and F50W. The reaction was stopped by mixing gently and storing at –20 °C. After adding 5 μL of 6X DNA sample loading buffer to each sample, DNA fragments were resolved in a 1% agarose gel (1% w/v agarose, 0.5 μg/mL ethidium bromide, 0.5X TBE) in 5X TBE at 80 V for 2 h. The gel was photographed on a UV illuminator using a Polaroid camera.

4. Preparation of SA/SB Double Site Mutant

Difficulty was experienced during attempts to construct SA/SB using mutagenic primers for SA and SB, presumably due to the fact that there is an unpaired stretch of only 10 bases on the template DNA between the two primers. Thus, a different strategy was employed, in which a DNA fragment encoding SA was obtained by double restriction enzyme digestion and used to replace the counterpart in a wild type plasmid. The resulting plasmid underwent a second round of mutagenesis using GeneEditor Mutagenesis System and mutagenic primer for SB.

Specifically, plasmids encoding wild type GST-ACP and SA were extracted from 100 mL each of overnight culture using QIAfilter Plasmid Midiprep Kit. Double restriction digestion mixture contained 3 μg of wild type GST-ACP DNA or 10 μg of SA DNA, 100 U of BamHI, 100 U of PstI, 2 μL of BamHI buffer, and 2 μL of 10X BSA in a total volume of 20 μL, and was incubated at 37 °C overnight. In-gel ligation was performed after resolving the reaction mixture in a 1% low melting point agarose gel (1% low melting point agarose, 0.5 μg/mL ethidium bromide, 0.5X TBE) at 80 V for 6 h. Gel slices corresponding to the 4 kb band of GST-ACP and the 1.2 kb band of SA were incubated at 65 °C for 2 min or until melted. Ligation mix consisting of 2 μL of T4 DNA ligase, 4 μL of 5X ligase buffer, and 4 μL of H_2O was pre-warmed at 37 °C before addition of 2 μL of melted gel containing fragment from GST-ACP and 8 μL of melted gel containing fragment from SA, followed by incubation at 16 °C overnight. T4 DNA ligase was inactivated at 65 °C for 10 min, and added to 180 μL of TCM on ice; 100 μL of this was added to 200 μL of thawed *E. coli* JM109 competent cells. Tubes containing the cells were kept on ice for 30 min, heat shocked in a 42-°C water bath for 90 s, and incubated on ice for 2 min. After addition of 900 μL of SOC medium, chemically transformed cells were incubated at 37 °C for 1 h with moderate

aeration (180 rpm). Cells were pelleted with centrifugation at 1,000 × g for 5 min at 4 °C, resuspended in 50-100 μL of fresh SOC medium, and spread on LB plus ampicillin plates. Plates were kept at room temperature for 15-30 min prior to incubation at 37 °C. Clones were tested for positive mutation by restriction digestion.

C. Preparation of ACP and Derivatives

1. Purification of Native *V. harveyi* ACP

V. harveyi wild type MAV or dark mutant M17 (Byers, 1988) was grown in 1 L of 1% complex medium at 25 °C in a rotary shaker (200 rpm) to an A_{660} of approximately 2. Cells were harvested by centrifugation at 9,000 × g for 20 min at 4 °C and stored at −20 °C or used immediately. Cell pellets were lysed by sonication in 15 mL of Buffer NA, and the cell free supernatant was retained after centrifugation at 27,000 × g for 30 min at 4 °C. An equal volume (approximately 15 mL) of isopropanol was added dropwise to the cell free supernatant with constant stirring and incubated at 4 °C for 30 min. The supernatant was collected after centrifugation at 27,000 × g for 30 min and kept at 4 °C overnight. After removal of newly formed precipitate by centrifugation at 27,000 × g for 30 min at 4 °C, the supernatant was syringe filtered through a MILLEX-GP 0.22 μm filter unit that had been prewashed using 30 mL of 50% isopropanol. The sample was applied to a SOURCE 15Q anion exchange column (13 × 70 mm) after equilibration of the column with 30 mL of Buffer NA on a Waters 650 Advanced Protein Purification System. Native ACP was purified to homogeneity using a linear gradient of 30 mL from Buffer NA to NB at a flow rate of 1 mL/min. Elution of ACP was monitored by A_{280} and confirmed using AAS assay and 20% SDS-PAGE. No more than three fractions with highest ACP level were pooled and syringe filtered through a MILLEX-GP 0.22 μm filter unit that had been prewashed with 5 mL of Buffer NA. Sample was applied to a 55-mL Superdex 200 gel filtration column on the Waters system that had been equilibrated with 120 mL of Buffer NA. ACP was eluted isocratically with Buffer NA. Based on AAS assay and SDS-PAGE, five to six 1-mL fractions containing ACP were pooled and applied to SOURCE 15Q column again using abovementioned buffers and gradient. Two to three 1-mL fractions containing ACP were

pooled, mixed with 1.6 μL of glacial acetic acid per mL of pooled sample to obtain an isoelectric pH of 4, and kept at 4 °C overnight. ACP was precipitated by centrifugation at 12,000 × g for 10 min at 4 °C and dissolved in 1 mL of 100 mM MES, pH 6.0, containing 10 mM DTT.

2. Purification of Recombinant Holo-ACP

Overnight cultures were prepared from *E. coli* BL21 cells transformed with wild type or mutant pGEX-ACP plasmids, and 20 mL was diluted into 2 L of fresh LB medium containing 50 μg/mL ampicillin and incubated at 37 °C for 3 h with vigorous aeration (250 rpm) or until A_{660} was between 0.6 and 0.8. GST-fused ACPs were produced by induction of mid-log phase cells with 0.25 mM IPTG for 3 h at 30 °C or overnight at 25 °C. Cells were harvested by centrifugation at 8,000 × g for 10 min at 4 °C. Pellets from each 2-L culture were resuspended in 16 mL of Dulbecco's PBS. Cell lysate after sonication (12 bursts of 30 s) was mixed gently with 2 mL of 10% Surfact-Amps Triton X-100 and incubated on ice for 30 min before centrifugation at 20,000 × g for 20 min at 4 °C. The supernatant was stored at −20 °C or used immediately for ACPS treatment and glutathione-Sepharose binding.

Before use, 5 mL (packed volume) of glutathione-Sepharose 4B was washed in a 2.5-cm diameter Econo column sequentially with 25 mL of Dulbecco's PBS, 10 mL of 5 M guanidine-HCl, and four times with 10 mL of Dulbecco's PBS. Drained resin was mixed end over end directly in the sealed column for 30 min at room temperature with 19-20 mL of the above supernatant, 250 μL of 100 mM CoA, 140 μL of 2 M $MgCl_2$, 140 μL of 1 M DTT, and 800 μL of ACPS cell extract (see section D2), which was sufficient to quantitatively convert apo- to holo- forms for most wild type and mutant rACPs. Overnight incubation with 2 mL of ACPS cell extract was required for SA but was still not enough for complete conversion of SA/SB to the holo form. After the ACPS reaction, the resin was drained and washed six times with 5 mL of Dulbecco's PBS. GST-ACP was eluted with 20 mL of freshly prepared 10 mM reduced glutathione in 50 mM Tris-HCl, pH 8.0; 2 mL fractions were collected. The resin was regenerated by washing sequentially with three cycles of high and low pH regeneration buffers (12 mL each time), followed by 10 mL of 75% ethanol, and 25 mL of Dulbecco's PBS, and stored in Dulbecco's PBS containing 20% ethanol at 4 °C.

Based on the A_{280} profile, five fractions containing the highest protein concentration were combined and mixed with 0.2 mL of 5 M NaCl, 5 µL of 2 M $CaCl_2$, and up to 80 U of Factor Xa protease (10 U for every mg of fusion protein) at 4 °C for not longer than 48 h. Factor Xa cleavage of the GST-ACP product yields a recombinant *V. harveyi* ACP (rACP) with an N-terminal extension of four amino acids (GIPL); this was confirmed by MALDI-TOF mass spectrometry (University of Victoria Proteomics Facility). The sample was heated in DuPont Corex tubes at 75 °C for 3 min or until the appearance of a white precipitate and cooled on ice prior to centrifugation at 21,000 × g for 10 min at 4 °C to remove precipitated GST, uncleaved GST-ACP, and Factor Xa. The supernatant was dialyzed against Buffer RA using Spectra/Por 3,500 Da molecular weight cutoff molecularporous membrane tubing (Spectrum Laboratories), filtered through a 0.45 µm 13 mm PVDF Syringe Filter, and was applied to a SOURCE 15Q anion exchange column (13 × 70 mm) after equilibration of the column with Buffer RA on an AktaFPLC. After unbound molecules were washed from the column with 10 mL of Buffer RA, holo-rACP was purified to homogeneity using a linear gradient of 60 mL from Buffer RA to RB at a flow rate of 1 mL/min. Elution of ACP was monitored by A_{280} and confirmed using AAS assay and 20% SDS-PAGE. Fractions containing the highest ACP concentration were combined and dialyzed against 10 mM Na^+-phosphate, pH 7.0, 0.1 mM EDTA before Micro BCA protein assay and storage at −20 °C.

3. Purification of Apo-ACP

GST-ACP was produced by induction of 2 L of mid-log phase cells with 0.25 mM IPTG at 25 °C overnight. Purification was similar to that of holo-ACP except that the cell free supernatant was not treated with *E. coli* ACPS cell extract. Apo-ACP typically eluted before holo-ACP and could be separated from the latter on an anion exchange chromatographic gradient because apo-ACP is less negatively charged than its holo counterpart.

4. Preparation and Purification of Acyl-ACP

To prepare β-hydroxymyristoyl-ACP substrates for LpxA assay, the reaction mixture contained 56 µM holo-ACP, 40 µg of partially purified AAS (0.16 U), 80 µM β-hydroxymyristic acid, 10 mM $MgSO_4$, 10 mM ATP, 5 mM DTT, 0.1 M Tris-HCl, pH 7.8 in a

total volume of 400 μL and was incubated at 37 °C for 3 h or room temperature overnight. β-Hydroxymyristoyl-ACP was further purified by Vivapure Q Mini M Spin Column equilibrated in 25 mM Tris-HCl, pH 7.8. Following elution with 0.2 M NaCl, ACP was eluted with 400 μL of 0.5 M NaCl and quantified using Micro BCA protein assay.

For tryptophan mutants, β-hydroxymyristoyl-ACP was prepared in a reaction containing 56 μM holo-ACP, 250 μg of partially purified AAS (1 U), 150 μM β-hydroxymyristic acid, 10 mM $MgSO_4$, 10 mM ATP, 5 mM DTT, 0.1 M Tris-HCl, pH 7.8 in a total volume of 2 mL and incubated at room temperature overnight prior to application to a SOURCE 15Q column. ACP was eluted in a linear gradient of 50 mL from Buffer BA to BB at a flow rate of 1 mL/min and confirmed by 20% native PAGE. DTT was not included in column buffers in order to minimize hydrolysis of acyl-ACP to form holo-ACP.

For biophysical conformational analyses, acyl-ACPs of various fatty acyl chain lengths were prepared in a total volume of 40 μL containing 56 μM holo-ACP, partially purified AAS (10 μg or 0.04 U for 6:0, 8:0, 10:0, and 12:0; 20 μg or 0.08 U for 14:0 and 16:0), 80 μM fatty acids, 10 mM $MgSO_4$, 10 mM ATP, and 1 mM DTT in 0.1 M Tris-HCl, pH 7.8. The reaction mixture was incubated at 37 °C for 4 h followed by heating at 75 °C for 5 min and centrifugation at 21,000 × g for 5 min to remove proteins from the AAS preparation. The supernatant was applied to a Zeba Desalt Spin Column equilibrated with H_2O, and desalted by centrifugation.

D. Enzyme Preparation and Assays

1. *V. harveyi* Fatty Acid Synthase

Partial purification and assay of *V. harveyi* FAS are essentially as described (Gong and Byers, 2003). Wild type *V. harveyi* MAV was grown overnight in 2 mL of 1% complex medium, which was diluted into 50 mL of fresh 1% complex medium and incubated at 25 °C for 5 h (250 rpm) or until the cells started to glow in the dark. Cells were harvested by centrifugation at 8,000 × g for 20 min at 4 °C and sonicated in 2.5 mL of 50 mM Na^+/K^+-phosphate buffer containing 5 mM DTT. After centrifugation to prepare cell free extract (CFE), FAS was separated from endogenous ACP by ammonium sulfate fractionation

between 40% and 75% saturation. The CFE or FAS fraction (FASF) was used immediately or stored at −20 °C for up to two weeks. Assay for FAS activity was performed at 37 °C or 25 °C for 1 h in a final volume of 40 μL containing 10 μM holo-ACP, 30 μg of total CFE or FASF protein, 23 μM [2-^{14}C]malonyl-CoA (48 dpm/pmol), 10 μM acetyl-CoA, 0.5 mM NADPH, 0.5 mM NADH, and 5 mM DTT in 10 mM Na^+/K^+-phosphate buffer, pH 7.0. The reaction was stopped with 40 μL of 1 M KOH and incubated at 60 °C for 1 h. After acidification with 40 μL of 2 M HCl, fatty acids were extracted into 1 mL of hexane and quantified by liquid scintillation counting (Beckman LS6500 Multi-purpose Scintillation Counter). Results were corrected for background values in the absence of ACP (0.01 pmol/min/μg). *E. coli* CFE and FASF were prepared in the same way as those of *V. harveyi*, and used for comparison.

2. *E. coli* Holo-ACP Synthase

Preparation and assay of *E. coli* ACPS were essentially as described (Lambalot and Walsh, 1997). ACPS was overexpressed from *E. coli* strain BL21 (DE3) pDPJ (Lambalot and Walsh, 1995) by induction of mid-log cells with 1 mM IPTG at 30 °C for 3 h. Each gram of harvested cells was resuspended in 3 mL of cold Buffer H, sonicated, and centrifuged at 24,000 × g for 30 min at 4 °C. The supernatant was stored at −20 °C for ACPS treatment during rACP purification or subjected to further purification as described below.

The ACPS cell extract was mixed for 15 min at 4 °C with 1 mL (packed volume) of DEAE-Sepharose FF that had been equilibrated with Buffer H. Following centrifugation at 5,000 × g for 15 min at 4 °C, the above step was repeated with the supernatant and 1 mL of fresh DEAE-Sepharose FF. The pH of the supernatant was then adjusted to 6.5 with 1 M MES prior to centrifugation at 14,000 × g for 15 min at 4 °C. The supernatant was syringe filtered and applied to a CM-Sepharose CL-6B column (1 × 10 cm) equilibrated with Buffer HA on the Waters system. ACPS was purified using a 30 mL linear gradient from Buffer HA to HB.

The ACPS assay was performed at 25 or 37 °C for up to 10 min in a final volume of 10 μL containing 50 μM apo-ACP, ACPS (0.06 μg of total protein in ACPS cell extract or 0.03 μg of purified ACPS), 50 μM [^{3}H]acetyl-CoA (63 dpm/pmol), 10 mM $MgCl_2$, and 5

mM DTT in 50 mM Tris-HCl, pH 7.0. At different time points the reaction was quenched by adding 4.5 μL of the mixture to 800 μL of cold 10% w/v trichloracetic acid containing 20 μL of 25 mg/mL BSA. Following incubation on ice for 15 min, the precipitate was obtained by centrifugation at 12,000 × g for 5 min, washed twice with 800 μL of cold 10% w/v trichloracetic acid, solubilized in 50 μL of formic acid, and quantified by liquid scintillation analysis.

3. *V. harveyi* Acyl-ACP Synthetase

AAS was partially purified by DEAE-Sepharose and Sephacryl S-300 chromatography (Fice et al., 1993). To determine AAS activity with mutant ACPs, the reaction mixture contained (in a total volume of 15 μL) 50 μM holo-ACP, 0.5 μg of partially purified AAS [0.002 U, one unit defined as 1 nmol of acyl-ACP formed per min using standard assay condition (Fice et al., 1993)], 0.1 mM [9,10-^{3}H]myristic acid (888 dpm/pmol), 10 mM $MgSO_4$, 10 mM ATP, 5 mM DTT, 1% glycerol, and 100 mM Tris-HCl, pH 7.8, 10 μL of which was spotted on a Whatman 3MM Chr cellulose filter disc (0.8 × 2 cm) after incubation at 37 °C or 25 °C for 10 min. The filter discs were washed three times with methanol/chloroform/acetic acid (6:3:1) and air-dried for liquid scintillation counting. Results were corrected for background values (~0.4 pmol/min/μg).

4. *E. coli* LpxA

Purified *E. coli* LpxA expressed as an N-terminal His_6-tagged protein was obtained from Dr. Christopher R. McMaster (Atlantic Research Centre, Dalhousie University). The assay was performed as described (Sweet et al., 2001). The LpxA reaction was conducted at room temperature in a total volume of 10 μL containing 10 μM β-hydroxymyristoyl-ACP, 0.4 μg of purified recombinant His_6-LpxA (1.2 μM), 2.5 μM [^{3}H]UDP-GlcNAc (10 000 dpm/pmol), and 10 mg/mL BSA in 40 mM Na^+-HEPES, pH 8.0. After 2, 5, and 10 min, during which product formation was linear with time, 2 μL of each reaction mixture was spotted on a silica gel G plate, which was developed in a mobile phase of chloroform/methanol/acetic acid/water (25:25:2:4). The TLC plate was air-dried for 3 h, scanned on a Bioscan System 200 Imaging Scanner, and quantified using WinScan software. The acylated product has an Rf value of approximately 0.6, whereas the unacylated substrate

UDP-GlcNAc remains at the origin. The LpxA reaction rate reaction was calculated from the percentage of product formed in each sample.

E. Biophysical Analyses

1. Native PAGE

Conformationally sensitive native gel electrophoresis at pH 9.2 is a method sensitive to the conformational stability of various forms of ACP (Rock et al., 1981), where both intrinsic charge and hydrodynamic properties play a role in determining the mobility of a protein. Apo-, holo-, and acyl-ACP samples were mixed with 0.33 volumes of 4X native PAGE sample buffer and resolved on a 20% polyacrylamide mini-gel (2.5 mL 40% Acrylamide/Bis Solution 29:1, 1.25 mL 1.5 M Tris-HCl, pH 9.2, 1.25 mL H_2O, 25 μL 10% ammonium persulfate, 2.5 μL TEMED) under 150 V at 37 °C or room temperature.

Native PAGE at neutral pH was performed under 150 V at 4 °C on a 20% polyacrylamide gel (using 40% Acrylamide/Bis Solution 29:1) in a continuous buffer system of 43 mM imidazole and 35 mM HEPES at pH 7.4 after pre-electrophoresing the gel for 2 h (McLellan, 1982). Protein bands were visualized by staining with GelCode Blue Stain. Gels were soaked in a solution containing 20% ethanol and 10% glycerol for 20 min before drying between two sheets of Ultraclear roll cellophane on Tut's tomb (Idea Scientific) to minimize formation of fissures.

2. Circular Dichroism

Spectra from a Jasco J-810 spectropolarimeter were recorded at 25 °C using a 0.1 cm water-jacketed cell. ACP was diluted to 30 μg/mL (3 μM) in 10 mM Na^+-phosphate, pH 7.0 containing 0.1 mM EDTA, and spectra were measured from 260 to 190 nm in continuous mode at a scanning speed of 20 nm/min directly or within 1 min after addition of $MgCl_2$, $MgSO_4$, $CaCl_2$, or $MnCl_2$. The CD signals were normalized to obtain the mean residue molecular ellipticity ($[\theta]$, $kdeg \cdot cm^2 \cdot decimol^{-1}$) using the following formula:

$$[\theta] = \frac{(10^{-7})\ (\theta)\ (M)}{(c)\ (n)\ (l)} \qquad (1)$$

where θ is CD signal in mdeg; M is the molecular weight of the rACP polypeptide; n is the

number of residues of rACP; c is protein concentration in g/mL; l is the pathlength of the cuvette in cm.

3. Steady-State Fluorescence Spectroscopy

i) *Emission Spectra*

All fluorescence measurements were carried out on a Perkin Elmer LS50B Luminescence Spectrometer in a Perkin Elmer 10 mm quartz cell at 25 °C. Slit widths of 5 and 10 nm were routinely used on the excitation and emission monochromators, respectively. The samples containing 1-10 μM ACPs in 10 mM Na^+-phosphate and 0.1 mM EDTA, pH 7.0, were excited at 280 nm and the emission spectra were recorded from 300 to 450 nm at 150 nm/min directly or immediately following addition of $MgCl_2$ or $MgSO_4$. Alternatively, samples were excited at 296 nm to selectively excite Trp and emission spectra were recorded from 310 to 450 nm with or without $MgCl_2$ or purified His_6-LpxA. These wavelength ranges were chosen to exclude the area of Rayleigh scatter that occurs at the excitation wavelength. The Raman band from the solvent was corrected by subtracting buffer fluorescence background from each spectrum.

ii) *Solute Perturbation*

Holo-ACPs (1 μM) in 10 mM Na^+-phosphate and 10 mM $MgCl_2$, pH 7.0, were titrated with 4 M stock solutions of soluble fluorescence quenchers acrylamide, KI, and CsCl. Excitation was at 280 nm and emission was measured from 300 to 450 nm after each addition. Fluorescence intensities and quencher concentrations were corrected for dilution. The stock solution of KI contained 1 mM $Na_2S_2O_3$ to prevent formation of I_3^-, which absorbs strongly at 280 nm. The dynamic and static quenching constants were obtained by fitting the data to the Stern-Volmer equation including an exponential term to account for static quenching (Eftink and Ghiron, 1976):

$$F_0 / F = (1 + K_{SV}[Q])\, e^{V[Q]} \qquad (2)$$

where F_0 and F are the fluorescence intensities at an appropriate emission wavelength in the absence and presence of quencher (Q), K_{SV} is the Stern-Volmer collisional quenching constant, and V is the static quenching constant that can be considered as a volume element surrounding the fluorophore. The fluorescence quenching of proteins can also be described

by a modification of the classical Stern-Volmer equation (Eq. 2), in which it is assumed that energy transfer between accessible and inaccessible fluorophores is negligible and that all fluorophores have identical absorptivities (Lehrer, 1971):

$$F_0 / (F_0 - F) = 1 / (f_a K_{SV} [Q]) + 1 / f_a \quad (3)$$

where f_a is the effective fractional maximum accessible protein fluorescence.

iii) *Determination of Dissociation Constant*

His_6-tagged *E. coli* LpxA was affinity-purified and dialyzed against 10 mM Na^+-phosphate, pH 7, to remove imidazole that has been reported to quench indole fluorescence (Eftink, 1997). LpxA (2.2 μM) was titrated with aliquots of 130 μM solutions of holo-ACP mutants with a total added volume not exceeding 10% of the initial volume so that $[LpxA]_{total}$ was treated as a constant. When there is a single binding site on LpxA, the fluorescence of ACP is described by (Eftink, 1997):

$$F_{LpxA} - F_{-LpxA} = \Delta F_{max} [ACP]_{free} / (K_d + [ACP]_{free}) \quad (4)$$

where F_{LpxA} and F_{-LpxA} are fluorescence intensities in the presence and absence of LpxA, $[ACP]_{free}$ is uncomplexed ACP concentration, ΔF_{max} is maximum signal change, K_d is the dissociation constant for binding of ACP to LpxA. Assuming that each LpxA molecule carries a single ACP binding site, $[ACP]_{free}$ can be expressed in relation to the known total concentrations of LpxA and ACP by solving the following quadratic equation (Eftink, 1997):

$$[ACP]_{free}^2 + [ACP]_{free} ([LpxA]_{total} - [ACP]_{total} + K_d) - [ACP]_{total} K_d = 0 \quad (5)$$

Data series of $F_{LpxA} - F_{-LpxA}$ at a given emission wavelength and $[ACP]_{total}$ were fitted to Eq. 4 to obtain ΔF_{max} and K_d using nonlinear regression analysis with GraphPad Prism (GraphPad Software).

F. ACP Homology Modelling

The model structure of *V. harveyi* ACP was obtained using SWISS-MODEL version 3.5 (http://www.expasy.org/swissmod/SWISS-MODEL.html), an automated comparative protein modelling server. Under First Approach mode, the *V. harveyi* ACP sequence was submitted in FASTA format. All templates with sequence identities above 25% and projected model size larger than 20 residues were found in the sequence database ExNRL-3D with the programs BLASTP2 and SIM. Models were generated with the program

ProModII using a structure database ExPDB, which is derived from the Protein Data Bank. During iterative template fitting, the layers of templates which did not fit well were removed. The solution structure of *E. coli* ACP (accession code 1ACP) was found with $P(N)=1 \times 10^{-20}$ and was chosen as the template for modelling. Energy minimization was conducted using the GROMOS 43B1 force field to optimize the side chain and backbone structures of the model. This force field allowed the evaluation of the energy of a structure in vacua and the subsequent repair of distorted geometries by moving atoms to release internal constraints. The resulting PDB file contained a model superimposed on the template. A manually optimized sequence alignment can be used alternatively under Optimize (Project) mode. A project file was generated with the Swiss-Pdb Viewer program, which contained the target sequence and all of the template structures with significant sequence similarities. Submission of the project file resulted in the same model as in the fully automatic procedure. Given the high identity (86%) between the two ACP sequences, the *V. harveyi* ACP model was almost identical to the structure of the *E. coli* ACP template with a backbone root mean square deviation less than 3 Å.

The electrostatic potentials of *E. coli* ACP and the *V. harveyi* ACP model were computed using Swiss-PDB Viewer version 3.7 (Guex and Peitsch, 1997) and were visualized by mapping to computed molecular surfaces. Solvent ionic strength, pH, dielectric contants for the solvent and the protein were set at 50 mM, 7.0, 80, and 4, respectively. The matrix-based Poisson-Boltzmann algorithm was used to compute atomic partial charges of the GROMOS 43A1 force field, giving a much reduced potential surface compared to using simple Coulomb interaction. Images were rendered using POV-Ray (Persistence of Vision Ray-Tracer from http://www.povray.org).

Chapter III. Identification of a Key Residue in ACP Required for *V. harveyi* Fatty Acid Synthase Activity[1]

A. Rationale

As ACP is essential for microbial growth and has a distinct architecture in mammals and bacteria, enzymes that interact with ACP are potential targets for the development of new antimicrobial agents (Heath et al., 2002). How ACP interacts with its multiple enzyme partners is largely unknown, and sequence analysis of these enzymes has not revealed any obvious ACP-binding motifs. A previous molecular docking study indicated that amino acids primarily in helix II of ACP interact directly with *E. coli* FabH, a rate-limiting enzyme in FAS (Zhang et al., 2001). Site-directed mutagenesis of FabH predicted an important electrostatic interaction between Arg249 of FabH and Glu41 of ACP, and between Ala253 of FabH and Ala45 of ACP to permit close approach of the interacting helices (Zhang et al., 2001). A similar basic/hydrophobic ACP docking site has been identified and confirmed on the reducing enzyme FabG (Zhang et al., 2003b). A role for helix II of ACP in binding to enzymes has also been indicated from the X-ray structure of *B. subtilis* ACP co-crystallized with ACPS (Parris et al., 2000) and fluorescence studies with HlyC (Worsham et al., 2003). On the other hand, different regions of *E. coli* ACP have been implicated in interactions with the glucosyltransferase involved in membrane-derived oligosaccharide biosynthesis (Tang et al., 1997), suggesting that some enzymes may bind to different regions of ACP.

Few studies have addressed the contribution of ACP residues to ACP-partner interactions. In this study, the *V. harveyi* ACP gene was used as a template for site-directed mutagenesis to assess the importance of specific ACP helix II residues for the activities of the FAS complex and AAS, both from *V. harveyi*. A radioisotope-based assay for *V. harveyi* FAS was developed and thoroughly characterized for this purpose. The results indicate that an acidic residue at position 41 is critical for FAS but not AAS activity, and that both activities tolerate replacements at position 45.

---

[1] This chapter is adapted from Gong and Byers, 2003.

B. Results

1. Conformational Analysis of ACP Mutants

The negative charge of Glu41 and the small size of Ala45 have been predicted by computational docking analysis to be important for the interaction of helix II of *E. coli* ACP with the fatty acid synthase condensing enzyme FabH (Zhang et al., 2001). On this basis, both acidic (E41D) and basic (E41K) residues were substituted for Glu41 of *V. harveyi* ACP by site-directed mutagenesis, and Ala45 was replaced with either smaller (A45G), slightly bulkier (A45C), or much bulkier residues (A45W). The primary structure of *V. harveyi* ACP is identical to that of *E. coli* over this region (between residues 31 and 71) and 86% identical over the entire protein (Shen and Byers, 1996). Not only is the predicted backbone structure of *V. harveyi* ACP obtained using SWISS-MODEL (Guex and Peitsch, 1997) virtually superimposable on that of *E. coli* ACP (Keating et al., 2002), the charge distributions on the molecular surfaces are also similar and dominated by negative charges (Fig. 6).

Nevertheless, CD spectra indicated that, unlike *E. coli* ACP, *V. harveyi* ACP is largely unfolded at neutral pH (Fig. 7) as previously reported (Flaman et al., 2001). This is presumably a result of electrostatic repulsion due to the greater negative charge of *V. harveyi* ACP. A native-like conformation containing ~ 50% α-helix was restored by addition of millimolar levels of Mg^{2+} ions. CD was also used to examine the effects of helix II mutations on the secondary structure of ACP (Fig. 7). Similar behavior to that of wild type rACP was observed for ACP mutants E41D, A45G and A45W, while mutants E41K and V43I exhibited substantial α-helical content even in the absence of Mg^{2+}, with little further change following its addition. In contrast, the A45C mutant contained little secondary structure either in the presence or absence of Mg^{2+}, but a Mg^{2+}-dependent conformational change of this mutant was restored by addition of the sulfhydryl reducing agent DTT (Fig. 7). This suggests that oxidation of Cys45 to form either intermolecular or intramolecular (i.e. with the phosphopantetheine sulfhydryl) disulfide bonds impairs proper folding of ACP. Overall, these results reveal that, although native-like structure is attainable in the presence of Mg^{2+} and/or DTT in all cases, ACP conformation is sensitive to mutations in the highly conserved helix II region.

The hydrodynamic properties of ACPs as monitored by native PAGE at pH 7.4 (Fig. 8A) were consistent with the CD data. In the presence of Mg^{2+} and DTT, all mutants

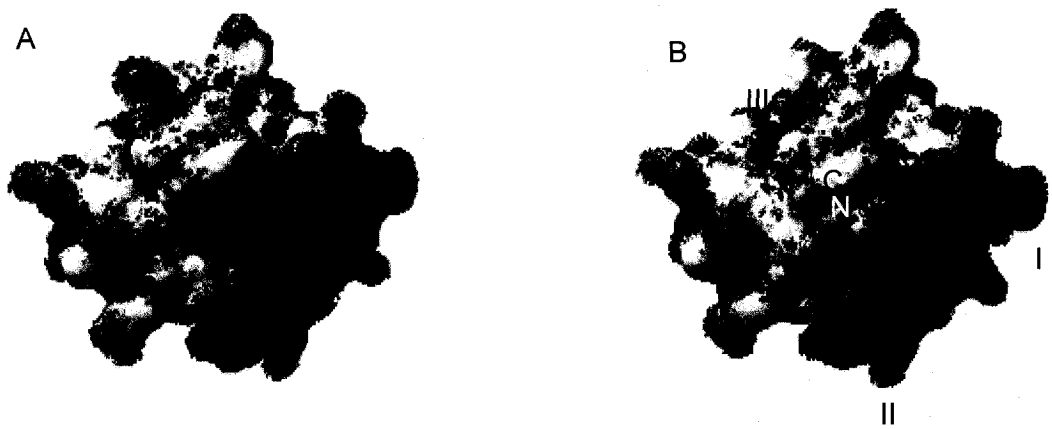

Figure 6. Surface electrostatic potential of ACP. Partial charges were used to compute the electrostatic potential surfaces of A) structural model of *V. harveyi* rACP and B) NMR structure of *E. coli* ACP as described in Chapter II, section F. Negative charges are in red. Positive charges are in blue. Shown in each image is the side of the molecule where the N- and C-termini reside. The three α-helices are indicated (I-III).

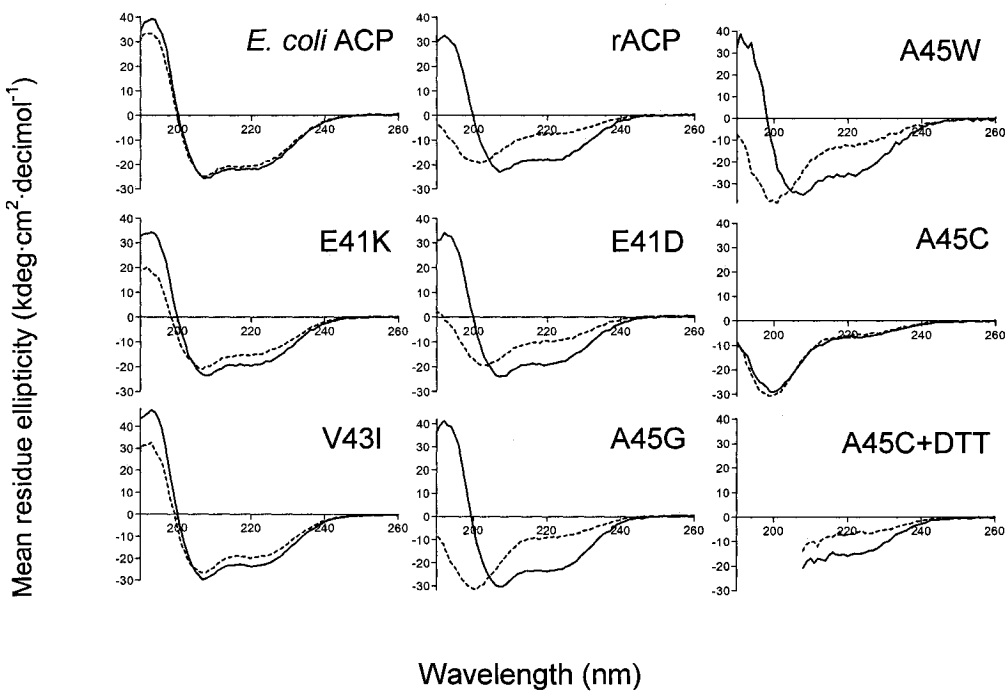

Figure 7. Effect of Mg^{2+} on secondary structure of wild type and helix II mutant ACPs. CD spectra of 3 μM purified holo-ACPs were recorded with (solid lines) and without (dashed lines) 2 mM $MgCl_2$. CD spectra of A45C were also recorded in the presence of 10 mM DTT. Results are representative of at least two separate preparations for each ACP mutant.

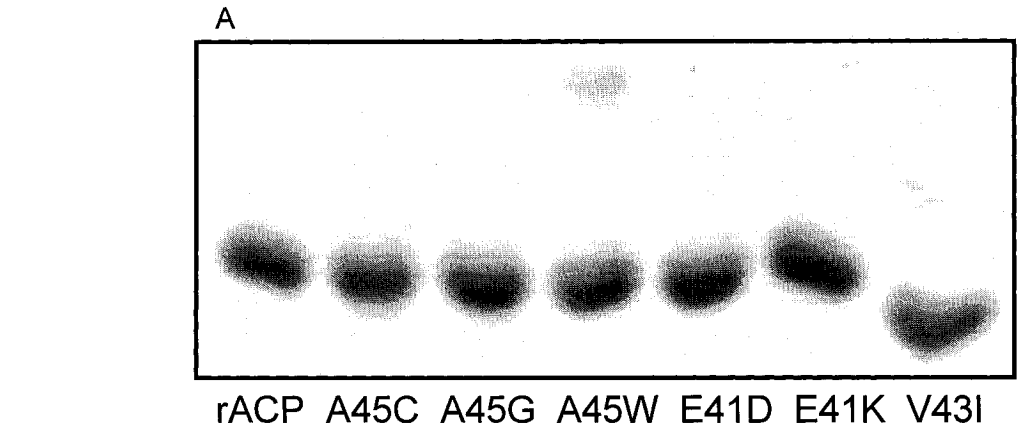

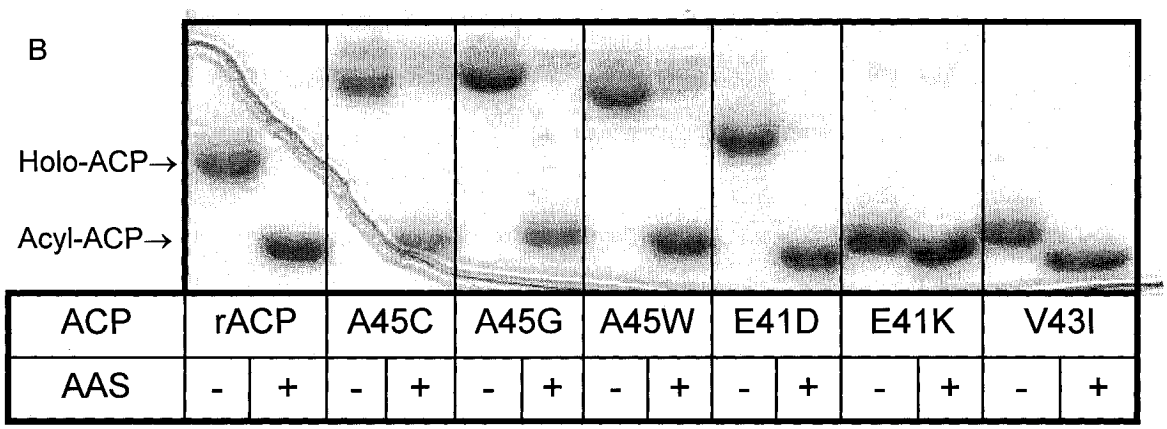

ACP	rACP		A45C		A45G		A45W		E41D		E41K		V43I	
AAS	-	+	-	+	-	+	-	+	-	+	-	+	-	+

Figure 8. Hydrodynamic analysis of ACPs using conformationally sensitive native PAGE. A) Holo-ACPs (4 μg each) were resolved on a 20% polyacrylamide gel at pH 7.4 in the presence of 10 mM $MgCl_2$ and 100 mM DTT. B) ACPs (2 μg each) were separated on a 20% polyacrylamide gel at pH 9.2 before (-) and after (+) ATP-dependent quantitative conversion into acyl-ACPs using AAS.

exhibited similar electrophoretic mobility to rACP. It is noteworthy that E41K should have a decreased negative charge relative to the other ACPs at this pH, so that its similar mobility might also be indicative of a more compact shape under these conditions.

ACPs exhibited hydrodynamic expansion due to electrostatic repulsion at elevated pH (Fig. 8B). Mutants A45C, A45G, and A45W all exhibited decreased mobility relative to rACP, indicating that these mutations further destabilize the native conformation of ACP at this pH. Interestingly, mutants V43I and E41K migrated faster than rACP, suggesting that these mutations counteract the high pH-induced expansion of ACP. Enzymatic attachment of fatty acid, which is known to interact with residues lining a hydrophobic fatty acid binding pocket and stabilize a more compact conformation of ACP (Rock et al., 1981), resulted in increased electrophoretic mobility which was similar for all ACPs (Fig. 8B). Thus, the combined CD and electrophoresis data indicate that all helix II mutants can adopt a native-like folded conformation upon either acylation or Mg^{2+} binding.

2. Effects of ACP Mutations on FAS and AAS Activities

To measure the ability of recombinant ACP mutants to support FAS activity, crude cell-free extract (CFE) of *V. harveyi* was fractionated using sequential precipitation by 40% and 75% saturated ammonium sulfate; a similar fraction has previously been shown to retain the *E. coli* FAS component enzymes while endogenous ACP remains soluble (Schulz, 1975). An in vitro *V. harveyi* FAS assay was developed to measure the incorporation of [2-^{14}C]malonyl-CoA into hexane-extractable fatty acid products. FAS activity with this ACP-free fraction (FASF) was completely dependent on added wild type or mutant ACP (Fig. 9), NADPH, and acetyl-CoA with background values < 3% of the complete mixture in each case. The assay was further optimized with regard to malonyl-CoA concentration (Fig. 10A), time, temperature, and enzyme concentration (Fig. 10B). FAS activity at 37 °C was fairly linear with time to 60 min and with enzyme concentration to 0.4 μg/μL, with less than 15% consumption of the limiting malonyl-CoA substrate. Mg^{2+} was not included in the assay mixture and was found to stimulate FAS activity by 15% at submillimolar levels but inhibit the enzyme at higher levels (data not shown). Despite the highly similar sequences of *E. coli* and *V. harveyi* ACPs, FASs from both bacteria preferred *E. coli* to *V. harveyi* ACP as their substrate (Fig. 9).

Kinetic analysis revealed that *V. harveyi* FAS exhibited a largely decreased maximal

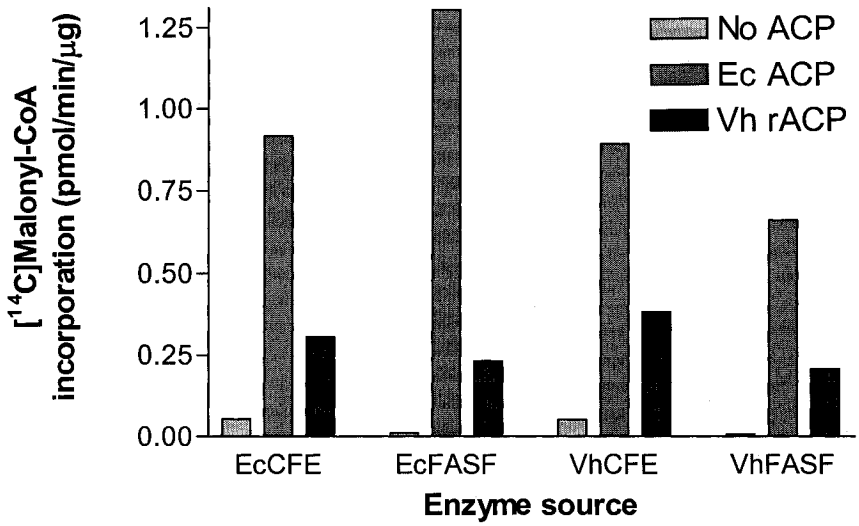

Figure 9. Cross-species activities of FAS with ACPs from *E. coli* and *V. harveyi*. FAS activity in crude extract (CFE) or after salt fractionation (FASF) from each bacterium was measured with 5 μM native ACP from *E. coli* (Ec) or wild type rACP from *V. harveyi* (Vh) at 25 °C. Background activities in the absence of exogenous ACP are also shown.

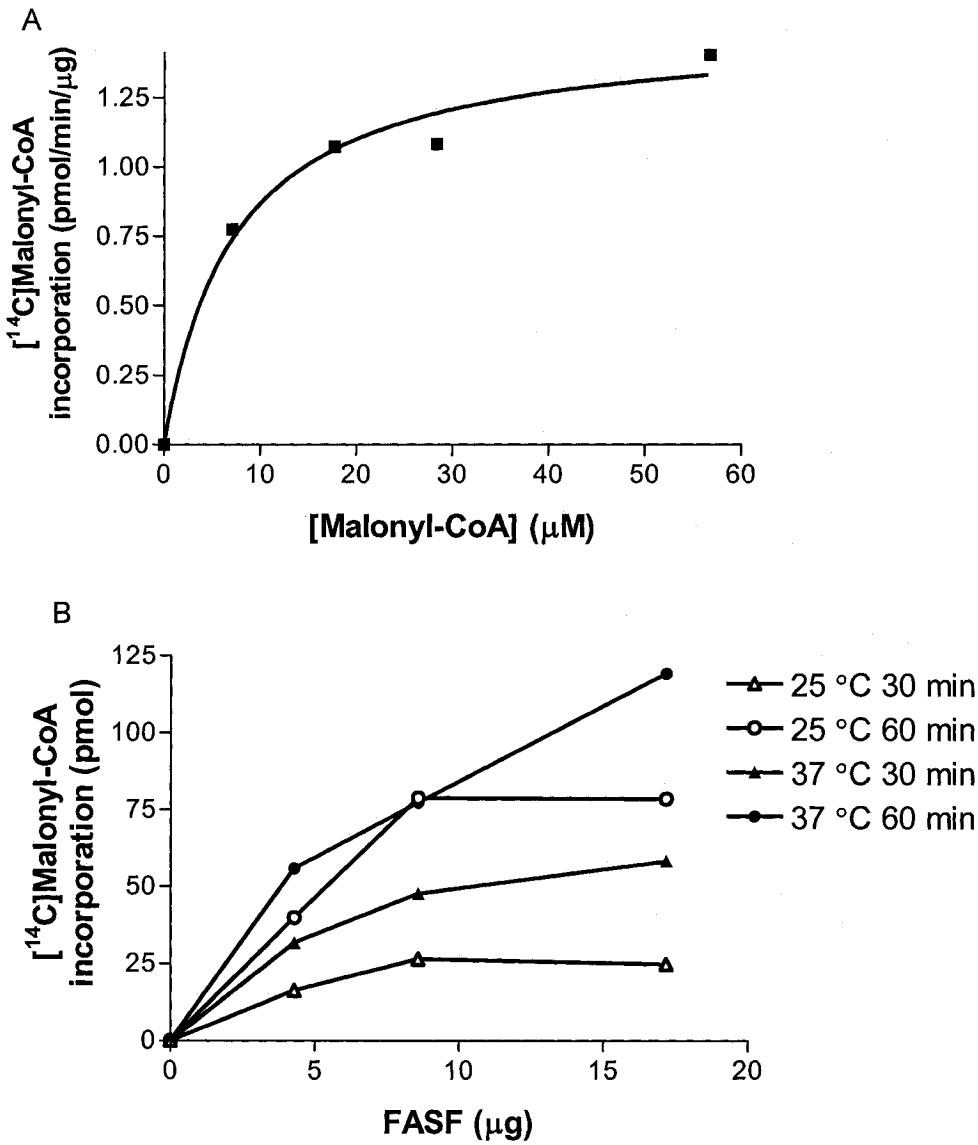

Figure 10. *V. harveyi* FAS assay characterization. A) FAS activity from *V. harveyi* FASF was measured with 10 µM *E. coli* ACP after incubation at 37 °C for 30 min. B) FAS from *V. harveyi* FASF was assayed with 5 µM rACP after incubation at 25 or 37 °C for 30 or 60 min.

activity with *V. harveyi* rACP vs *E. coli* ACP and a similar K_m with both ACPs (Table 2). The K_m values with A45C, A45G, A45W, and V43I were in the micromolar range similar to that with rACP, and increased for E41D and E41K despite a conservative replacement in the case of E41D. FAS had similar V_{max} with rACP and most mutants but a drastically decreased value with E41K. For comparison, the effect of amino acid replacements in ACP helix II on activity of *V. harveyi* AAS was also investigated. AAS is a soluble enzyme that directly activates a broad range of free fatty acids to ACP in an ATP-dependent manner (Fice et al., 1993). The K_m of AAS with most helix II mutants were similar to that with rACP except that the values were elevated with E41D, E41K, and A45C, and decreased with V43I, suggesting differences in binding affinity for the enzyme. Nonetheless, AAS exhibited similar V_{max} with all ACPs tested.

As shown graphically in Fig. 11A, FAS activity was not affected when Glu41 of ACP was replaced by another acidic residue (E41D), but was completely abolished with the E41K ACP mutant. In contrast, replacement of Ala45 with either Gly, Cys, or Trp had no apparent effect on FAS activity. Moreover, mutation of Val43 in this region to Ile, which has been shown to stabilize a more compact conformation of *E. coli* ACP (Keating and Cronan, 1996), also had no effect relative to rACP. All ACPs tested at 50 μM were equally effective substrates for AAS (Fig. 11B). Thus, FAS, but not AAS, is sensitive to ACP mutations that reverse the charge at position 41, while both activities are insensitive to replacements of Ala45.

C. Discussion

Although early studies demonstrated that *E. coli* FAS activity requires native ACP conformation (Abita et al., 1971; Schulz, 1975), more detailed structural information implicating specific amino acids in interactions between ACP and FAS enzymes has only recently begun to emerge. The observation that an acidic residue at position 41 of ACP is essential for FAS activity supports a key electrostatic interaction formed between this residue and Arg249 of the FAS condensing enzyme FabH (Zhang et al., 2001). Glu is found at this position in almost all ACPs, and a similar interaction has been observed between Glu41 of ACP and Arg221 of ACPS in the crystal structure of the *B. subtilis* complex (Parris et al., 2000). Indeed, all ACP-dependent enzymes of known structure possess a basic/hydrophobic patch, adjacent to the active site, which is predicted to dock the ACP substrate (Zhang et al.,

Table 2. Kinetic parameters of FAS and AAS with wild type and mutant ACPs.

ACP type	FAS		AAS	
	K_m (μM)	V_{max} (pmol/min/μg)	K_m (μM)	V_{max} (pmol/min/μg)
E. coli ACP	3.4±0.3	2.03±0.07		
rACP	4±1	0.58±0.06	13±4	2.5±0.5
E41D	21±5	0.68±0.07	58±14	3.2±0.5
E41K	53±24	0.07±0.02	30±8	2.3±0.4
A45C	5±2	0.30±0.04	57±19	1.8±0.4
A45G	7±2	0.28±0.03	15±8	3±1
A45W	0.6±0.4	0.35±0.03	13±7	1.0±0.4
V43I	1.8±0.4	0.57±0.06	3.6±0.6	1.4±0.1

FAS activity was measured as described in Materials and Methods using FASF from *V. harveyi* and varying concentration of wild type or mutant ACPs. Shown are standard errors derived from curve fitting.

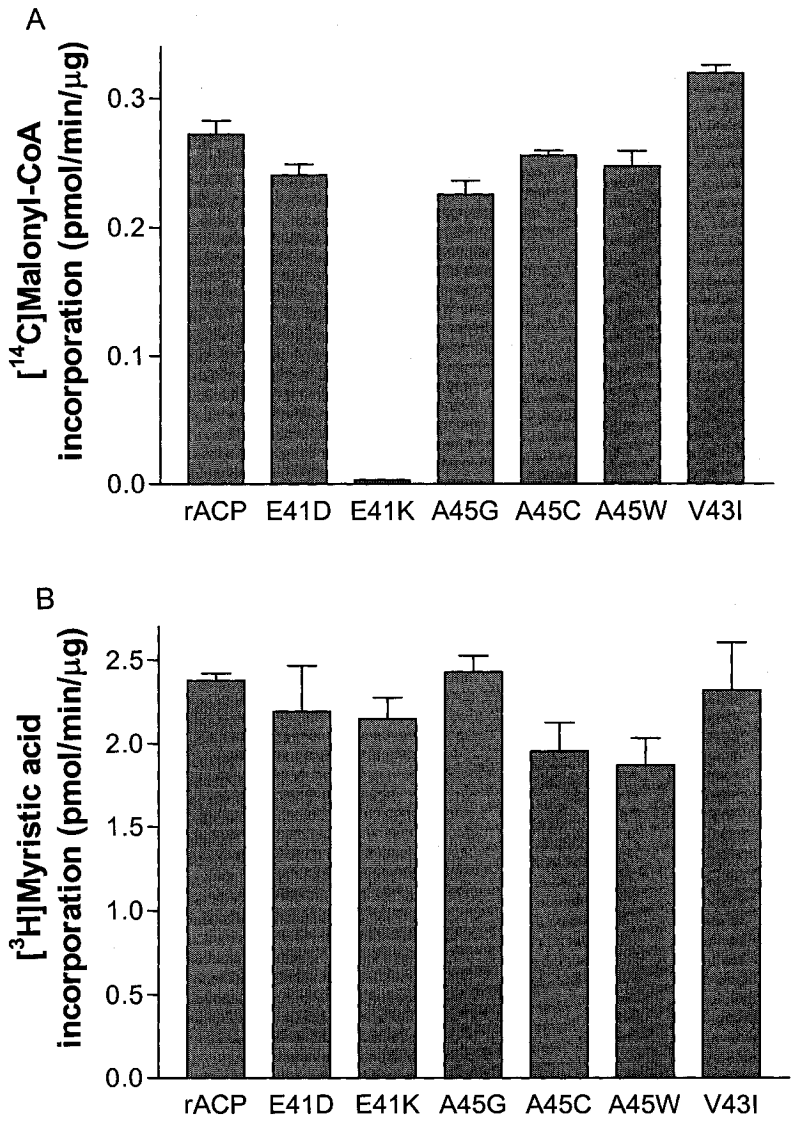

Figure 11. Activities of *V. harveyi* FAS and AAS with wild type and mutant ACPs. A) FAS activity with 10 μM ACPs. B) AAS activity with 50 μM ACPs. The mean and standard deviation (SD) from four independent reactions are shown in each case.

2001).

Somewhat surprisingly, I found no evidence that Ala45 of ACP is essential for FAS activity. Based on modelling this residue is thought to interact with Ala253 of FabH, allowing close contact between helix II of ACP and α-helix C2 of the enzyme, and mutation of the FabH Ala253 to a bulkier residue blocked its activity (Zhang et al., 2001). One obvious explanation for this result would be differences between the FabH enzymes of *E. coli* and *V. harveyi*. The amino acid sequence of *V. harveyi* FabH has not been determined, although other FAS components from this species (i.e. FabG, FabF) are >75% identical to the corresponding *E. coli* enzymes (Shen and Byers, 1996). Another possibility is that replacement of Ala253 with Tyr hindered enzyme catalysis more than ACP binding. A decreased apparent K_m of FAS with A45W may reflect an enhanced hydrophobic interaction in the molecular interface as a result of this substitution. Finally, FabH may not be rate-limiting in the overall FAS reaction measured with the *V. harveyi* complex; in this case effects of Ala45 substitutions on FabH activity might go undetected. On the other hand, the interaction between FAS and ACP may be rather weak and transient, as evidenced by the shortage of available co-crystal structures of ACP and FAS component enzymes despite much effort. In any case, Ala45 is clearly not universally required for FAS activity.

The effects of ACP helix II mutations on FAS activity must be interpreted in light of their influence on ACP conformation. While all the mutants examined in this study were capable of attaining a compact helical structure under optimal conditions, native PAGE experiments indicated that helix II mutations can either destabilize (e.g. A45G, A45W, A45C) or stabilize (E41K, V43I) a more compact ACP conformation in the absence of Mg^{2+}. The lack of FAS activity with E41K ACP could result from impaired electrostatic interaction with a basic residue on a FAS component enzyme(s), as predicted for FabH (Zhang et al., 2001). Alternatively, this mutation could decrease FAS activity by restricting the conformational flexibility of ACP, as *E. coli* ACP is known to exist in at least two conformers that are in dynamic equilibrium (Kim and Prestegard, 1989). This flexibility is thought to be important for the ability of ACP to reversibly interact with multiple enzyme partners, undergoing conformational changes as the attached fatty acid moiety alternately switches between interaction with an enzyme active site and the fatty acid binding pocket of ACP (Zhang et al., 2001). However, the V43I mutant also exhibited Mg^{2+}-independent helical content and increased conformational stability without any loss of FAS activity,

suggesting that an impaired specific electrostatic interaction is the correct explanation for the effect of the E41K mutation. In agreement, elevated apparent K_m of FAS with the conservative mutant E41D further indicates that FAS component enzyme(s) are sensitive not only to the charge but also to the specific structure at position 41.

Basic residues are known to be important for the maintenance of native *E. coli* ACP conformation (Schulz, 1975), and divalent cations can reverse unfolding of *E. coli* ACP that occurs at elevated pH or upon acetylation of its free amino groups (Schulz, 1975). E41K and V43I mutations probably stabilize ACP conformation by different mechanisms. The E41K mutation introduces a positive charge into the highly acidic helix II and, like binding of divalent cations which also occurs in this region (Frederick et al., 1988), neutralizes electrostatic repulsion. It has previously been shown that a similar mechanism is likely responsible for the increased conformational stability of *E. coli* versus *V. harveyi* ACP, due to the presence of a basic residue (His75) near the C-terminus of *E. coli* ACP (Keating et al., 2002). The V43I mutation was previously shown to decrease the hydrodynamic radius of *E. coli* ACP (Keating and Cronan, 1996), and (like fatty acid binding) likely stabilizes by increasing the hydrophobic character of the protein core.

In contrast to the important role of Glu41 in FAS activity, replacement of this residue with Lys had no effect on the V_{max} of the *V. harveyi* AAS reaction although the K_m was substantially increased. Previous work has demonstrated that native ACP conformation is essential for AAS activity; residues near the ACP fatty acid binding pocket (e.g. Ile54) have been implicated in enzyme binding (Flaman et al., 2001). While participation of helix II in interaction with AAS may be of secondary importance on the basis of the present results, an acidic residue at position 41 is clearly not required for this activity. Another enzyme shown to interact with a different region of ACP is the *E. coli* glucosyltransferase involved in membrane-derived oligosaccharide synthesis, where helix I and the adjacent extended loop of ACP have been implicated (Tang et al., 1997). This may reflect the unique nature of ACP's participation in the glucosyltransferase reaction, in which the phosphopantetheine moiety is not required. It is interesting to speculate that different classes of ACP-dependent enzymes, such as synthetases, synthases, acyltransferases, glucosyltransferase, etc., might recognize distinct features of ACP.

Chapter IV. Roles of Divalent Cation Binding Residues in Maintaining ACP Structure and Function[2]

A. Rationale

E. coli ACP has an inherently mobile structure that maintains a dynamic equilibrium of at least two conformers, with the loop region and helix II being particularly flexible (Kim and Prestegard, 1989; Andrec et al., 1995). Electrostatic repulsion undoubtedly contributes to conformational flexibility of ACP in this very acidic central region (with 13 acidic and no positive residues between positions 30 and 60); this flexibility, in turn, is thought to be important in facilitating rapid association and dissociation of ACP with its various partner enzymes. As noted in the preceding chapter, docking, crystallographic, and mutagenic studies with *E. coli* FAS components, ACPS and other enzymes (Parris et al., 2000; Zhang et al., 2001; Zhang et al., 2003b; Worsham et al., 2003) have implicated the conserved acidic helix II of ACP as a "recognition helix" for universal enzyme interaction (Zhang et al., 2003a).

NMR (Tener and Mayo, 1990), CD (Keating et al., 2002) and proteomic (Herald et al., 2003) approaches have revealed specific binding of divalent cations to ACPs and stabilization of ACP conformation by cation binding. Two divalent cation binding sites exist on *E. coli* ACP with average K_d/site of about 80 μM at neutral pH (Tener and Mayo, 1990), and relaxation perturbed 2D NMR studies have identified seven residues involved in these relatively low affinity interactions (Frederick et al., 1988). Site A (consisting of Glu30, Asp35, and Asp38) resides at the N-terminal end of helix II and site B (Glu47, Asp51, Glu53, and Asp56) at the other. Six of the seven putative cation binding residues are identical in *V. harveyi* ACP with Asp replacing Glu at position 30 (Fig. 12). Unlike *E. coli* ACP, however, *V. harveyi* ACP is largely unfolded at neutral pH in the absence of millimolar concentrations of Mg^{2+} or attached acyl chains (Flaman et al., 2001).

The role of acidic helix II residues in maintaining the stability or flexibility of ACP conformation, as well as their contributions to ACP interaction with specific enzyme partners, remains largely uncharacterized. Moreover, whether divalent cations influence ACP

[2] This chapter is adapted from Gong et al., 2006.

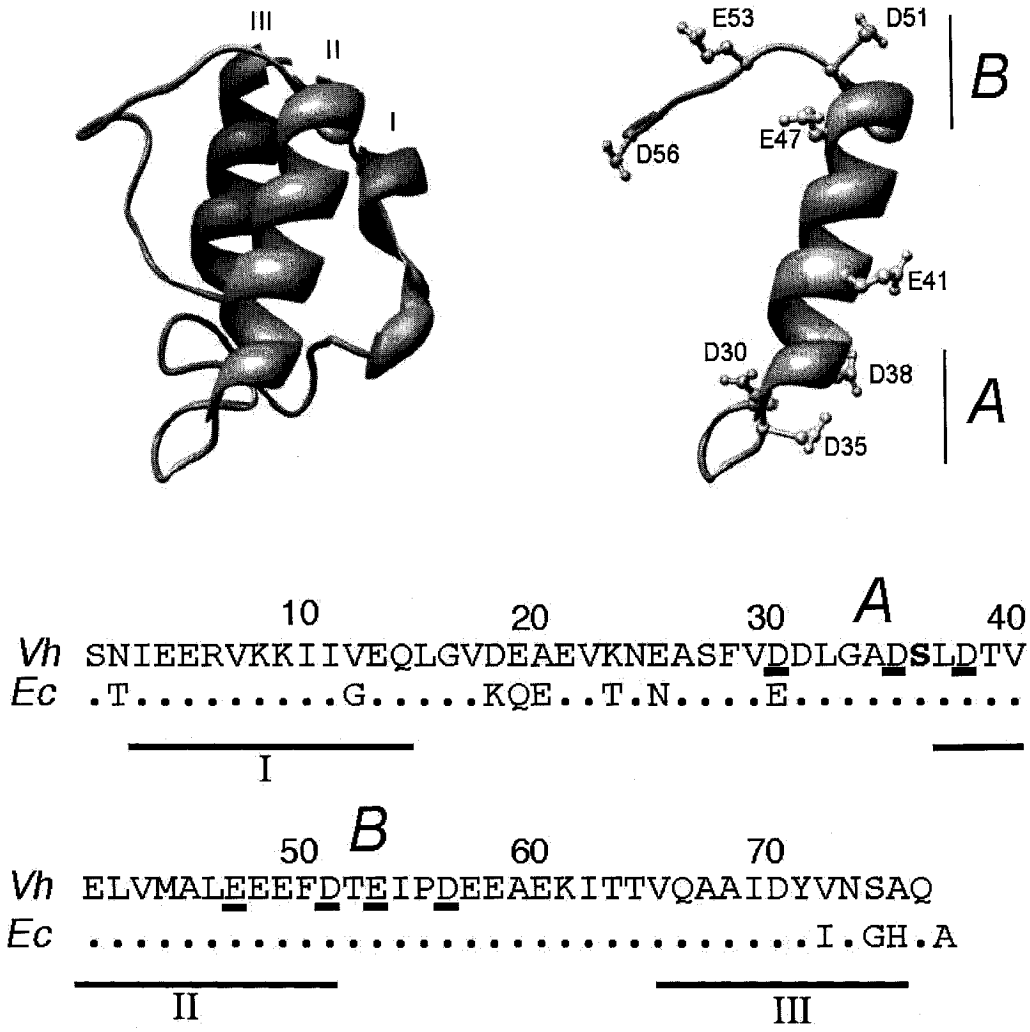

Figure 12. Divalent cation binding sites of *E. coli* ACP. Top: UCSF Chimera (Pettersen et al., 2004) ribbon representation of the model for *V. harveyi* ACP showing the three α-helices I-III (left) and helix II with putative divalent cation binding residues in sites A and B (right). Bottom: amino acid sequences of *V. harveyi* (*Vh*) and *E. coli* (*Ec*) ACPs, highlighting site A and B residues (underlined), helices I-III, and the site of PP attachment at Ser36 (bold). Residues conserved between the two species are indicated by a dot in the *E. coli* sequence.

structure and function in vivo is also unknown, as these sites would be expected to be occupied by Mg^{2+} under physiological conditions. In the present project, putative divalent cation binding residues on rACP were mutated (alone or in combination) to corresponding neutral amide forms and the consequences on ACP conformation were examined. Four enzyme systems that employ ACP in different reactions were also investigated to identify ACP regions or residues engaged in each interaction.

B. Results

1. Mutant ACP Preparation

Of the seven acidic residues implicated in divalent cation binding by *E. coli* ACP (Fig. 12), positions 35, 38, 47, 56, and to a lesser extent positions 30 and 53, are invariant or highly conserved among ACPs from plants and bacteria (Fig. 4). Position 51 in site B is the least conserved and tolerates various non-conservative replacements. The conserved acidic residues are likely to not only play a role in cation binding, but may also be important in the interaction of ACP with specific enzymes. To examine the individual and combined contribution of these acidic residues, site-directed mutagenesis was employed to substitute the corresponding neutral amino acids. Nine mutants were constructed, expressed and purified to homogeneity, i.e. six individual mutants D30N, D35N, D38N, E47Q, E53Q, and D56N, and three site elimination mutants SA (D30N/D35N/D38N), SB (E47Q/D51N/E53Q/D56N), and SA/SB. Attempts to construct the D51N individual mutant were not successful. ACPs were expressed in *E. coli* BL21 cells and isolated as GST fusion proteins in order to eliminate contamination of the mutant proteins with host cell ACP. All mutant ACPs exhibited roughly comparable levels of expression with rACP, and none appeared to be lethal to *E. coli* cells.

2. Mg^{2+}-Induced ACP Folding

CD was used to examine the effects of divalent cation binding site mutations on the secondary structure of ACP and dependence of ACP folding on $MgCl_2$ (Fig. 13). As noted earlier, *V. harveyi* ACP is largely unfolded at physiological pH, but adopts a largely helical conformation in the presence of millimolar levels of Mg^{2+} (Flaman et al., 2001). Addition of 2 mM Mg^{2+} to rACP increased the magnitude of ellipticity at 220 nm by 2.4 $\pm$ 0.3 fold (mean

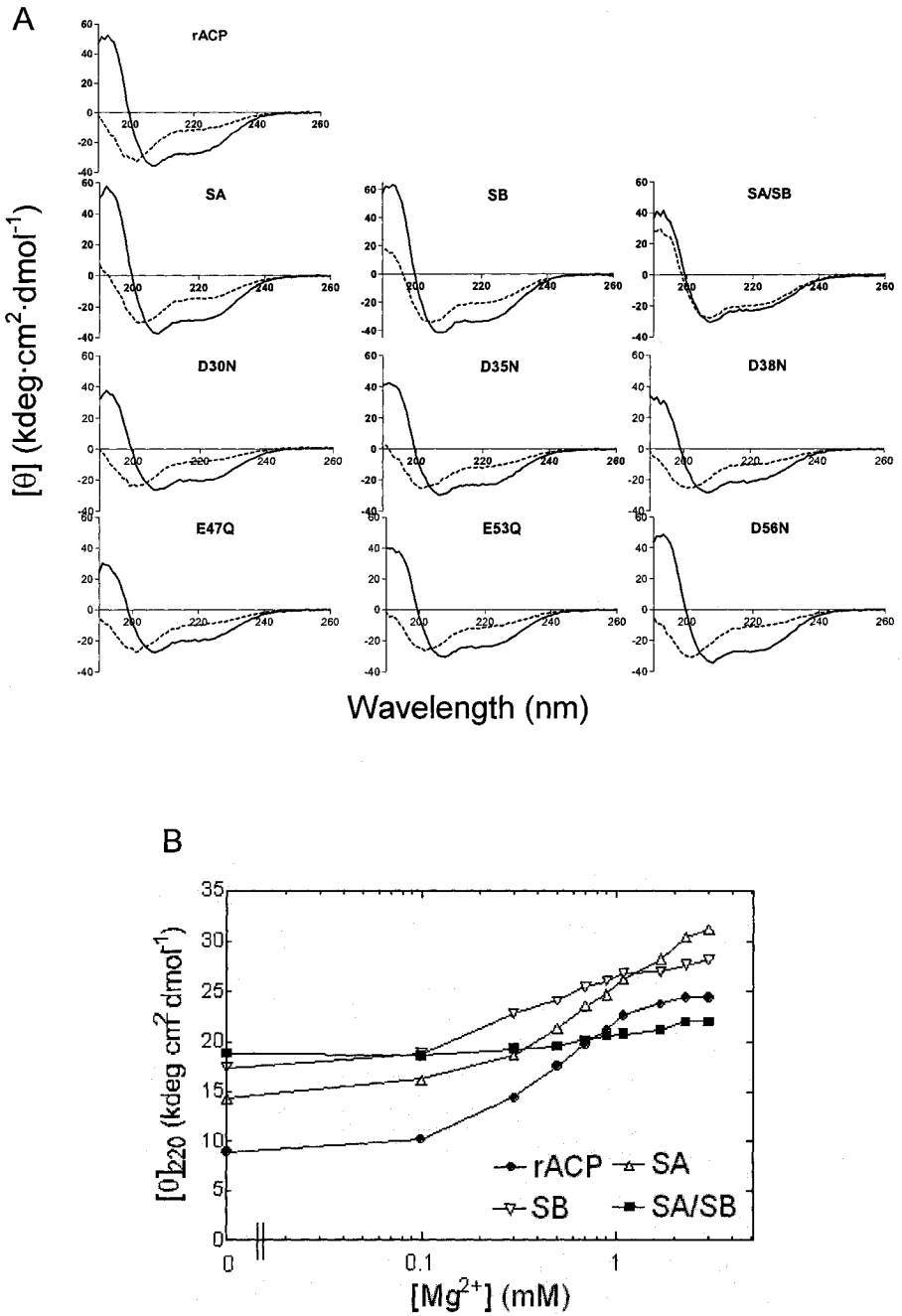

Figure 13. Effect of Mg^{2+} on the CD of rACP and mutant ACPs. A) CD spectra of the indicated holo-ACPs (10 μM) were obtained at 25 °C at pH 7.0 in the absence (dashed line) or presence (solid line) of 2 mM $MgCl_2$. B) ACPs (10 μM) were titrated with $MgCl_2$ and mean residue ellipticity at 220 nm ($[\theta]_{220}$) measured. Results are representative of at least three independent experiments.

± SD, n=3) and shifted the negative trough at 201 nm to 208 nm indicative of increased α-helical content; similar Mg^{2+}-dependent conformational transitions were observed for the six individual mutants (Fig. 13A). In contrast, the two single-site mutants SA and SB exhibited more residual helical content in the absence of divalent cations, and became folded to the same extent as rACP upon addition of Mg^{2+}. The effect of Mg^{2+} on $[\theta]_{220}$ was significantly greater for the SA mutant (1.9 ± 0.1) than for SB (1.5 ± 0.2). The double-site mutant SA/SB contained substantial helical content even in the absence of Mg^{2+}, with only a modest further effect of Mg^{2+} on $[\theta]_{220}$ (1.12 ± 0.04). The mid-point of the Mg^{2+}-induced conformational transition ($[\theta]_{220}$) for SA (0.7 ± 0.1 mM, n=3) was slightly higher than those for SB (0.43 ± 0.03 mM) and rACP (0.44 ± 0.08 mM) (Fig. 13B). The mid-points of CD response to Mg^{2+} for the individual mutants in site B (E47Q, E53Q, and D56N) were similar to that for SA (data not shown). These results suggest that Mg^{2+} binding to either site A or B alone allows ACP to adopt a native-like conformation.

Conformational change of rACP was also monitored in response to Ca^{2+} and Mn^{2+}, which like Mg^{2+} increased α-helical content in the 0.1 - 1.0 mM range (Fig. 14). However, although all three divalent cations elicited a maximum conformational change at around 5 mM, higher levels of Ca^{2+} and Mn^{2+} (but not Mg^{2+}) decreased the secondary structure content of rACP. Results from the CD deconvolution program k2d (Andrade et al., 1993) indicated that 50 mM Ca^{2+} or Mn^{2+} caused a 40% decrease in α-helical content of rACP, relative to 5 mM Ca^{2+} or Mn^{2+}.

3. Native PAGE Analysis of Mutant ACP Derivatives

Most apo- and holo- individual mutants had electrophoretic mobilities that were comparable to the corresponding forms of rACP, with the exception of apo- and holo-D35N which migrated considerably faster than its rACP counterparts (Fig. 15). In contrast to individual mutants, the three site elimination mutants SA, SB, and SA/SB exhibited increased mobility relative to their apo- and holo-rACP counterparts. These mutants would be less negatively charged than rACP at pH 9.2 and might be expected to migrate slower, indicating that they must have a decreased hydrodynamic radius or a more compact conformation under these conditions, consistent with CD results. Upon enzymatic myristoylation, all ACP mutants exhibited further increased mobility relative to holo-ACPs,

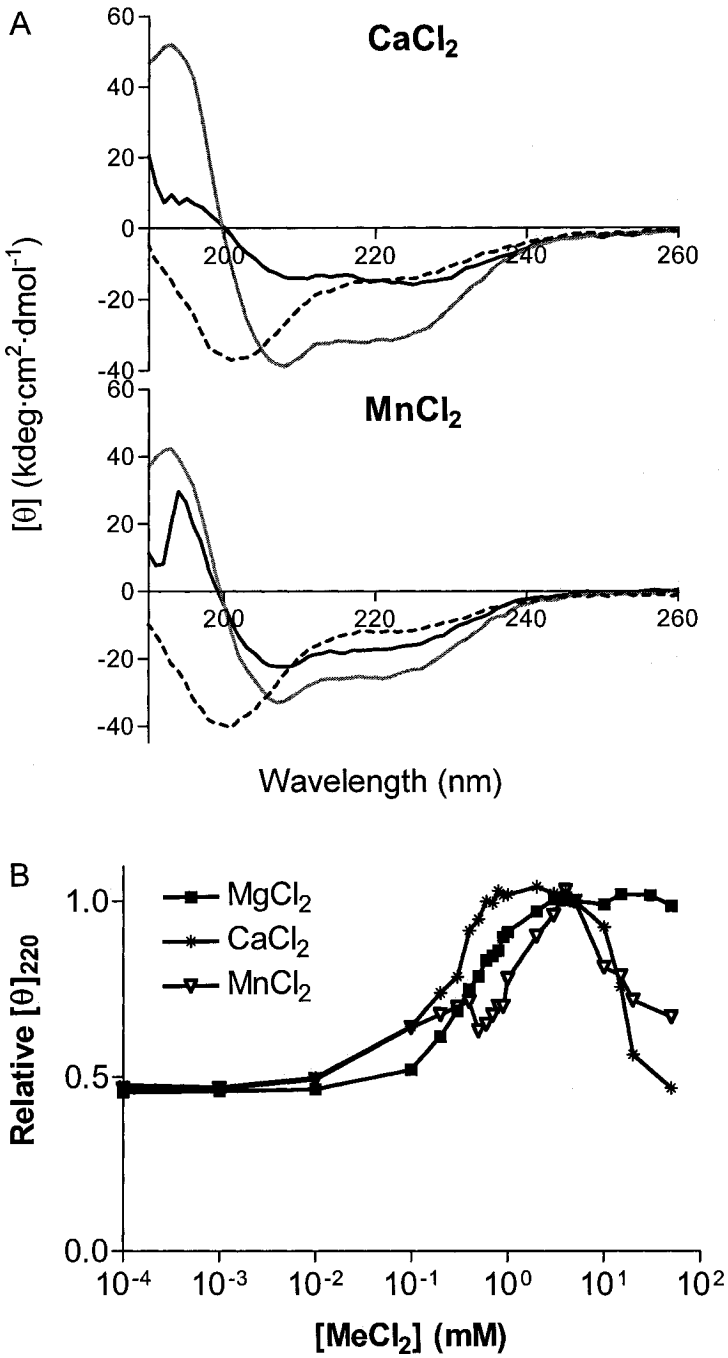

Figure 14. Effects of Mg^{2+}, Ca^{2+}, and Mn^{2+} on the CD of ACPs. A) CD spectra of holo-rACP (3 μM) were obtained in the absence (dashed line) and presence of 5 mM (grey solid line) or 50 mM (black solid line) of $CaCl_2$ or $MnCl_2$. B) CD signal at 220 nm of holo-rACP was recorded at the indicated levels of Mg^{2+}, Ca^{2+}, or Mn^{2+}. The ellipticity relative to holo-rACP in the presence of 5 mM of each cation (Me) is shown.

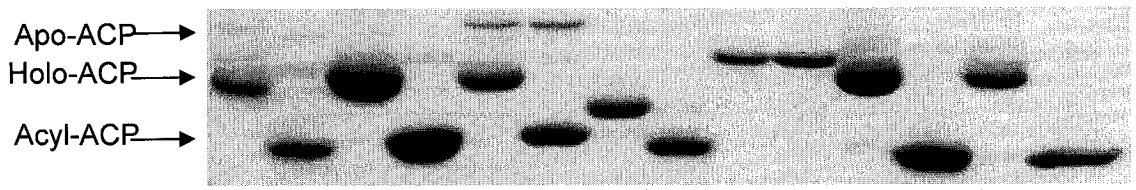

ACP	rACP		D30N				D35N				D38N			
ACPS	+	+	+	+	-	-	+	+	-	-	+	+	-	-
AAS	-	+	-	+	-	+	-	+	-	+	-	+	-	+

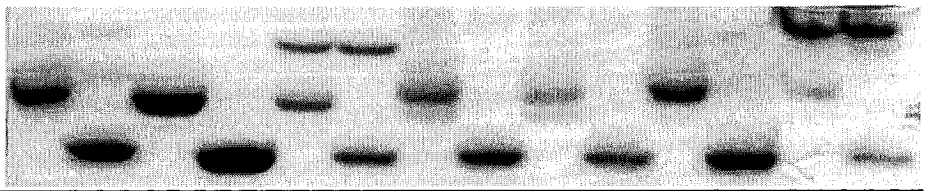

ACP	rACP		E47Q				E53Q				D56N			
ACPS	+	+	+	+	-	-	+	+	-	-	+	+	-	-
AAS	-	+	-	+	-	+	-	+	-	+	-	+	-	+

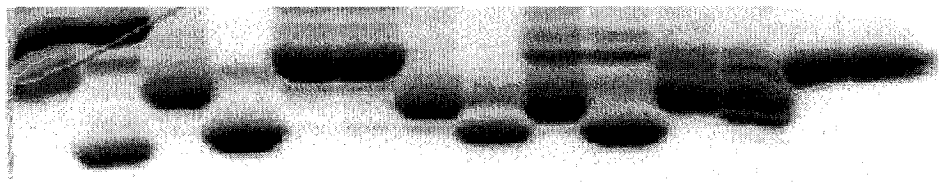

ACP	rACP		SA				SB				SA/SB			
ACPS	+	+	+	+	-	-	+	+	-	-	+	+	-	-
AAS	-	+	-	+	-	+	-	+	-	+	-	+	-	+

Figure 15. Conformationally sensitive native PAGE analysis of wild type and mutant ACPs. ACPs were prepared with (+) or without (-) modification by exogenous *E. coli* ACPS during purification and separated on a 20% polyacrylamide gel at pH 9.2, before (-) or after (+) ATP-dependent conversion into acyl-ACPs using AAS. An equal volume of the extract was loaded and rACP was included on each gel for comparison.

indicating that compact conformation was further stabilized by the interaction with the covalently bound acyl chain although the stabilization was only minor for the SA/SB mutant (Fig. 15).

Overexpression and preparation of *V. harveyi* rACP and mutant ACPs without treatment with exogenous *E. coli* ACPS during purification resulted in a mixture of apo- and holo-ACPs in most cases (Fig. 15). Wild type rACP was over 50% converted to holo form in vivo by host cell ACPS. D35N, D56N, SA, and SA/SB were poorly converted and appeared mainly as apo-ACPs. E47Q and SB showed a holo/apo ratio similar to that of rACP. Surprisingly, D30N, D38N, and E53Q were modified to the holo form to a greater extent than the wild type protein and appeared as mainly holo-ACPs. Incubation with ACPS and coenzyme A increased conversion to holo-ACP for all mutants, but SA/SB was not quantitatively converted.

4. Role of Divalent Cation Binding Residues in Supporting Enzyme Activities

Differences in the relative amounts of apo-, holo-, and acyl- forms of various mutant ACPs suggest that divalent cation binding site mutations may affect their substrate properties with specific ACP-dependent enzymes. A more quantitative assay measuring [^{3}H]acetyl-CoA incorporation at 25 °C (a temperature chosen for direct comparison with biophysical experiments) into apo-ACP using *E. coli* ACPS confirmed that activity of this enzyme is impaired with apo-ACP substrates containing the D35N or site A-eliminating mutations (SA or SA/SB), with less than 10% activity observed relative to apo-rACP (Fig. 16). In contrast, activity with the apo-SB mutant was even greater than with rACP, and other site A mutants (e.g. D30N) also supported significant levels of ACPS activity. Results were qualitatively similar when the assay was conducted at 37 °C, although ACPS activity relative to rACP was decreased for apo-SB and higher for *E. coli* apo-ACP at this temperature.

Other ACP-dependent enzymes with different catalytic functions were also investigated (Fig. 17). In marked contrast to ACPS, activity of *V. harveyi* AAS with the SA mutant was indistinguishable from that with rACP at 25 °C, while the SB and SA/SB mutants supported 40% and 10% activity with this enzyme, respectively (Fig. 17). Most individual mutants were comparable substrates for AAS at 37 °C (Fig. 18), i.e. less effective

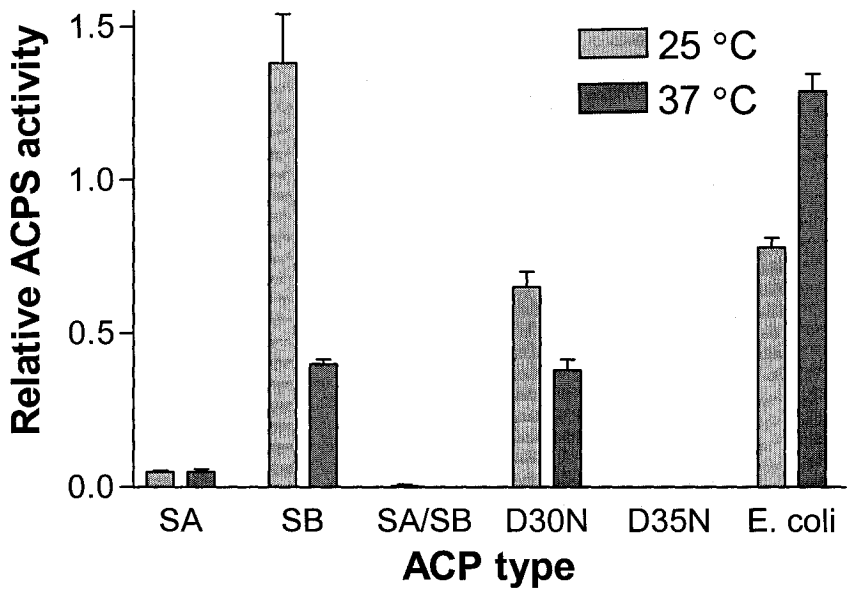

Figure 16. Relative activity of *E. coli* ACPS with selected mutant apo-ACPs. Assays were performed at 25 or 37 °C and formation of [^{3}H]acetyl-ACP (mean ± SEM of at least three independent experiments) was expressed relative to that using apo-rACP as a substrate. The rate of ACPS reaction with apo-rACP was 65 pmol/min/μg at 25 °C and 86 pmol/min/μg at 37 °C.

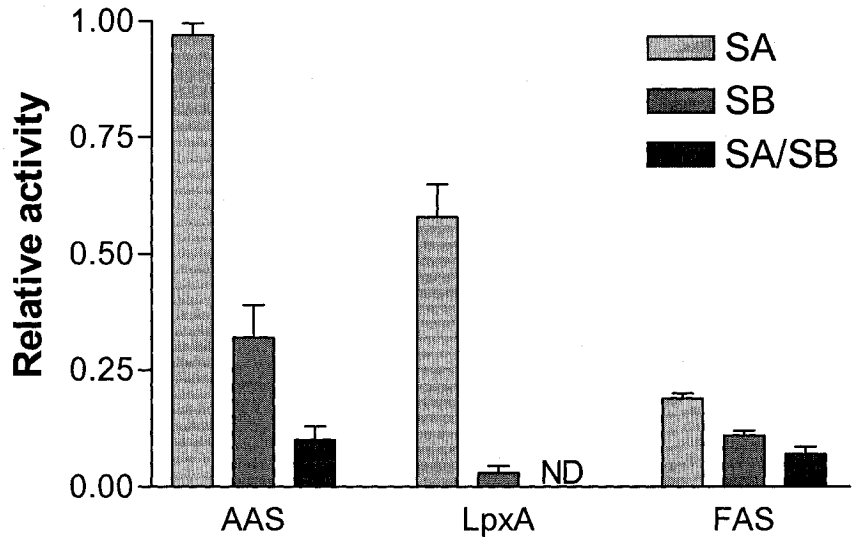

Figure 17. SA, SB and SA/SB mutant ACPs as enzyme substrates. *V. harveyi* AAS, *E. coli* LpxA, and *V. harveyi* FAS assays were performed at 25 °C with the indicated ACP substrates. The control values using the corresponding rACP substrates were 1.6, 2.2, and 0.2 pmol/min/μg for AAS, LpxA, and FAS, respectively. The mean ± SEM (n = 3-6) activity for each mutant ACP is expressed relative to the control values. The activity of LpxA with SA/SB was not determined (ND).

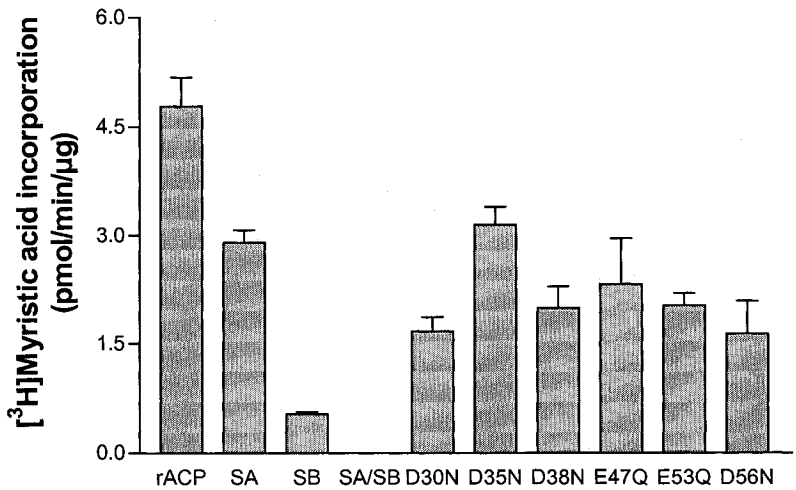

Figure 18. Activity of *V. harveyi* AAS with wild type and mutant ACPs. Shown are mean ± SD obtained from triplicate experiments performed at 37 °C.

than rACP but more so than SB and SA/SB, suggesting a cumulative effect of site B mutations on AAS activity. The poor activity of AAS with the SA/SB double mutant is also evident from electrophoresis (Fig. 15), as it is the only mutant not quantitatively acylated by AAS under these conditions.

As with AAS, combined mutations at site B had a substantially greater effect on *E. coli* LpxA activity than site A mutations, although 40% impairment of LpxA was also noted with β-hydroxymyristoyl-SA relative to the corresponding rACP substrate (Fig. 17). LpxA activity for the double site SA/SB mutant could not be determined due to difficulty in preparation of the corresponding acyl-ACP substrate (which requires both ACPS and AAS reactions), although little or no LpxA activity would be anticipated with this substrate.

V. harveyi FAS was substantially (>80%) inhibited when SA, SB or SA/SB holo-ACPs were used instead of rACP (Fig. 17). FAS activity was also decreased by 50% or more with all individual mutants except D56N, for which activity was similar to rACP (Fig. 19). These results suggest that acidic residues in both divalent cation binding sites are involved in interaction with one or more of the FAS component enzymes, and their mutation may have an additive effect on FAS activity.

C. Discussion

1. Importance of Carboxylates in Shaping ACP Conformation

Unlike previously examined *V. harveyi* ACP mutants A75H (Keating et al., 2002) or E41K (Chapter III), in which strategic placement of a +1 or +2 charge difference abolishes the Mg^{2+} requirement for conformational stability, all individual site A and B mutants were similar to the rACP template, undergoing transition from largely unfolded to helical conformation in the presence of Mg^{2+}. Metal ion binding is believed to stabilize folded ACP conformation at these sites through reduction of electrostatic repulsion between carboxylate groups (Schulz, 1975).

As these experiments did not directly measure Mg^{2+} binding (i.e. in the absence of an observable conformational change), it is not known whether Mg^{2+}-induced folding of individual mutants was the result of cation binding to both sites or to the single unaffected site. However, mutation of even a single acidic residue would be expected to result in a substantial decrease of Mg^{2+} affinity at that site, leading to a biphasic CD titration response

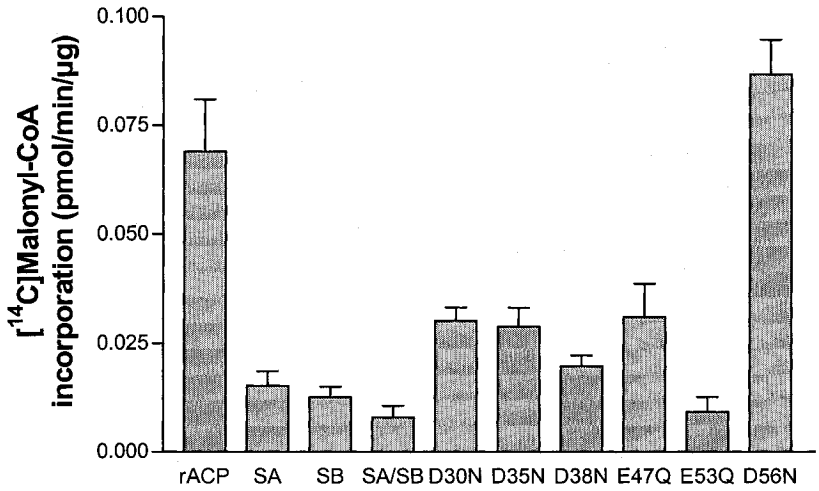

Figure 19. Activity of *V. harveyi* FAS with wild type and mutant ACPs. Shown are mean ± SD obtained from triplicate experiments performed at 37 °C.

which was not observed. Thus, the more logical conclusion is that Mg^{2+} binding at either site is sufficient to elicit complete conformational change from the unfolded ACP. Combined neutralizing mutations at either site did result in partial stabilization of folded ACP in the absence of Mg^2, a conclusion supported by increased mobility in native PAGE. The greater helical content of SA (+3 charge difference), SB (+4), and SA/SB (+7) mutants suggests additive stabilization in response to decreasing electrostatic repulsion in this region of the protein. In the event that Mg^{2+} binding to ACP is positively cooperative, binding at one site would provide coordinated molecular scaffold to facilitate binding at the other site. Consistent with this scenario, conformational transition of SB occurred at lower Mg^{2+} levels than SA and the individual mutants, which are significantly less folded than SB in the absence of Mg^{2+}.

2. Distinct Binding Determinants of Various ACP-Dependent Enzymes

In contrast to the similar consequences of abolishing cation binding site A vs site B on ACP conformation and response to Mg^{2+}, these mutations had markedly diverse consequences on individual ACP-dependent enzyme activities. Among these enzymes, ACPS is quite distinct in that it modifies the ACP polypeptide chain directly: the N-terminus of helix II must be positioned at the ACPS active site for the Mg^{2+}-dependent transfer of PP from CoA. The X-ray structure of the *B. subtilis* ACP-ACPS complex has revealed several acidic residues in the vicinity of helix II, including Asp35, Asp38, Glu41, Glu47, and Asp56, that participate in electrostatic interactions with basic residues of ACPS (Parris et al., 2000). Of these, the most important contact is between Arg14 of ACPS and both Asp35 (salt bridge) and Asp38 (H-bond) of ACP, and helix II is displaced toward the enzyme in the complex relative to the corresponding free ACP in solution (Xu et al., 2001). The present results are completely consistent with this model: mutation of Asp35 in site A had the greatest impact on ACPS activity, followed by Asp38 and Asp30. The basis of the slight increase in ACPS activity with the SB mutant at 25 °C is not known, but could be due to the enhanced conformational stability of this ACP or to a possible positive effect of removing the Mg^{2+} ion that might normally occupy this site in the assay. It is noteworthy that ACPS appears to require a native ACP substrate conformation, as this enzyme is inactive with an ACP mutant (I54A) that is incapable of folding even in the presence of Mg^{2+} (Flaman et al., 2001).

In contrast to ACPS, activities of both AAS and LpxA were much more sensitive to neutralization of cation binding site B than site A in the ACP substrate. These enzymes are respectively involved in the attachment to and transfer of acyl groups from the PP sulfhydryl moiety. Previous work from Byers and coworkers has implicated this region of ACP interaction with enzyme, in particular Phe50 and Ile54 (Flaman et al., 2001). None of the individual acidic residues in site B appeared to be critical for AAS activity in the present study, perhaps indicating a more general importance of maintaining an acidic character (or conformational flexibility) in this region, rather than involvement of specific site B residues. Mutation of Asp35 in *E. coli* ACP to cysteine was found to inhibit *E. coli* acyl-ACP synthetase activity, while similar alterations at Glu30, Asp38 and Asp56 had less effect (Worsham et al., 2003). However, acyl-ACP synthesis is only part of the reaction catalyzed by the membrane-bound *E. coli* enzyme, which is not believed to be related to *V. harveyi* AAS (Fice et al., 1993).

The results are a little more surprising in the case of LpxA. TROSY NMR spectra of *E. coli* ACP has recently revealed that residues 35-41 (i.e. site A region) undergo the greatest chemical shift perturbation upon addition of LpxA, and molecular docking analysis further suggested specific roles for Asp35, Asp38 and Glu41 in LpxA binding (Jain et al., 2004). Although some inhibition of LpxA activity was noted with the β-hydroxymyristoyl-SA substrate relative to rACP, activity was affected to a much greater extent with the SB mutant (Fig. 17). It must be emphasized that in the present study, enzyme activity was measured using the acyl-ACP substrate, rather than monitoring LpxA interaction with holo-ACP. It is possible that requirement for these site A residues (Glu41 would still be present) could be partially overcome under the assay conditions in which acyl-ACP concentration was ~ 10-fold higher than the reported K_m (Anderson et al., 1993), or that different residues are involved in acyl-ACP binding. Nevertheless, little evidence of LpxA interaction with any ACP site B residues was obtained by chemical shift perturbation in the NMR study (Jain et al., 2004). One possible explanation for the dramatic effect of site B combined mutations on LpxA activity could be altered dynamics of ACP unfolding to release the acyl group to the enzyme active site. Glu53 and Asp56 from site B reside in loop II region that makes up the "lid" of the fatty acid binding pocket and must move to allow the sequestered acyl chain to interact with the LpxA active site (Zornetzer et al., 2006). Note that Mg^{2+} is not required for

LpxA activity, so it seems unlikely that an inability to bind this cation at site B would explain these results.

Although early studies pointed to the involvement of ACP carboxylates in FAS activity (Abita et al., 1971), the current investigation has further shown that most of the acidic residues around helix II are important for overall activity of the bacterial Type II FAS complex. Recent experimental and modelling analyses have supported a role for residues in this region in interaction with specific FAS component enzymes: Glu41 and Ala45 in the case of the rate-determining condensing enzyme FabH (Zhang et al., 2001), Asp35, Asp38 and Ile54 for ketoacyl-ACP reductase FabG (Zhang et al., 2003b), and Asp35 for malonyl-CoA:ACP transacylase FabD (Worsham et al., 2003). Clearly, interpretation of the present results is limited in that it is not clear which component(s) of the FAS complex are affected by specific site A or site B mutations. However, unlike E41K (Chapter III), none of the individual mutations analyzed in the current study caused complete loss of FAS activity, while combined mutations at either site A or site B had a greater impact. Not surprisingly, FAS displayed normal activity with the D56N mutant, as this residue is exposed on the opposite face of ACP relative to most of the helix II residues implicated in enzyme interaction. Some loss of FAS activity with the mutant ACPs could be due to impaired Mg^{2+} binding, as optimal *E. coli* FAS activity in the presence of 5-10 mM divalent cations has been attributed to interaction of cations with the negatively charged ACP substrate (Schulz et al., 1969). A similar trend has been observed with the *V. harveyi* FAS system (data not shown).

In summary, the role of acidic ACP residues has been investigated in four separate enzyme systems that catalyze distinct ACP-dependent reactions. Overall, results in this study support the emerging consensus that helix II is the principal recognition motif for most enzymes that utilize ACP or its acylated derivatives as substrates. However, the data have also revealed that the relative importance of acidic residues at either end of this helix varies among these different enzymes, thus providing additional insight into the structure-function relationships of this small but essential bacterial protein.

Chapter V. Probing ACP Microenvironment: Insights from Tryptophan Fluorescence

A. Rationale

Several avenues have been explored previously in investigations of interactions between ACP and its partner enzymes, including examination of cocrystal structures (Parris et al., 2000; Rafi et al., 2006), NMR perturbation (Zhang et al., 2003b; Jain et al.,. 2004), computational docking (Zhang et al., 2001; Keatinge-Clay et al., 2003; Lee and Suh, 2003), and functional mapping using chemical modifications (Abita et al., 1971; Keating et al., 2002; Worsham et al., 2003). The focus of my project was to study ACP conformation and the effects of acylation, Mg^{2+} binding, and enzyme interaction on ACP conformation using fluorescence techniques, with the goal of providing insight into specificity of ACP-enzyme interactions.

Fluorescence spectroscopy is well suited for studying protein-protein interaction in the micromolar range because of its high sensitivity and exemption of the requirement for physically separating bound and unbound protein molecules (Eftink, 1997). ACP contains no intrinsic Trp residues, which are widely used environmental probes of protein conformation whose fluorescence emission intensity, wavelength maximum, as well as band shape are sensitive to polarity of its immediate surroundings. Thus, using site-directed mutagenesis, observation points were installed at various locations on the ACP molecule, allowing study of ACP conformational changes at micromolar levels that more closely reflect ACP behavior under physiological conditions.

LpxA serves as a good starting point because it is a well-studied enzyme with no intrinsic Trp, and thus suited for fluorescence studies with Trp mutants of ACP. Requirement for ACP as the obligatory donor of an acyl substrate for LpxA points to the importance of protein-protein interactions in substrate delivery (Raetz, 1993). Unlike *E. coli* LpxA, which utilizes β-hydroxymyristoyl-ACP (C14), *Leptospira interrogans* LpxA exhibits an absolute selectivity for 12-carbon β-hydroxylauroyl-ACP (Sweet et al., 2004). All of the active site and substrate binding residues (Fig. 3B) are conserved between these two enzymes with the exception that Lys76 of *E. coli* LpxA implicated in ACP binding is replaced by Gly

in the enzyme from *Le. interrogans*. This leads to the hypothesis that LpxA enzymes may be able to sense the slight variations in ACP conformation between acyl-ACPs of various fatty acyl chain lengths and modifications. Thus, investigation of ACP conformation under various conditions using Trp reporter groups will shed light on how ACP interacts with LpxA both globally and locally.

The hypothesis is that ACP undergoes conformational changes upon acylation, binding of divalent cation, and binding of partner enzymes. ACP flexibility, i.e. the ability of ACP to adopt certain recognizable conformations may be a significant driving force in conveying specificity to enzyme interactions. To test this hypothesis, Trp mutants of *V. harveyi* ACP were constructed and the effects of acylation, Mg^{2+} binding, and LpxA binding were examined using various conformational analysis techniques including CD, native PAGE, and steady-state fluorescence spectroscopy.

B. Results

1. Preparation and Functional Analysis of Mutant ACPs

The polypeptide chain of rACP contains one tyrosine (Tyr71), two phenylalanines (Phe28, Phe50), and no tryptophan. In order to use Trp as an intrinsic fluorescence probe of ACP microenvironment, site-directed mutagenesis was used to substitute Trp for residues in helix II (Ala45, Leu46, Phe50), helix III (Val72), and the loop region between helices I and II (Glu25). As indicated from the crystal structure of butyryl-ACP from *E. coli*, positions 25 and 45 reside on the surface of the protein, whereas positions 46, 50, and 72 are oriented towards the hydrophobic protein core (Fig. 20). Position 50, and to a lesser extent, positions 46 and 72 are highly conserved in ACPs from plants and bacteria, yet tolerate some conservative replacements. Positions 25 and 45 are less conserved and tolerate various non-conservative replacements (Fig. 4). Therefore, introduction of hydrophobic Trp residues at these positions is not expected to be deleterious to the effectiveness of ACP in supporting enzyme activities or the maintenance of overall ACP conformation.

The Trp mutants of ACP were overexpressed in *E. coli* BL21 cells as GST fusion proteins and purified to homogeneity after removal of the GST tag. Partially purified *V. harveyi* AAS exhibited normal activity with all mutants (Fig. 21A), which is supported by the fact that all ACPs could be quantitatively acylated by this enzyme (Fig. 22A). All ACP

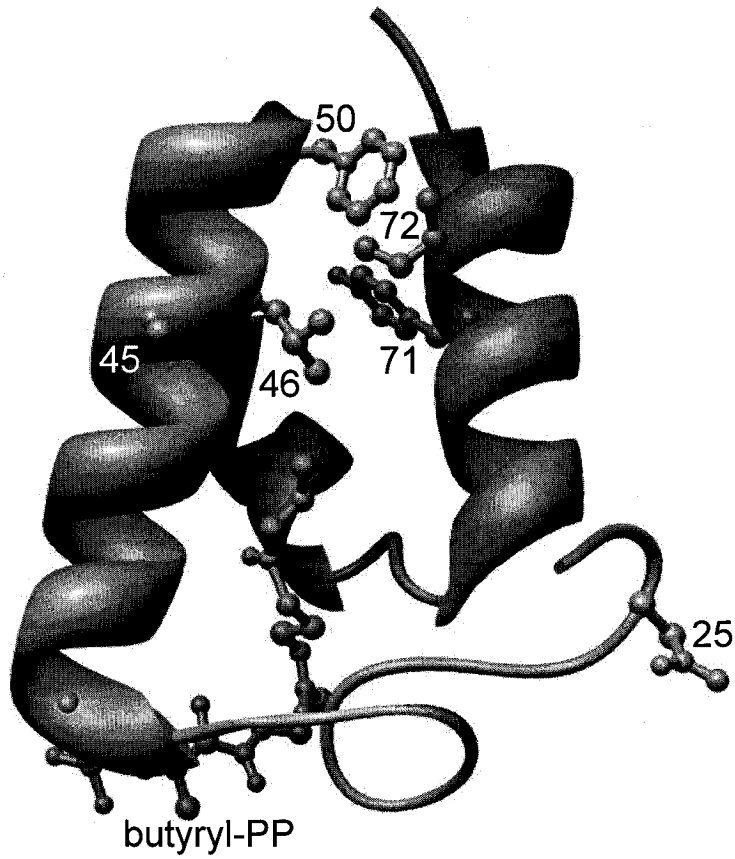

Figure 20. Ribbon representation of *E. coli* butyryl-ACP (Roujeinikova et al., 2002). Residues shown in ball and stick representation are those selected for site-directed mutagenesis on *V. harveyi* rACP (25, 45, 46, 50, 72), the lone Tyr (71), and butyrylated phosphopantetheine group. Helix I is hidden for clarity.

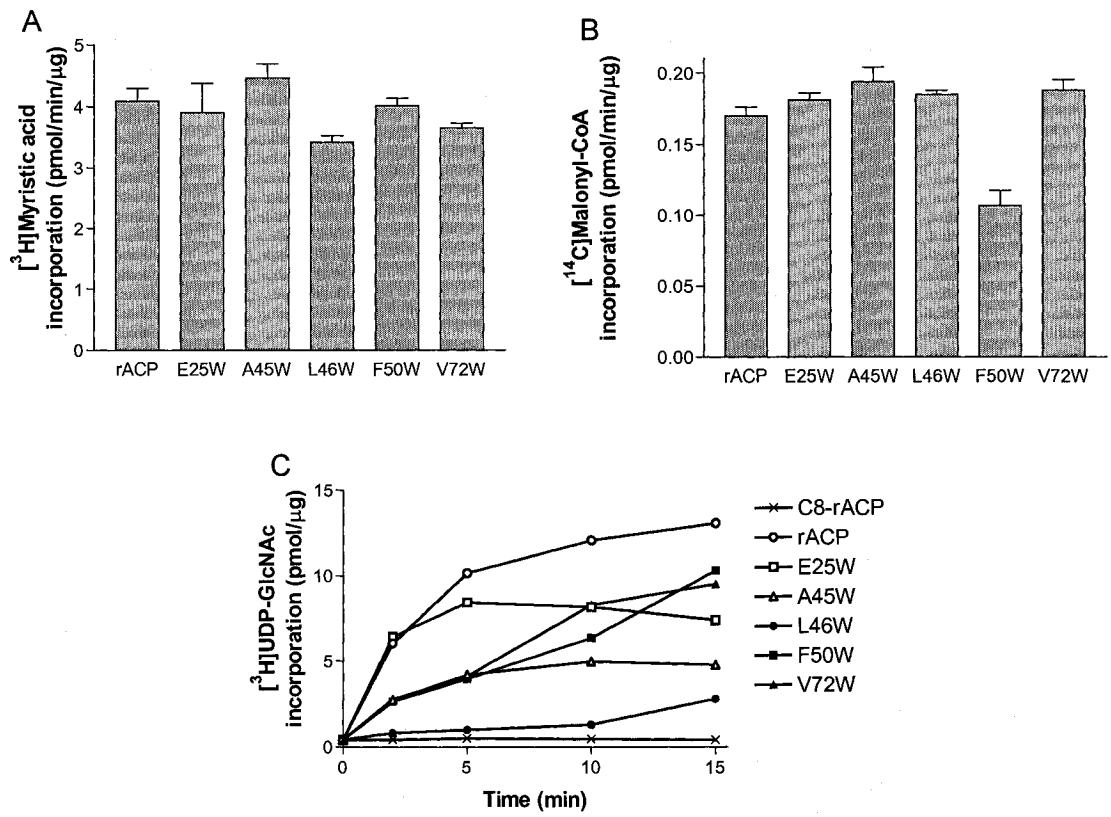

Figure 21. Enzyme activities with wild type and mutant ACPs. A) AAS activity at 37 °C. B) FAS activity at 37 °C. Shown in A and B are means and standard deviations from six assays. C) LpxA activity at 25 °C with β-hydroxymyristoylated wild type and mutant ACPs as well as octanoyl-rACP (C8-rACP).

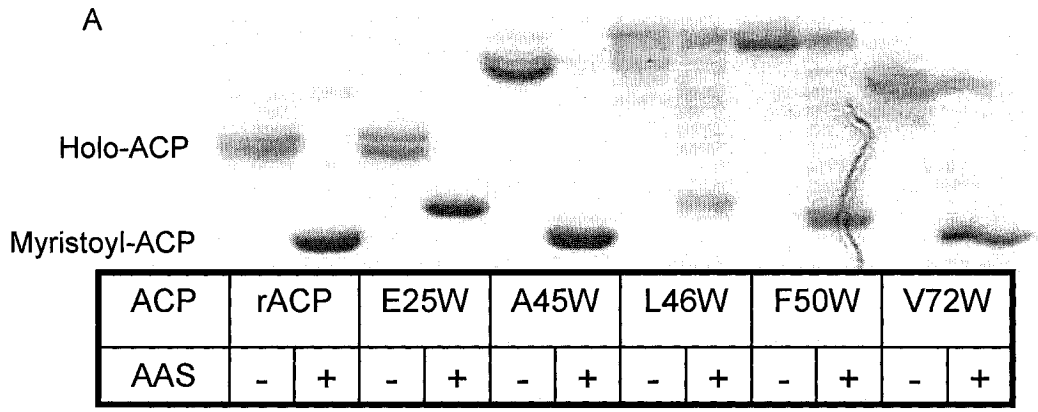

ACP	rACP		E25W		A45W		L46W		F50W		V72W	
AAS	-	+	-	+	-	+	-	+	-	+	-	+

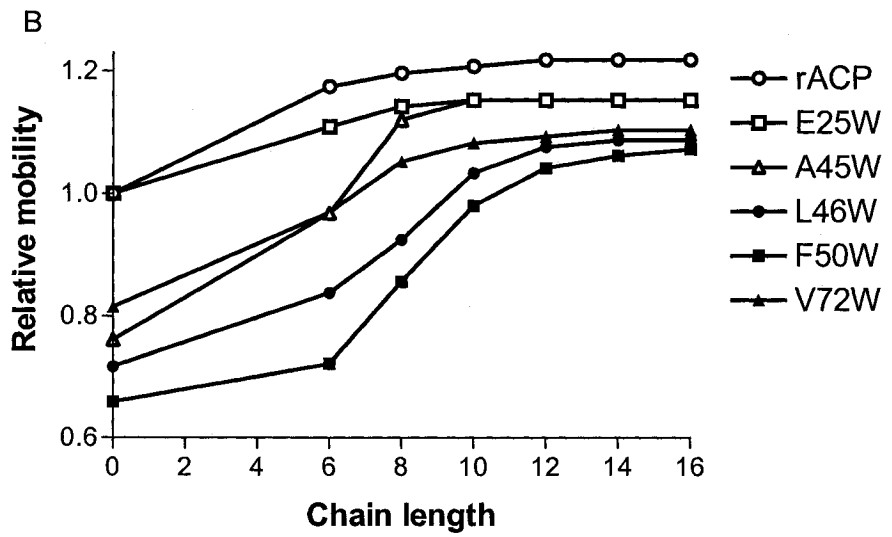

Figure 22. Hydrodynamic analysis of holo- and acyl-ACPs using conformationally sensitive native PAGE. A) ACPs (2 μg) were separated on a 20% polyacrylamide gel at pH 9.2 before or after ATP-dependent conversion into myristoyl-ACPs using AAS. B) Relative mobility of various holo- and acyl-ACPs relative to holo-rACP on 20% native gels at pH 9.2.

mutants were also effective substrates for partially purified *V. harveyi* FAS, although activity with F50W was less than with rACP and other mutants (Fig. 21B). LpxA required β-hydroxymyristoyl derivatives of wild type and mutant ACPs and had no activity with octanoyl-rACP (Fig. 21C). The initial rate of LpxA with acylated A45W, F50W, and V72W was over 50% lower than that with rACP and E25W. The activity of LpxA was least effectively supported by β-hydroxymyristoyl-L46W, which exhibited 7% of initial activity with rACP, suggesting the participation of helix II and interior residues in the overall reaction. Nevertheless, all mutants were substrates for LpxA despite variability in time required to reach equilibrium and effectiveness of the reaction.

2. Conformational Analyses of ACP Mutants Using Native PAGE and CD

Most holo- and myristoyl-ACP mutants had slower native PAGE mobility than their rACP counterparts except for holo-E25W and myristoyl-A45W, which migrated similar to the corresponding forms of rACP (Fig. 22A). However, all acylated ACPs exhibited an increased mobility relative to the holo forms, indicating that they were all able to interact with the covalently attached acyl chain to stabilize a more compact conformation. Conformational stabilization was also examined as a function of attached acyl chain length. A stepwise increase in migration of acyl-ACPs with acyl chains ranging from six carbons to 12 carbons in length was observed for all ACPs (Fig. 22B). This native PAGE protocol was not able to resolve differences in migration of acyl-ACPs with an acyl chain longer than 12 carbons.

CD was used to monitor changes in the secondary structure content of Trp mutant ACPs as a result of divalent cation binding or acylation. Like rACP, all mutants were largely unfolded at physiological pH and adopted a native-like conformation containing a significant amount of α-helix upon addition of millimolar levels of Mg^{2+} (Fig. 23). Octanoylation of rACP rendered a folded conformation that was insensitive to Mg^{2+}. Similarly, acylation of ACP mutants with β-hydroxymyristic acid caused ACP to attain native-like levels of helical structure in the absence of Mg^{2+}. Addition of Mg^{2+} had little further effect on CD spectra although some changes were noted for L46W and V72W.

In order to examine the effect of acyl chain length on Mg^{2+} dependence of ACP secondary structure, rACP was quantitatively acylated by AAS with saturated fatty acids of

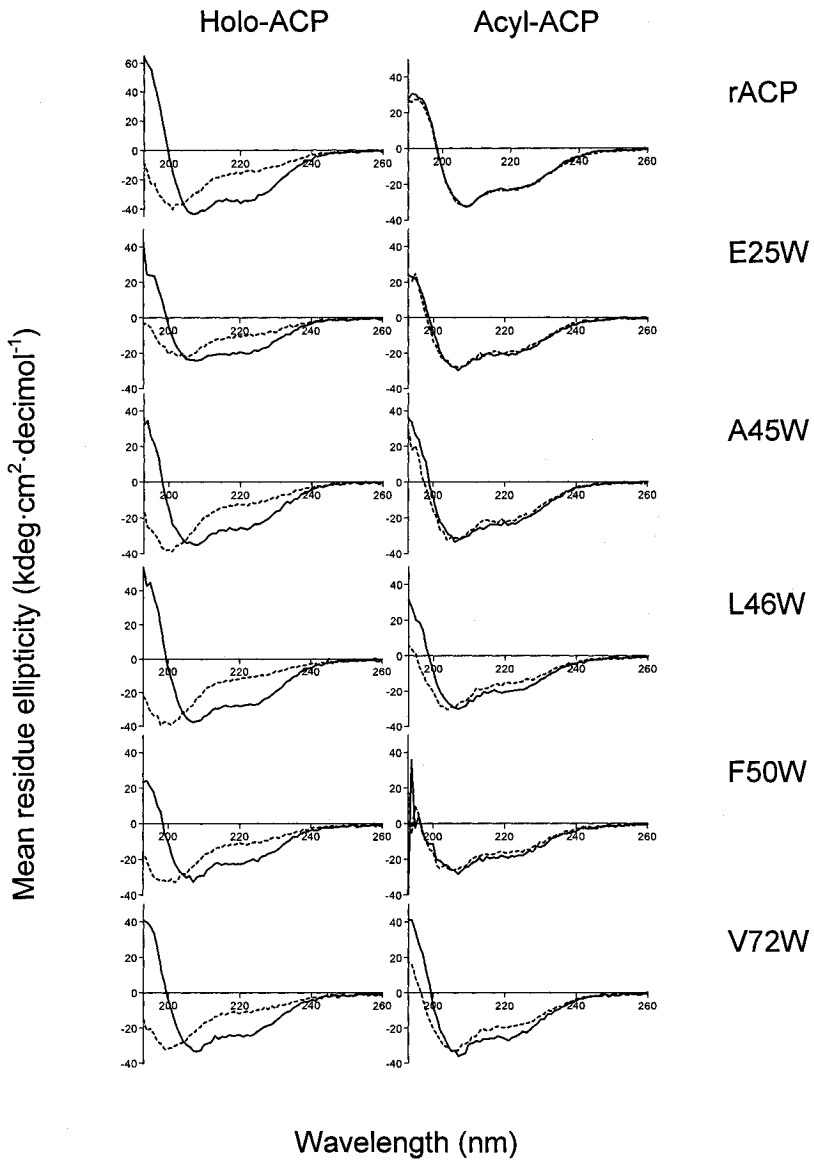

Figure 23. Effect of Mg^{2+} on secondary structure of holo- and acyl-ACPs. Shown are CD spectra of purified holo- and acyl-ACPs (3 μM) in the absence (dashed lines) and presence (solid lines) of $MgCl_2$. Wild type rACP was acylated with octanoic acid, while mutant ACPs were acylated with β-hydroxymyristic acid. $MgCl_2$ concentrations used were 2 mM for all except 1 mM for octanoyl-rACP.

six (hexanoic acid) to 14 carbons (myristic acid). Samples were heated to remove AAS and contaminating proteins from the completed reactions. The resulting heat-resistant acyl-ACPs were diluted 13-fold in 10 mM sodium phosphate containing 1 mM EDTA, pH 7 and analyzed using CD. The level of salts that originated from AAS reactions were decreased to lower than 8 mM after dilution, which likely had minimal effect on ACP conformation. Acylation caused a progressive increase in α-helical content of rACP as monitored by the mean residue ellipticity at 220 nm (Fig. 24), the extent of which could be correlated with the length of the covalently attached acyl group. In the presence of Mg^{2+}, acyl-rACP exhibited high helical content, which was independent of the length of the acyl group. In other words, a longer acyl chain may provide a larger hydrophobic surface for the interaction with the nonpolar residues in the fatty acid binding pocket so that ACP conformation is progressively stabilized with increasing chain length. A similar trend was observed with the five Trp mutants (data not shown). Thus, CD data are in general agreement with native PAGE results, showing that acylation stabilizes a more compact helical conformation of ACP.

3. Steady-State Fluorescence Emission Spectra of Tryptophan Mutants of ACP

The effect of Mg^{2+} on holo-ACP fluorescence emission was examined using purified Trp mutants of ACP (Fig. 25). Upon excitation at 280 nm, fluorescence responses of all holo-ACP mutants in the absence of Mg^{2+} were characterized by a broad emission peak with a full-width at half maximum value of 62-66 nm, a wavelength maximum (λ_{max}) centered near 355 nm, and a similar intensity, suggesting that Trp in all mutants resides in a similar polar microenvironment and probably exposed to the aqueous buffer when ACP is unfolded (Vivian and Callis, 2001). Upon addition of 10 mM $MgCl_2$, holo-L46W exhibited the most dramatic hypsochromic (blue) shift of nearly 40 nm as well as a two-fold increase in fluorescence intensity, suggesting a highly hydrophobic environment for Trp at this position. Similarly, holo-F50W and holo-V72W responded to Mg^{2+} with blue shifts of 16 and 20 nm, respectively, despite a modest decrease in integrated intensity, also suggesting a transfer of Trp at these two positions from a hydrophilic to a more apolar environment during Mg^{2+}-induced ACP folding. By contrast, Mg^{2+} caused significant increase in intensity of holo-E25W and holo-A45W fluorescence with not more than 3 nm of bathochromic (red) and hypsochromic shifts, respectively. The wild type rACP exhibited low-intensity fluorescence

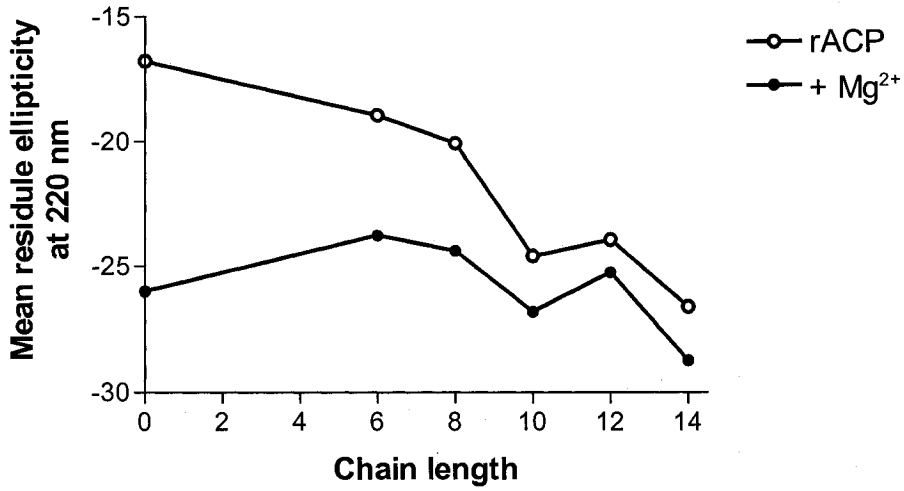

Figure 24. Effects of acylation and Mg^{2+} on helical content of rACP. CD spectra of 3 μM rACP from heat-treated AAS reactions diluted in 10 mM Na^{+}-phosphate, pH 7.0, 1 mM EDTA were recorded in the absence and presence of 10 mM $MgCl_2$. Shown are normalized CD signals at 220 nm.

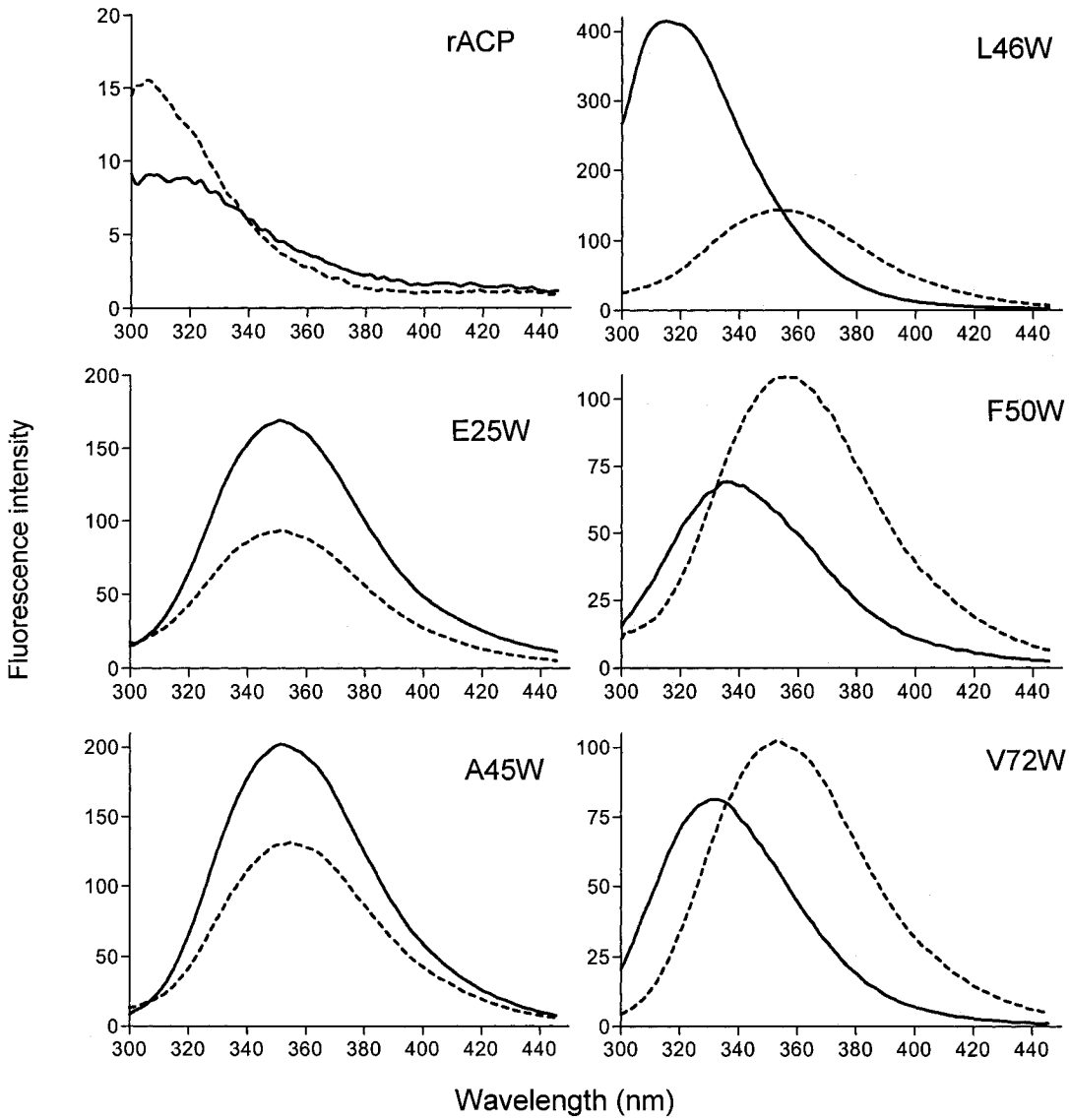

Figure 25. Fluorescence emission spectra of wild type and mutant ACPs. Purified holo-ACPs were diluted to 1 μM in 10 mM Na^+-phosphate, pH 7.0. Fluorescence emission spectra were recorded with excitation at 280 nm in the absence (dashed lines) and presence (solid lines) of 10 mM $MgCl_2$.

centered between 300 and 310 nm both in the absence and presence of Mg^{2+}, presumably as a result of Tyr excitation at 280 nm.

Fatty acylation produced a similar but not identical effect to that of Mg^{2+}. Acylated Trp mutants of ACP were prepared from a reaction catalyzed by AAS as described above and diluted for fluorescence emission spectra measurement with excitation at 280 nm (Fig. 26-27). The control reaction contained all reagents except fatty acids so that holo-ACPs were not converted to acyl forms. Proteins from the AAS preparation were removed from ACP by precipitation after heat-induced denaturation. In the absence of Mg^{2+}, acylated E25W and A45W both experienced an increase in intensity and a small red (E25W) or blue (A45W) shift of up to 3-4 nm (Fig. 26). Acylation of L46W, F50W and V72W all exhibited blue-shifted spectra with slight change in integrated intensities for L46W (Fig. 27) and V72W, and up to 50% decrease in intensity for F50W (Fig. 26). The extent to which acylation of A45W, L46W, F50W, V72W, and to a lesser degree E25W, induced fluorescence change was correlated with the number of carbons the acyl group contained.

A summary of the effects of Mg^{2+} and fatty acylation on fluorescence of all Trp mutant is shown in Fig. 28. Consistent with CD experiments, fluorescence intensity data indicate that acylation with longer chain fatty acids progressively causes ACP to fold and become independent of Mg^{2+} (Fig. 28B). Comparison of positions of emission maxima, however, suggests that acylation provides Trp with a microenvironment that is distinguishable from binding of Mg^{2+}. Although attachment of long chain fatty acids to E25W and A45W caused these two mutants to exhibit an emission maximum independent of Mg^{2+}, the difference between emission maxima of acylated L46W, F50W, and V72W with (Fig. 28D) and without (Fig. 28C) Mg^{2+} decreased with increasing chain length but persisted with a gap of about 8 nm even in the case of myristoylation.

CD and fluorescence emission spectra are two independent methods of monitoring protein conformational transition. The former is a measure of overall secondary structure whereas the latter monitors localized changes in protein tertiary structure. Mean residue ellipticity of holo-L46W at 220 nm in response to magnesium concentration was monitored and expressed as fraction of folded protein molecules in the population. A sigmoidal curve with a midpoint around 1.2 mM Mg^{2+} was observed (Fig. 29), which is consistent with a two-state folding model (Pace and Scholtz, 1997) though indicating a requirement for higher Mg^{2+} levels by L46W than by rACP (Fig. 13-14). The conformational transition profile

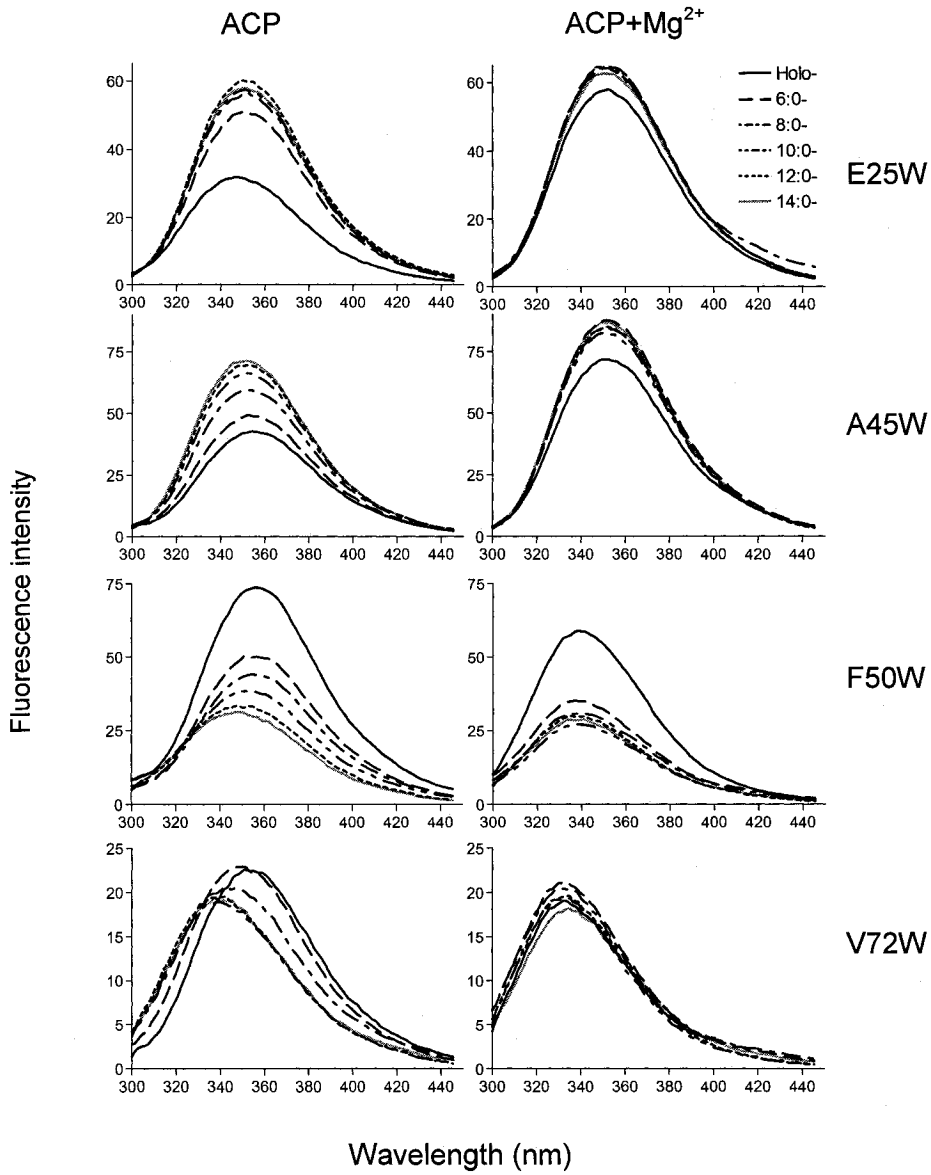

Figure 26. Fluorescence emission spectra of holo- and acyl-ACP mutants. ACPs from heat-treated AAS reactions were diluted to 1 μM in 10 mM Na^+-phosphate, pH 7.0 containing 1 mM EDTA. Fluorescence emission spectra were recorded with excitation at 280 nm in the absence (left) and presence (right) of 10 mM $MgCl_2$.

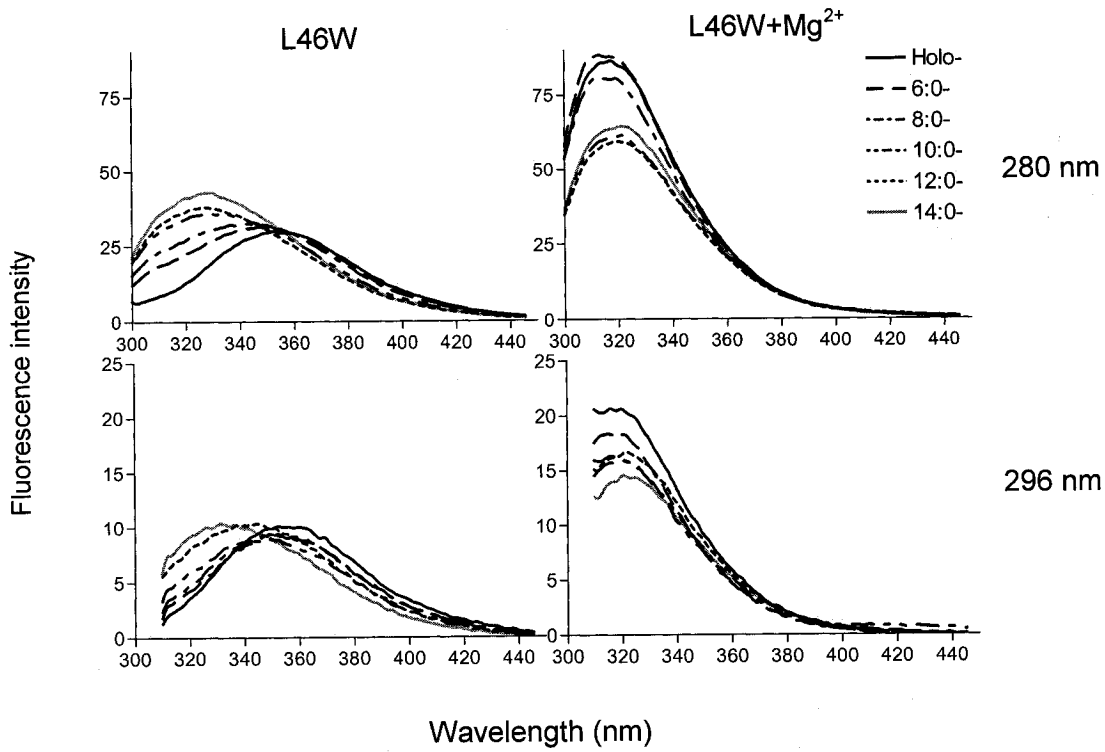

Figure 27. Fluorescence emission spectra of holo- and acyl-L46W. L46W from heat-treated AAS reactions was diluted to 1 μM in 10 mM Na^+-phosphate, pH 7.0 containing 1 mM EDTA. Fluorescence emission spectra were recorded with excitation at 280 nm (upper) and 296 nm (lower) in the absence (left) and presence (right) of 10 mM $MgCl_2$.

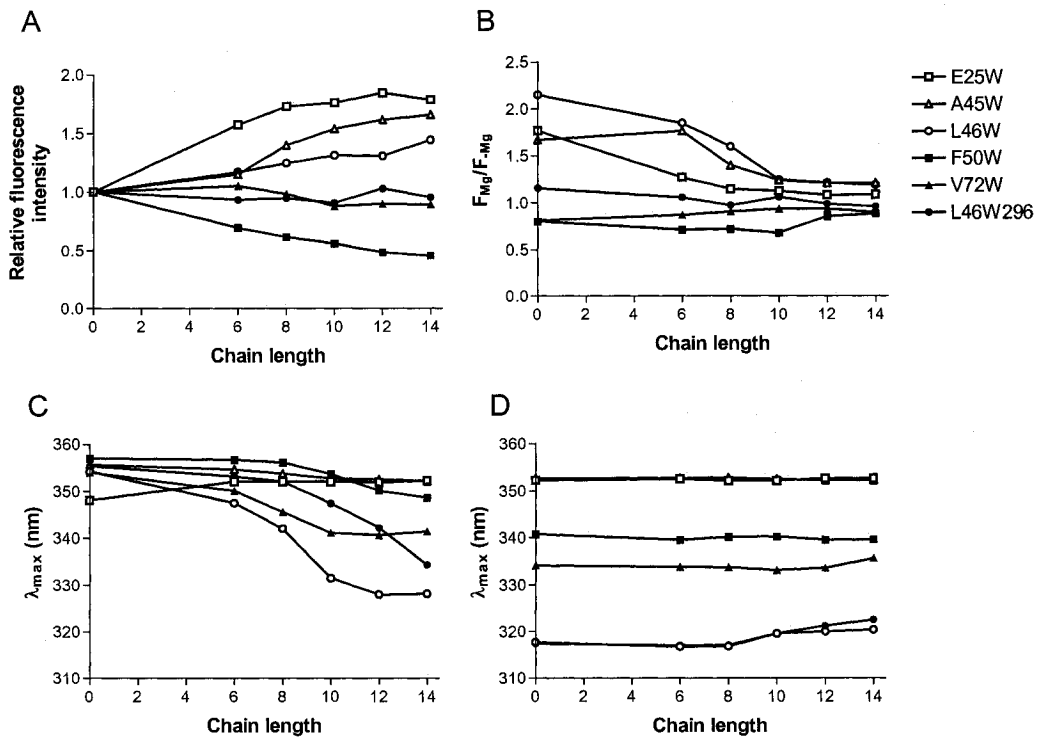

Figure 28. Effects of acylation and Mg^{2+} binding on fluorescence intensities and wavelength maxima of tryptophan mutants of ACP. A) Fluorescence intensities of acyl-ACPs relative to holo-ACPs in the absence of Mg^{2+}. B) Fluorescence intensities of acyl-ACPs in the presence of 10 mM $MgCl_2$ relative to the corresponding acyl-ACPs in the absence of Mg^{2+}. Integrated fluorescence intensity values were obtained as areas under the curves from 300 to 400 nm for excitation at 280 nm, and from 315 to 415 nm for excitation at 296 nm. C) Emission wavelength maxima of holo- and acyl-ACPs in the absence of Mg^{2+}. D) Emission wavelength maxima of holo- and acyl-ACPs in the presence of 10 mM $MgCl_2$.

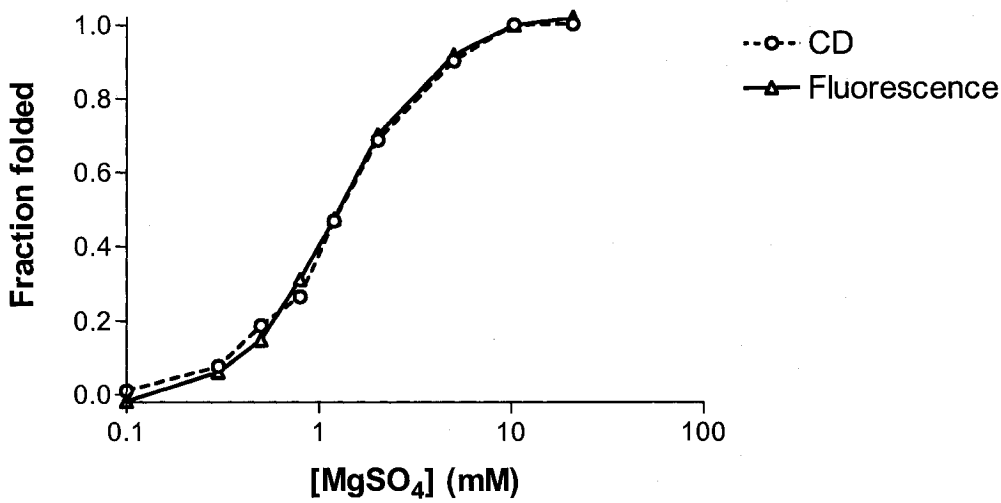

Figure 29. Mg^{2+}-induced ACP structural transition monitored by CD and fluorescence. Holo-L46W was diluted to 10 μM in 10 mM Na^{+}-phosphate, pH 7.0 in 0.1 mM EDTA and titrated with $MgSO_4$ to 20 mM. CD and fluorescence signals were converted to the fraction of folded molecules using the expression $(X-X_{min})/(X_{max}-X_{min})$, where X is CD at 220 nm or fluorescence emission at 320 nm with excitation at 296 nm.

monitored by fluorescence under the same conditions corresponded well with the CD data, suggesting not only that the folding of holo-L46W is a cooperative two-state process, but also that no stable folding intermediate is detectable by these methods.

4. Examination of Tryptophan Exposure by Fluorescence Quenching

Wavelength maximum provides limited information about the polarity of a Trp microenvironment, but does not directly indicate whether a particular Trp residue is exposed on the protein surface or buried in the inner core. Fluorescence quenching studies were carried out using soluble quenchers to further examine the solvent accessibility of Trp in these ACP mutants (Fig. 30, Table 3). Acrylamide (Eftink and Ghiron, 1976) and iodide (Lehrer, 1971) are efficient indole fluorescence quenchers commonly used in aqueous solutions to quench Trp fluorescence. Polar uncharged acrylamide has effective access to some buried fluorophores, while iodide only has access to fluorophores on the protein surface as well as those in a positively charged environment as a result of electrostatic interaction. Likewise, cesium ions (Eftink and Ghiron, 1981) can quench fluorescence of surface fluorophores and those in negatively charged surroundings. Two types of quenching occur in solute perturbation: collisional (or dynamic) quenching described by the Stern-Volmer quenching constant K_{SV} and static quenching described by the constant V (Lakowicz, 1983). K_{SV} obtained from the slope of a linear Stern-Volmer plot describes the extent of quenching as a result of quencher molecules colliding with excited-state fluorophore, which is proportional to the product of a bimolecular diffusion rate constant k_d and quenching efficiency γ. Static quenching constant V accounts for the exponential component of an upward curving Stern-Volmer plot, and represents an active volume element surrounding the excited fluorophore (Eftink and Ghiron, 1981). Intuitively, the value of V reflects the likelihood of a quencher molecule being within this volume element at the time of photon absorption, leading to instantaneous quenching.

Fluorescence quenching of holo forms of E25W, A45W and L46W was monitored at 360 nm with excitation at 280 nm in the presence of Mg^{2+} to ensure a folded ACP conformation with minimal structural perturbation by added quenchers (Fig. 30). Little change in band shape or wavelength maximum of L46W fluorescence emission was observed with the levels of any of the quenchers tested. A45W emission was not shifted in the presence of acrylamide or iodide, but displayed a 7 nm blue shift in the presence of

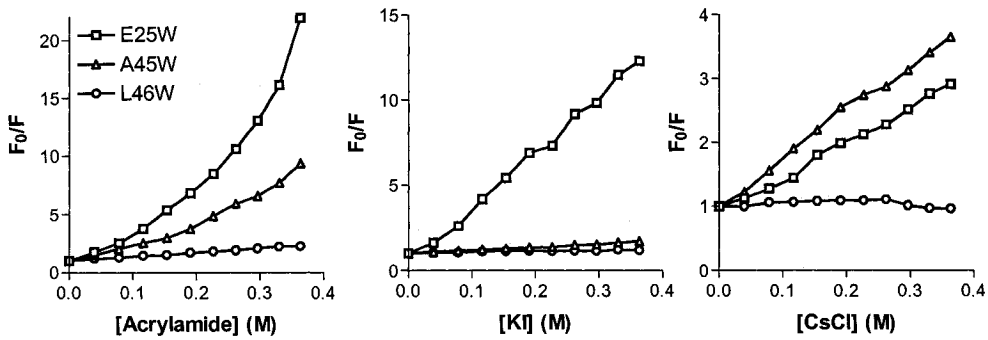

Figure 30. Fluorescence quenching of holo-ACPs in the presence of Mg^{2+}. Stern-Volmer analyses of the quenching of 1 μM holo-ACP mutants in the presence of 10 mM $MgCl_2$ by acrylamide, iodide and cesium, performed at 25 °C in 10 mM Na^+-phosphate, pH 7.0 with excitation at 280 nm and emission at 360 nm to minimize contribution from the tyrosine residue. Shown are the ratios of fluorescence intensities in the absence (F_0) versus the presence (F) of indicated concentrations of each quencher. Values have been corrected for small increases in volume caused by addition of quencher stock solutions.

Table 3. Fluorescence quenching parameters for holo-ACP mutants in the presence of Mg^{2+}.

Quencher	ACP	K_{SV} (M^{-1})	V (M^{-1})	Quenching %[3]
Acrylamide	E25W	23±1	2	85.3
	A45W	7.3±0.8	2.5±0.2	73.3
	L46W	0.48±0.07	2	41.4
Iodide	E25W	25±2	0.6±0.2	85.5
	A45W	1.4±0.4	0.3±0.3	26.3
	L46W	0.60±0.05	0	13.3
Cesium	E25W	5.1±0.1	0	49.7
	A45W	7.4±0.1	0	60.8
	L46W	0.13±0.08	0	8.2

Quenching data in Fig. 29 were fitted to a one-component model (Eq. 2) to obtain K_{SV} and V values that are listed with standard errors from curve fitting. Static quenching constant was assumed to be 2 or 0 in some cases as indicated.

[3] Extent of quenching by 0.2 M of quenchers was observed at 360 nm.

cesium (data not shown). E25W also exhibited a 4-5 nm blue shift in the presence of each of the three quenchers tested, which may reflect a collisional quenching mechanism in which lower energy emission is preferentially quenched, rather than a global protein conformational change (Lakowicz, 2000). Acrylamide quenching experiments yielded exponential Stern-Volmer plots, clearly indicating the existence of a static quenching component. The static quenching constant V was fitted in the case of A45W or assumed to be 2 to facilitate curve fitting of datasets for E25W and L46W (Table 3). This appears to be a reasonable assumption since V values are often found to be in the range of 1-3 M^{-1}, corresponding to a volume element having a radius reaction distance of ~10 Å (Eftink and Ghiron, 1981).

The collisional quenching constant K_{SV} for acrylamide was found to be higher with E25W than with A45W or L46W, suggesting that Trp at position 25 is the most exposed of the three. Iodide quenching yielded predominantly linear Stern-Volmer curves with K_{SV} parameters exhibiting a similar trend as quenching by acrylamide (Fig. 30). K_{SV} of E25W for acrylamide was comparable to that for iodide and over four times that for cesium, suggesting that the Trp at position 25 is completely exposed to the solvent, which is consistent with the emission wavelength maximum of E25W both in the absence and presence of Mg^{2+}. The extent of quenching by 0.2 M of quenchers was in general agreement with the K_{SV} parameters (Table 3).

Although the efficiencies (γ) of fluorescence quenching of free Trp in solution for acrylamide and iodide are unity, which is five times that for cesium (Eftink and Ghiron, 1981), quenching of A45W by iodide was dramatically lower than by acrylamide or cesium, suggesting that Trp45 is partially buried in the folded protein, where the uncharged acrylamide could diffuse but the negatively charged iodide had little access. Interestingly, K_{SV} for the inefficient quencher cesium with A45W was not only comparable to that of acrylamide, but also higher than that of E25W for cesium, which likely resulted from binding of cesium to acidic sites near Trp at position 45, where effective quenching could occur by a mechanism that does not involve free diffusion. Thus, diminished quenching by I^- and enhanced quenching by Cs^+ indicate a negative charge barrier shielding the Trp microenvironment at position 45. The polar surroundings of Trp as indicated by the emission wavelength maximum of A45W are likely provided more by the predominant negatively charged residues in helices I and II than by the aqueous solvent.

Among all three mutants, fluorescence of L46W in the presence of Mg^{2+} was the least effectively quenched by all three compounds which, consistent with its blue-shifted wavelength maximum, indicates that Trp at 46 is buried in a nonpolar microenvironment in a folded ACP. Interestingly, a downward curvature was observed in the Stern-Volmer plot when ionic quenchers were used, suggesting that the population of fluorophores is heterogenous. The modified Stern-Volmer plot (Eq. 3) was employed to confirm this, estimating the fraction of L46W fluorophores accessible (f_a) to iodide or cesium at 0.2 and 0.1, respectively. The accessible fraction value, when significantly lower than 1, indicates that there exists more than one class of fluorophores with quenching constants differing by a factor of four or more (Eftink and Ghiron, 1981), all contributing to the total fluorescence. By contrast, the f_a values for E25W and A45W using various quenchers and for L46W using acrylamide were found to be near 1 (ranging from 0.7 to 1.3). This suggests that the entire population of fluorophores are accessible to quenchers under these conditions.

Although Trp is the major environmentally-sensitive intrinsic fluorophore, the contribution from other aromatic residues needs to be taken into consideration when interpreting fluorescence results. Phe emission can be ignored since the fraction of light absorbed by Phe is negligible above 275 nm, and the quantum yield of Phe is more than one order of magnitude lower than that of Trp and Tyr. With excitation at 280 nm, both Tyr and Trp are excited, whereas protein fluorescence produced by excitation at 296 nm is due almost entirely to Trp. Subtraction of emission spectra for excitation at 296 nm from those at 280 nm, after normalization at 400 nm where only Trp fluoresces, yielded the profiles of Tyr emission. In the absence of Mg^{2+}, there was only a weak Tyr contribution to fluorescence of holo-L46W that accounted for about 6% of total fluorescence with excitation at 280 nm (Fig. 31A), suggesting that the singlet-singlet energy transfer from Tyr to Trp is efficient. By contrast, Mg^{2+} caused a significant Tyr component that contributed almost 30% to holo-L46W fluorescence at λ_{ex} of 280, suggesting that radiationless singlet energy transfer from Tyr to Trp is less efficient in a folded holo-L46W. Like that of holo-L46W without Mg^{2+}, Tyr components of all other holo-ACP mutants were found to be weak both in the absence and presence of Mg^{2+} (data not shown). A closer examination of Tyr emission of acyl-L46W with increasing fatty acyl chain length indicated a progressive decrease in resonance energy transfer without Mg^{2+} and an increase with Mg^{2+} (Fig. 31B), which resulted in blue-shifted emission spectra with 280-nm excitation (Fig. 27-28). Thus,

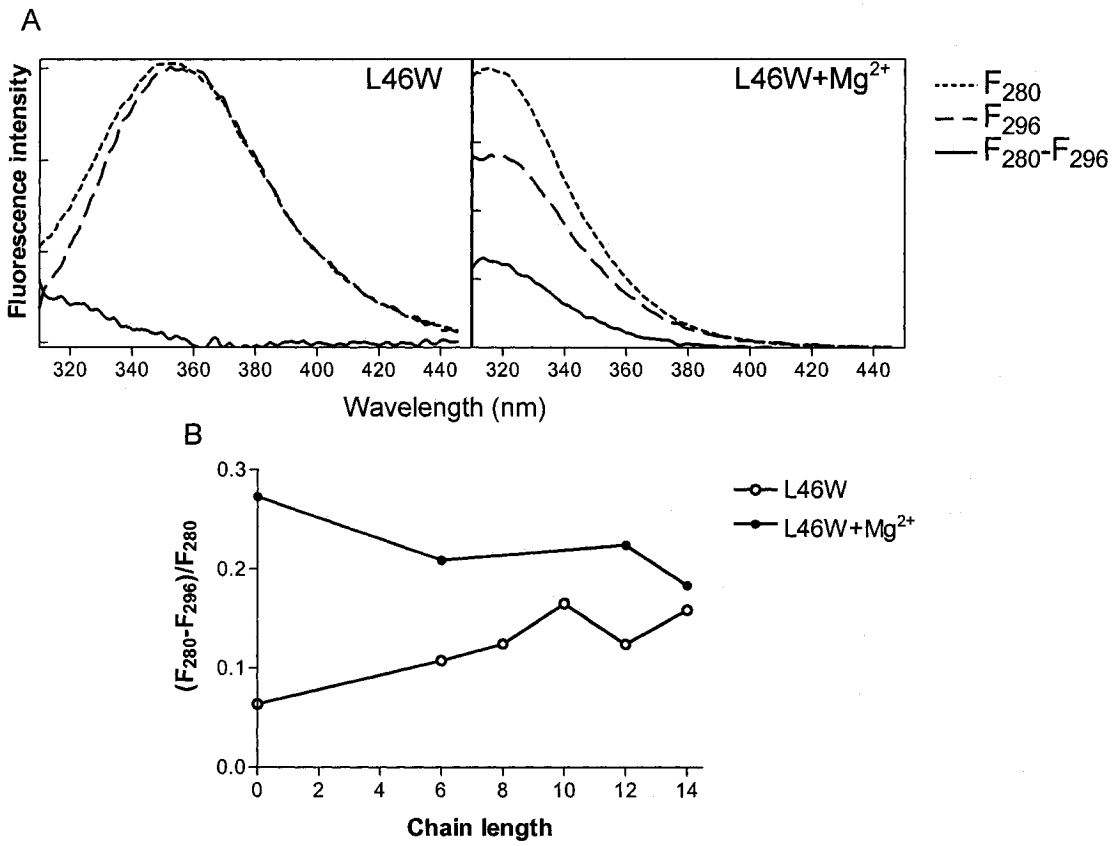

Figure 31. Effects of Mg^{2+} binding and acylation on tyrosyl contribution to intrinsic fluorescence of L46W. A) Normalized fluorescence emission profiles of holo-L46W with and without 10 mM $MgCl_2$ with excitation at 280 and 296 nm, and their difference spectra. B) The areas under the curves from 315 to 415 nm of the difference spectra for the indicated acyl-L46W ACPs are shown relative to the normalized spectra for excitation at 280 nm.

consistent with fluorescence intensity and peak wavelength data, a decrease in Mg^{2+} dependence with increasing chain length was also observed by monitoring the Tyr contribution.

5. Interaction between LpxA and Holo-ACP

E. coli LpxA contains ten Tyr residues but no intrinsic Trp; this makes it an excellent ACP partner enzyme to study using fluorescence techniques as no mutagenesis or chemical modification of LpxA is required. With excitation at 296 nm, the observed fluorescence should all be produced by the lone Trp on mutant ACPs. Like Mg^{2+}, adding purified LpxA enhanced the fluorescence intensities of holo-E25W and holo-A45W (data not shown) and shifted holo-L46W (Fig. 32) and holo-V72W (data not shown) peaks to lower wavelengths in a concentration dependent manner, clearly indicating that LpxA binds to holo-ACP and causes changes in the environment of each Trp.

To assess whether changes in fluorescence behavior of tryptophan mutants of ACP result from an ACP-folding event or from direct contact of Trp with the LpxA protein, data need to be interpreted in light of spatial location of each Trp residue in a native ACP scaffold. The concentration-dependent effect of LpxA on L46W fluorescence was similar to that of Mg^{2+} binding. Quenching studies have demonstrated that Trp in L46W is buried in the hydrophobic core of ACP (Fig. 30), consistent with the structure of butyryl-ACP from *E. coli* (Fig. 20), suggesting that holo-L46W becomes folded upon contact with LpxA. Similar conclusions were drawn for holo-E25W and holo-V72W, for which the effect of LpxA was similar to that of Mg^{2+}. Intriguingly, holo-A45W exhibited not only an enhanced fluorescence emission in response to LpxA as with Mg^{2+}, but also a blue shift of about 5 nm, which was distinct from the effect of Mg^{2+}. Fluorescence quenching analysis indicates that Trp in A45W is not fully buried (Fig. 30), which is in general agreement with the fact that Ala45 in folded *E. coli* ACP constitutes part of the acidic/hydrophobic patch on the protein surface. No LpxA-induced blue shift was observed with Trp of E25W, which appears to be a surface residue (Fig. 30) and resides on the opposite side of the ACP molecule according to the *E. coli* ACP structure (Fig. 20). Thus, changes in holo-A45W fluorescence behavior caused by LpxA are likely the consequences of both an ACP-folding event and a local interaction between Trp and surface residues on LpxA.

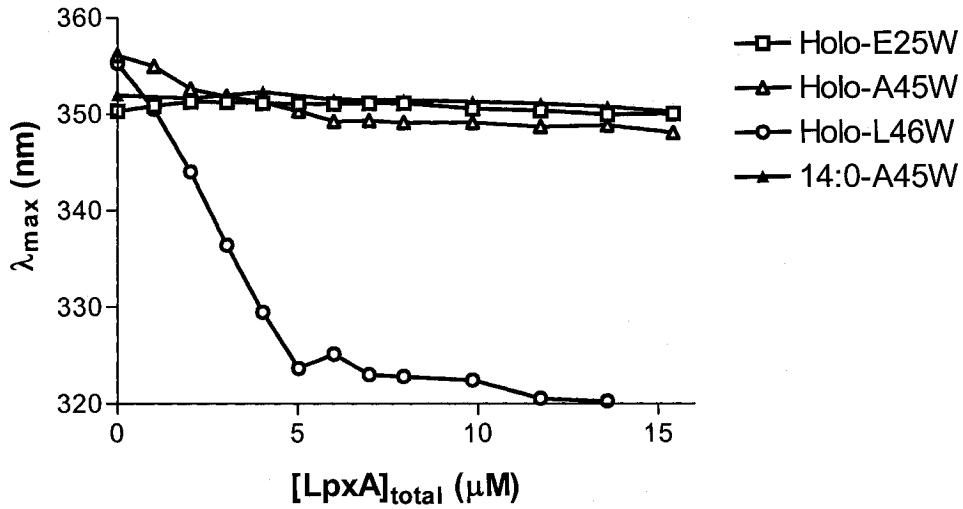

Figure 32. Fluorescence indicator of LpxA interaction with ACP. ACPs (4 μM) in 10 mM Na^+-phosphate, pH 7.0, 1 mM EDTA were titrated with LpxA in the same buffer at 25 °C. Wavelength maximum of fluorescence emission was plotted as a function of LpxA concentration. Excitation wavelength was 296 nm.

Distinct effects of LpxA and Mg^{2+} on holo-A45W fluorescence were further evaluated by adding Mg^{2+} to holo-ACP alone and to the ACP-LpxA complex (Table 4). The effect of Mg^{2+} on holo-ACP emission with excitation at 296 nm was comparable to that observed with excitation at 280 nm (Fig. 26-27). Mg^{2+} had some further effect on E25W, L46W, and V72W in the presence of LpxA, probably as a result of uncomplexed ACP becoming folded. Interestingly, Mg^{2+} did not cause any further change in maximum wavelength of A45W (Table 4) despite a further increase in intensity (data not shown). Mg^{2+} had little effect on holo-A45W at saturating LpxA level (4 μM and 16 μM for holo-A45W and LpxA, respectively), where the concentration of uncomplexed ACP was presumably minimal (data not shown). The slight blue shift of A45W emission peak cause by Mg^{2+} alone (2 nm) was smaller than that caused by LpxA (5 nm), indicating that Trp45 resides in distinct environments in the presence of Mg^{2+} and LpxA. Similar changes in wavelength maximum were not observed with myristoyl-A45W (Fig. 32), perhaps suggesting a different binding mechanism for holo and acyl forms of ACP. Overall, these results suggest that Trp45 may be present at the molecular interface, allowing it to be in direct contact with residues on the surface of LpxA.

Although the binding between ACP and LpxA is presumably weak and difficult to characterize, the high sensitivity of fluorescence spectroscopy made the study of micromolar levels of binding partners possible. It also dispenses with the need for laborious physical separation of bound and free states by monitoring fluorescence changes upon binding. Data collected during titration of LpxA with holo-ACPs were fitted to a hyperbolic binding curve (Eq. 4), assuming that each LpxA monomer contains a single ACP binding site. Although large errors precluded quantitative interpretation, nonlinear regression curve fitting suggested dissociation constant (K_d) values in the low micromolar range for E25W, A45W, and L46W (data not shown).

C. Discussion

1. Introduction of Tryptophan Residues into ACP Using Site-Directed Mutagenesis

Trp has long been recognized as an intrinsic fluorophore for probing protein internal electrostatics, i.e. the polarity of the local environment of the indole side chain (Lakowicz, 1983). Under various conditions a protein may undergo conformational and structural

Table 4. Effect of Mg^{2+} on holo-ACP and ACP-LpxA complex.

ACP type	Fluorescence emission wavelength maxima (nm)			
	Holo-ACP	ACP+Mg^{2+}	ACP+LpxA	ACP+LpxA+Mg^{2+}
E25W	351	353	352	352
A45W	356	354	351	352
L46W	355	317	322	318
V72W	354	334	339	335

$MgCl_2$ (10 mM) was added to 10 μM holo-ACP alone or 8 μM holo-ACP in the presence of 17 μM LpxA. Shown are wavelength maxima (nm) of fluorescence emission spectra when exciting at 296 nm.

changes, which often lead to alterations of Trp fluorescence properties such as emission intensity, wavelength maximum (λ_{max}), band shape, anisotropy, fluorescence lifetimes, and energy transfer (Royer, 1995). Steady-state emission spectra are the most readily measured among all fluorescence properties, from which quantitative parameters such as emission intensity and wavelength maximum are derived. Wavelength maximum of Trp in proteins reported to date ranges from ~ 355 nm in glucagons, where both faces and the edge of the indole side chain are exposed to water, to ~ 308 nm in azurin where Trp has no exposure to water (Vivian and Callis, 2001). An increase in fluorescence intensity can also occur as the microenvironment of Trp becomes more hydrophobic, which may or may not be accompanied by a shift of the fluorescence band to higher energy (lower wavelengths) (Pace, 1986; Schmid, 1997).

ACP contains no intrinsic Trp, which allows introduction of a single Trp at any position using site-directed mutagenesis to provide an environmental fluorescence probe of ACP local structure. Unlike many extrinsic fluorescence probes whose applications are restricted to the protein surface (Worsham et al., 2003), the amphipathic nature of Trp allows its role of intrinsic probe to be fulfilled both on the outside and the inside of the protein. By employing the high sensitivity of fluorescence, alterations in the molecular environment of Trp residue as a result of protein conformational changes can be determined and analyzed even when the conformational changes are minor and local, and may not otherwise be detected. Trp shares some chemical similarity with other aromatic or apolar residues and is commonly substituted for Tyr and Phe in closely related homologues (Li and Meighen, 1995). Thus, introduction of Trp in ACP or other proteins of interest is not expected to dramatically alter its function or three-dimensional fold.

Residues of *V. harveyi* rACP were selected to be mutated to Trp at various locations, i.e. protein surface (Glu25 and Ala45) vs protein inner core (Leu46, Phe50, and Val72), as well as helix II (Ala45, Leu46, and Phe50) vs helix III (Val72) and loop region (Glu25). Trp residues at these positions appear to be valid environmental probes with minimal disturbance of overall protein conformation for several reasons. First, like wild type rACP, all mutants exhibited unfolded conformation as monitored by CD and adopted comparable α-helical content upon addition of Mg^{2+} (Fig. 23). Second, covalently attached long chain acyl groups were able to interact with all mutant ACPs, modifying their hydrodynamic properties to a similar extent (Fig. 22) and also dispensing the requirement for Mg^{2+} to adopt

a highly helical conformation (Fig. 23). Third, none of the mutations significantly hampered the activity of AAS (Fig. 21A), an enzyme known to require a native conformation of ACP (Flaman et al., 2001), indicating that these mutants efficiently interact with the partner enzyme despite placement of a bulky Trp side chain on protein surface or in the recognition helix II. FAS had comparable activity with all Trp mutants except F50W (Fig. 21B), likely as a result of the alteration of the highly conserved Phe50 that is thought to be directly involved in fatty acid binding (Mayo and Prestegard, 1985). Finally, the fluorescence properties of each Trp residue in the presence of Mg^{2+} were consistent with its predicted environment in a folded ACP.

Despite being unfolded at neutral pH, *V. harveyi* ACP presumably follows a two-state folding model with rapid interconversion between states, similar to *E. coli* ACP (Kim and Prestegard, 1989), spinach ACP-I (Kim and Prestegard, 1990a), and frenolicin ACP (Li et al., 2003). Thermodynamic analysis has demonstrated that *E. coli* ACP exhibits a near two-state unfolding both in the absence and presence of Ca^{2+} (Horvath et al., 1994). No multiphasic change was observed during pH titration of *V. harveyi* rACP (Keating et al., 2002) or fluorescence quenching of Trp mutants of ACP (Fig. 30). Complete correlation of Mg^{2+} responses of L46W monitored by CD and fluorescence is also consistent with the dynamic two-state model with no stable intermediate in the ACP folding pathway (Fig. 29). Thus, the conformational changes captured by steady-state biophysical techniques employed in the current study can be understood as the shifting of equilibrium between two states.

2. Probing Tryptophan Exposure by Soluble Fluorescence Quenchers

Exposure of these Trp residues to solvent was also investigated by fluorescence quenching analyses using a water-soluble uncharged quencher acrylamide and ionic quenchers iodide and cesium. Findings were in general agreement with the prediction of the local environment of these residues in a folded ACP scaffold. With excitation at 280 nm, Tyr71 likely also contributes and is presumably accessible to quenchers as it resides in helix III with one edge in contact with interior of ACP and the other edge exposed to the solvent according to the butyryl-ACP structure from *E. coli* (Fig. 20). This is also consistent with the solution structure of *B. subtilis* ACP (Xu et al., 2001) and absorption spectroscopy of *E. coli* ACP (Rock, 1983) that demonstrated the partially buried nature of the Tyr71 side chain. It has been reported that Tyr fluorescence quenching behavior is in all respects similar to the

Trp fluorescence quenching (Brown et al., 1977). Fluorescence emission from holo-rACP containing the lone Tyr71 was less than one tenth of the total fluorescence from a Trp mutant of ACP (Fig. 25). Thus, the tyrosyl component of ACP fluorescence can be treated as a second quenchable fluorophore that has minor contribution to fluorescence emission in the wavelength range where Trp emits. Therefore, the general conclusions drawn from current quenching studies should still hold true when quenching experiments are carried out with excitation at 295 nm or higher where excitation of Tyr is negligible.

Millimolar levels of Mg^{2+} were included in quenching experiments to ensure a folded conformation of holo-ACP. It has been previously demonstrated that high levels of monovalent salt cause rACP to fold in a similar fashion as Mg^{2+} (Keating et al., 2002). Thus, addition of ionic monovalent quenchers KI and CsCl was not expected to further alter ACP conformation, as indicated by the CD behaviors of rACP in the presence of 10 mM $MgCl_2$ and 0.4 M CsCl (data not shown). Acrylamide, however, has been reported to induce intermediate states of aldolase, inactivating this enzyme reversibly at levels up to about 1.2 M, and irreversibly at levels above 3.5 M (Dobryszycki et al., 1999). Earlier work by Eftink and Ghiron demonstrated that acrylamide has only a small effect on protein structure in the range of 0-1.0 M (Eftink and Ghiron, 1977) and exhibits a weak interaction with proteins with an association constant in the range of 0.5-2.0 M^{-1} (Eftink and Ghiron, 1987). The relatively low concentrations of acrylamide used in the current study (0-0.4 M) appeared to have minimal effect on ACP conformation because both the emission maximum and the band shape remained constant.

The observed fluorescence quenching is governed by one or both of two distinct processes (Lakowicz, 1983). Dynamic or collisional quenching of fluorescence results from the encounter of the excited-state Trp with quenching groups on added solutes or neighboring amino acids. Static quenching results from the formation of ground-state nonfluorescent complexes between the Trp and quenching groups (Royer, 1995). Static quenching is readily detected in proteins that are denatured, or contain only a single fluorophore (Eftink and Ghiron, 1976), yet static quenching constant V values are less reproducible than collisional quenching constant K_{SV} values because of the usual presence of impurities of the protein or errors from scattered light (Eftink and Ghiron, 1981). There is no general response of intrinsic Trp fluorescence intensity to unfolding or refolding of a polypeptide chain. Increase of fluorescence intensity of holo-E25W and holo-A45W upon

folding induced by Mg^{2+} or acylation may involve structural reorganization as a result of ACP global conformational change such that the intrinsic fluorescence quenching groups are removed from the surroundings of Trp. Known protein quenching moieties include disulfides, amines, charged side chains (Chen and Barkley, 1998), peptide bonds (Chen et al., 1996), and other electron accepting groups on neighboring residues (Harris and Hudson, 1990).

Acrylamide and iodide were equally effective in quenching E25W fluorescence, indicating that Trp25 in the flexible loop region between helices I and II is fully exposed to aqueous solvent. The fact that iodide has a smaller K_{SV} constant than acrylamide for A45W indicates that there is less accessibility to the former. Moreover, the elevated quenching by cesium compared to iodide suggest that the Trp is not hidden from ionic quenchers but rather shielded by a negatively charged barrier that can not be readily penetrated by quenchers carrying charges of the same nature. This is consistent with the expected nature of position 45 in folded ACP, which is in a polar/nonpolar interface of the amphipathic helix II and is encompassed by a cluster of acidic residues in helices I and II.

The conserved Leu46 is one of the residues lining the putative fatty acid binding cavity in the *E. coli* acyl-ACP crystal (Roujeinikova et al., 2002). In ACPs from *B. subtilis* (Xu et al., 2001) and *H. pylori* (Park et al., 2004), Leu46 is also involved in hydrophobic packing that includes in close contact residues Ile/Val7, Ile/Val10, and Ile11 in helix I; Val39, Leu42, and Ile/Val43 in helix II; Val65, Ala68, Val69, and Ile72 in helix III. Consistent with published structures, three lines of evidence indicate that Trp of folded *V. harveyi* recombinant L46W is buried in the hydrophobic interior. First, the emission peak was centered around 320 nm, which places this Trp residue in class I as buried with no exposure to water (Burstein et al., 1973, Vivian and Callis, 2001). Second, there was lack of efficient quenching by any of the three soluble quenchers used, as demonstrated by the low K_{SV} values and low extent of quenching at any given concentration. Third, the effective accessible fraction for iodide or cesium was well below 1 and that for acrylamide was near 1, indicating the existence of a fluorophore population devoid of physical contact with ionic quenchers. Studies by Calhoun and coworkers have argued against the long-held belief that small molecules quench buried Trp by moving into and through the native protein (Calhoun et al., 1983). Rather, the Trp-quencher contact is governed by protein unfolding, which supports the proposal of acrylamide as a "kinetic ruler" since it appears to quench even fully

buried Trp. Intuitively, the degree of exposure of Trp to solvent reported by acrylamide quenching can be considered as an index of not only the actual depth of Trp burial but also the time that the protein stays in an open position as opposed to a closed conformation. Taken together, holo-L46W in the presence of Mg^{2+} contains a fully buried Trp and is mostly folded on a fluorescence time scale.

3. Effects of Acylation vs Mg^{2+} Binding on ACP Conformation

Early structural analyses of *E. coli* ACP in solution suggested that the attached fatty acyl moiety is immobilized by interaction with ACP polypeptide (Gally et al., 1978) and constrained to an orientation parallel to the helices (Jones et al., 1987a), which is now consistent with the recent crystal structure of butyryl-ACP (Roujeinikova et al., 2002). Despite a similar overall fold, octanoylation of *E. coli* ACP at neutral pH significantly decreased affinity of ACP for divalent cations and increased Tyr71 exposure (Tener and Mayo, 1990), suggesting structural reorganization at a local level. In pursuit of a better understanding of the roles of fatty acylation and Mg^{2+} binding in shaping ACP conformation, acylated Trp mutants of ACP were prepared with a spectrum of fatty acyl chain lengths. The difference in secondary structural content between acyl-ACP in the presence and absence of Mg^{2+} was notably minimized when a long chain fatty acid is attached (Fig. 23-24). This trend was also observed in terms of tertiary structure indicated by fluorescence parameters (Fig. 26-28) except that some dependence of the Trp environment on Mg^{2+} persisted even with the longest acyl group tested in the context of L46W, F50W, and V72W. Trp located at these interior positions may be more sensitive to the detailed structure of its environment since it can report environmental changes in two fluorescence parameters, namely intensity change and wavelength shift, as opposed to surface Trp residues that report mostly intensity changes. Lower wavelength maxima associated with Mg^{2+} binding indicate a more hydrophobic environment of Trp reporters at various locations along the hydrophobic pocket, suggesting that the protein core of acyl-ACP with Mg^{2+} may be more apolar than without. Paradoxically, early NMR studies on octanoyl-ACP from *E. coli* indicated that divalent cations such as Ca^{2+} and Mg^{2+} significantly enhance the degree of Tyr71 exposure (Tener and Mayo, 1990), also providing evidence for distinct effects of divalent cation binding and acylation on ACP conformation. Interestingly, even in the presence of Mg^{2+} the environment of Trp in L46W (Fig. 27, 28D), and to a lesser degree

A45W, F50W, and V72W (Fig. 26), varied with the acyl chain length. NMR studies of acyl-ACP from spinach indicated that the acyl group of 18:0-ACP is more exposed to solvent than that of 10:0-ACP despite a larger hydrophobic pocket for fatty acid accommodation in the former ACP derivative (Zornetzer et al., 2006). It seems likely that local conformational changes of a folded ACP induced by the attachment of a longer acyl chain leaves the protein interior slightly more open and consequently less apolar. This supports the possible role of unique average conformation adopted by various ACP derivatives in achieving specific enzyme interaction.

Fluorescence changes caused by increasing chain length seem to also correlate with the location of the Trp probe, specifically the distance of Trp from the phosphopantetheine attachment site Ser36 in the 3D structure (Fig. 20). Trp in E25W is positioned the lowest in this view. Attachment of only a six-carbon chain caused the biggest change in fluorescence intensity that constituted the majority of the increase that acylation could have caused (Fig. 28A). Longer acyl groups did not have as much contribution to the increase. Thus, changes of Trp25 fluorescence appear to be mere reflection of ACP folding. Trp residues in A45W, L46W and V72W are located at similar distances from Ser36. Correspondingly, it was with attachment of fatty acids from C6 to C10 that the biggest changes in fluorescence intensity of A45W and wavelength shift of L46W and V72W were observed (Fig. 28A, Fig. 28C). This is in full agreement with the crystal structure of butyryl-ACP from *E. coli*, where the putative fatty acid binding pocket lined by the side chains of Val7, Leu46, Ile54, Met62, Ala68, Tyr71, and Ile72 is large enough to accommodate eight carbons of a lipophilic acyl chain (Roujeinikova et al., 2002). Trp in F50W is furthest from Ser36 along the hydrophobic groove. The emission peak of acyl-F50W underwent the steepest shift between C8 and C12 as expected (Fig. 28C). Evidence from the native PAGE is less compelling (Fig. 22B), likely because alterations in Trp microenvironment do not correlate directly with overall compactness of the protein and the behavior of ACP at pH 9.2 may be different from that at neutral pH. However, it is clear that the acyl chain of increasing number of carbons progressively stabilizes ACP conformation and exerts a cumulative effect on hydrodynamic properties of ACP, which is also consistent with increasing hydrophobicity of *E. coli* acyl-ACP with increasing length of the fatty acyl chains (Rock and Garwin, 1979; Cronan, 1982).

Analysis of Tyr to Trp energy transfer offers insight into effects of acylation vs Mg^{2+} binding on local structure of ACP from a different perspective. Fluorescence energy transfer

was not observed between free Tyr and Trp amino acids in an aqueous solution, but can occur to a significant extent when both residues are bound to a single polypeptide chain (Lakowicz, 1983). The distance between an energy donor and acceptor along a single polypeptide chain is not thought to be a determinant of efficiency of the energy transfer since the diameter of a protein is usually well within the range for efficient energy transfer to take place. Rather, it is the relative orientation of the aromatic side chains that dictates transfer efficiency; for instance, resonance dipole coupling is not allowed when the Trp plane is orthogonal to the tyrosyl transition dipole moment (Brown et al., 1977). Difference spectra profiles of the holo forms of all Trp mutants in the absence of Mg^{2+} showed slight Tyr emission (Fig. 31), reflecting efficient Tyr-Trp resonance dipole coupling as a result of freely rotating residues in an unfolded ACP polypeptide chain. By contrast, holo-L46W but not the other mutants exhibited a significant Tyr emission component in the presence of Mg^{2+}, which is likely a result of Trp at position 46 participating in the packing of the inner core, and thus less free to rotate. Consistent with steady-state spectra (Fig. 27), acylation with increasing chain length progressively decreased the extent of Tyr-Trp energy transfer and its dependence on Mg^{2+} (Fig. 31B).

The biological implications of acyl-ACPs of different chain lengths adopting locally different conformations in the presence of Mg^{2+} could lie in the regulatory role of various ACP derivatives and the chain length specificity of ACP-dependent enzymes. Negligible levels of apo-ACP (Rock and Jackowski, 1982) and low levels of acyl-ACP pools in *E. coli* (Rock and Jackowski, 1982) and spinach (Post-Beittenmiller et al, 1991) support a regulatory role of these ACP forms. Indeed, apo-ACP inhibits bacterial cell growth, likely by inhibiting PlsB and the biosynthesis of phospholipids (Keating et al., 1995). Medium to long chain acyl-ACPs but not holo-ACP inhibit *E. coli* FabH (Heath and Rock, 1996a), FabI (Heath and Rock, 1996b), and ACC (Davis and Cronan, 2001). Potency of inhibition increases with chain length (Heath and Rock, 1996a). However, chemical properties of the acyl moiety alone are not sufficient for this feedback regulation: ACP specificity is also required. For example, palmitoyl-ACP from spinach fails to inhibit *E. coli* ACC despite 44% sequence identity between ACPs from these two species (Davis and Cronan, 2001). Overexpression of plant acyl-ACP thioesterases in *E. coli* cells causes reductions in acyl-ACP levels in vivo, leading to unregulated fatty acid biosynthesis (Voelker and Davies, 1994; Dormann et al., 1995), suggesting that acyl-ACPs rather than fatty acids are primary physiological regulators

of fatty acid biosynthesis. FAS components utilize a wide variety of acyl substrates delivered by ACP, so they must be more forgiving than those enzymes that have a "hydrocarbon ruler" such as LpxA. Nevertheless, *E. coli* FabB and FabF exhibit increasing K_m with acyl-ACP substrates of increasing chain length (Garwin et al., 1980). Lauroyl-ACP exhibits non-competitive inhibition of the condensing enzyme KAS III from the plant *Cuphea wrightii* with regard to malonyl-ACP; the distinct binding site on KAS III for regulatory acyl-ACPs can be knocked out with only slight reduction of condensing activity with malonyl-ACP (Abbadi et al., 2000). These observations suggest that ACP partner enzymes can distinguish between various forms of ACP, possibly by recognizing subtly different ACP conformations.

4. ACP Interaction with LpxA

Despite adopting a folded conformation with similar helical content, the β-hydroxymyristoylated derivatives of ACP mutants differed widely in support of LpxA activity (Fig. 21C). LpxA activity was about 50% with A45W, F50W, and V72W, and almost negligible using L46W as the acyl donor. Replacing an interior residue with Trp could impair LpxA function by two mechanisms.

First, introduction of a bulky Trp side chain to the ACP hydrophobic core may cause a packing defect, which perhaps interferes with binding of ACP to LpxA or positioning of the fatty acyl moiety in a correct orientation. This possibility is supported by the observations that both holo and acyl forms of L46W, F50W, and V72W migrated more slowly than their rACP counterparts (Fig. 22), and that holo-L46W required higher levels of Mg^{2+} to adopt significant helical content than rACP (compare Figures 14 and 29). It has been well documented that conserved hydrophobic residues at positions 46 and 72 stabilize the packed ACP inner core by participating in extensive contacts with other hydrophobic side chains (Xu et al., 2001; Wong et al., 2002; Li et al., 2003; Park et al., 2004) and line the cavity for potential fatty acid interaction (Roujeinikova et al., 2002). Ile72 (*V. harveyi* numbering) of *M. tuberculosis* ACP forms hydrophobic contacts with Ile54 (Wong et al., 2002), which is implicated in fatty acid binding (Jones et al., 1987a; Roujeinikova et al., 2002) and ACP interaction with ACPS (Parris et al., 2000) and FabG (Zhang et al., 2003b). Along with Ile54, Ala59, and Tyr71 (Jones et al., 1987a), the importance of Phe50 in hydrophobic interaction with fatty acyl groups has been established by NMR (Mayo and Prestegard, 1985), absorption spectroscopy (Rock, 1983) and mutational analysis (Flaman et al., 2001).

Second, these mutations could have detrimental impact on ACP flexibility required for efficient enzyme catalysis. Internal motion around residues Leu46, Phe50, and Ile72 is thought to be responsible for the flexibility required to accommodate a growing acyl chain during fatty acid biosynthesis (Kim and Prestegard, 1989). In particular, Leu46 and Ile72 of *E. coli* ACP undergo rapid backbone amide exchange (Andrec et al., 1995). Substitution of a bulky Trp residue at these highly flexible positions may lead to disruption of dynamic mobility of ACP such that the acyl group is not efficiently delivered to the LpxA active site upon ACP interaction.

By contrast, reduced LpxA activity with ACP mutants containing substitutions of exposed residues such as E25W and A45W may be an indicator of altered protein interaction at the molecular interface. The N-terminal half of loop I, where Glu25 resides, is found to lack long-range atomic interaction constraints and is not well-defined in a number of ACP structures. There are few residues available for hydrophobic packing, indicating extensive solvent exposure (Crump et al., 1997; Findlow et al., 2003; Reed et al., 2003). The biological function of loop I is not well established except for a possible role in allowing space for fatty acids of varying length and shape. The N25C mutant of *E. coli* ACP supported normal activities of *E. coli* AAS, FAS, FabD, and HlyC, and this position was not found to interact with HlyC by fluorescence spectroscopy (Worsham et al., 2003). Chemical shift perturbations of *E. coli* ACP in the presence of *E. coli* LpxA were minimal in loop I, corresponding to residues 18-32 (Jain et al., 2004). Consistent with this NMR analysis, the nonconservative substitution E25W did not alter the solvent exposed nature at this position (Fig. 30) or affect LpxA activity (Fig. 21C), suggesting that LpxA is not sensitive to the detailed surface structure of Glu25 or that this residue is not critical to maintaining the required flexibility of ACP structure.

On the other hand, Ala45 of *E. coli* ACP has been predicted to partake in the electrostatic/hydrophobic interaction between ACP and partner enzymes such as FabA, FabB, FabD, FabF, FabI, and LpxA (Zhang et al., 2001). Electrostatic and hydrogen bonding interactions are thought to be just as important as hydrophobic contacts in protein-protein interactions (Xu et al., 1997). In a survey of 136 protein interfaces, only one third contained large concentrated hydrophobic patches, reflecting the importance of polar interactions involving surface residues and bridging water molecules (Larsen et al., 1998). Thus, although decreased LpxA activity with A45W may suggest the disruption of a smooth

fit between ACP and LpxA by Trp at position 45, it does not preclude the effect of a presumably less compact conformation as judged by native gel electrophoretic migration (Fig. 22). Superoxide dismutase dimer interface is one of the smallest known, and consists of two hydrogen bonds, six hydrophobic contacts, and a few water molecule (Larsen et al., 1998). Similarly, the predicted protein interaction patch on ACP contains only five acidic and two hydrophobic residues (Zhang et al., 2001), which suggests that the binding between ACP and partner enzymes through this region may be weak and transient.

The current fluorescence analysis has revealed for the first time that ACP-LpxA binding and ACP conformational changes as a result of this binding occur at micromolar levels, which more closely reflect physiological conditions in contrast to previous NMR studies with millimolar levels of ACP and LpxA (Jain et al., 2004). Holo-ACP mutants E25W, A45W, and L46W exhibited fluorescence changes upon LpxA binding that were similar to those caused by Mg^{2+} binding (Fig. 32), clearly indicating that holo-ACP binds to LpxA. This is somewhat surprising because holo-ACP did not inhibit LpxA activity at levels as high as 18 μM (data not shown), yet the data are consistent with the role of holo-ACP as a substrate of LpxA in the reverse reaction. It seems unlikely that the buried Trp in L46W would somehow flip to the surface and become associated with hydrophobic residues on LpxA, strongly suggesting that holo-ACP folds upon binding to LpxA. In addition to an increase in fluorescence intensity, holo-A45W clearly exhibited a more significant blue shift that is distinct from that induced by Mg^{2+} (Table 4). This was not observed with the exposed Trp in E25W, which indicates that position 45 may be involved in direct contact with LpxA surface, providing a slightly more hydrophobic environment.

Little is known about the biological significance of ACP folding upon binding to LpxA. *V. harveyi* ACP exhibits several properties in common with natively unfolded proteins, whose conformation is shaped through interactions with protein binding partners (Tsai et al., 1998). The natively unfolded conformation of these proteins, which has often eluded structural characterization due to the low population of corresponding conformers, is believed not to be a random coil but rather in a predominant conformation that can be induced to interact with different partners (Tsai et al., 2001). The entropic cost during folding of ACP could be compensated by formation of stable electrostatic/hydrophobic contacts with partner enzymes, ensuring that ACP only binds to specific targets (Wright and Dyson, 1998). Besides *V. harveyi* ACP, *H. pylori* ACP is also found to be partially unfolded at

neutral pH (Park et al., 2004). Thus, binding-induced folding may be a common trait for ACPs from certain organisms.

Myristoyl-ACP is not a substrate but rather a known inhibitor of LpxA with an IC_{50} value of 2 μM (Anderson et al., 1993), i.e. similar to the K_m for its natural substrate β-hydroxymyristoyl-ACP (Wyckoff and Raetz, 1999). Curve fitting of fluorescence data suggested LpxA binding constants for holo-E25W, A45W, and L46W in this range. The reported K_m of *E. coli* FabB and FabF for myristoyl-ACP is 30 times higher than that of LpxA for β-hydroxymyristoyl-ACP, which is in accord with genetic evidence that LpxA competes with FAS for β-hydroxymyristoyl-ACP substrate due to a higher affinity for this fatty acid synthesis intermediate (Mohan et al., 1994). However, binding between myristoyl-A45W and LpxA was not detected in the experimental system used in this study (Fig. 32), perhaps because further changes in the fluorescence intensity of already-folded myristoylated A45W would be expected when LpxA binds. Moreover, unlike holo-A45W, a blue shift of myristoyl-A45W emission was not observed upon addition of micromolar levels of LpxA (Fig. 32), which did not appear to result from the low LpxA concentrations in the assay system. A small shift in emission band of myristoyl-A45W, if there is one, would also likely be masked by experimental errors.

Another possibility is that myristoyl-ACP and holo-ACP might bind to LpxA at similar sites of distinct conformations. Holo-ACP is present as a predominant species in the total ACP pool (0.1 mM) in vivo (Jackowski and Rock, 1983), but was not found to be an inhibitor of the LpxA forward reaction in vitro (data not shown). Holo- (this chapter), myristoyl- (Anderson et al., 1993), and β-hydroxymyristoyl-ACP (Wyckoff and Raetz, 1999) appear to bind to LpxA with similar affinities, yet each assumes a distinct role in supporting or inhibiting the LpxA reaction, which may be related to LpxA functioning as a trimer. Binding of a holo- or acyl-ACP molecule to one of the three ACP binding clefts at each subunit interface may trigger specific conformational changes of LpxA, which in turn could hamper or facilitate the binding of another ACP molecule at the other two sites. Cooperativity has been observed for some oligomeric ACP-dependent enzymes, including *B. subtilis* ACPS trimer (Mootz et al., 2001) and *E. coli* FabG tetramer (Price et al., 2001b). Whether binding cooperativity is a characteristic of LpxA awaits further investigation.

Chapter VI. Conclusions

In the current project, several individual and combined ACP mutants were constructed using *V. harveyi* rACP as the template. The roles of these residues in ACP structure and function were investigated employing various biochemical and biophysical techniques with four distinct enzyme systems, i.e. FAS, AAS, ACPS, and LpxA. One of the advantages of studying *V. harveyi* ACP is that, unlike the *E. coli* counterpart, *V. harveyi* ACP is unfolded at neutral pH and can refold as a result of various factors. This makes it possible to monitor the effect of acylation, salt, pH, or ACP binding proteins on ACP conformation. Based on my results, some general themes have emerged:

i) *Neutralization of acidic residues in and around helix II of ACP generally stabilizes folded ACP conformation.* CD and native PAGE analyses indicate that ACP adopts increasingly compact conformation with increasing number of acidic residues neutralized. In the absence of Mg^{2+}, SA (+3 charge difference) and SB (+4) mutants were partially folded, compared to largely unfolded rACP and individual mutants (+1). SA/SB (+7) was completely folded independent of Mg^{2+}. By contrast, a single substitution in the middle of helix II (E41K) had the same effect as combined mutations in SA/SB, similar to the A75H mutant of *V. harveyi* ACP previously characterized in our laboratory. These results suggest that, like divalent cation binding, mutagenic replacement of acidic residues at either end of helix II with corresponding amides favors the native-like ACP conformation by reducing the overall electrostatic repulsion between charged side chains. Strategic replacement with basic residues such as His75 or Lys41 may have an even more dramatic stabilizing effect, by balancing specific intrinsic negative charge in the helix II or other regions.

ii) *Mutations that stabilize ACP conformation do not appear to impair enzyme activities through general stabilization of a folded ACP.* V43I, A75H, E41K, and SA/SB all adopted a folded conformation at neutral pH independent of Mg^{2+}, but supported enzyme activities to various degrees. V43I and A75H were effective substrates for FAS and AAS. E41K supported AAS but not FAS activity. SA/SB was a poor substrate for FAS, AAS, and ACPS. These findings indicate that the stabilization of ACP structure is not a general basis for effects of mutations on enzyme function. Rather, it is the presence of selected surface residues residing in the ACP-enzyme interface that determine enzyme activities. This is further supported by the fact

that more stable ACPs, such as *E. coli* ACP, are often as good or better substrates for these enzymes.

iii) *ACP-dependent enzymes can have specific functional determinants on ACP.* The enzyme systems examined have distinct catalytic mechanisms. Thus, they might be expected to bind to different regions of ACP or require a specific set of structural characteristics, e.g. the need for conformational transition. FAS is an array of component enzymes, and may prefer a versatile ACP with a rapid on and off rate. FAS had little activity with E41K, suggesting that Glu41 is critical for supporting FAS function while all other enzymes studied tolerated this mutation with little difficulty. Mutations of the acidic residues implicated in divalent cation binding had a cumulative effect on FAS but are not individually essential for catalytic function, suggesting that most of the acidic residues along helix II are required for optimal FAS activity. AAS and LpxA both catalyze conversion between holo- and acyl-ACP, and may require that ACP undergo fast conformational reorganization, particularly in the loop II region, to deliver or accept an acyl group. Consistent with this, activities of these two enzymes were more affected by mutations around the C-terminus of helix II. LpxA was more sensitive than AAS and also exhibited largely reduced activity with helix II Trp mutants such as L46W, which required higher levels of Mg^{2+} to fold than rACP and other mutants. Unlike the enzymes that utilize acylated substrates, ACPS modifies apo-ACP, suggesting that the DSL motif would be significant in this interaction. Thus, Asp35 from the DSL signature motif was critical for ACPS activity, possibly by forming a critical salt bridge with a conserved arginine from ACPS. In all cases, correct binding and positioning of reactive groups in the enzyme active site is a prerequisite, and conformational changes may also be important. Overall, my results are consistent with the notion that helix II serves as the primary recognition motif for ACP-dependent enzymes.

iv) *Two mechanisms previously thought to similarly stabilize the native folded conformation of ACP (divalent cation binding and fatty acylation) produce distinct environments of specific residues in the hydrophobic core.* CD analysis indicated that acylation of ACP with a medium to long chain saturated fatty acid caused ACP to adopt native-like helical content independent of Mg^{2+}. Using tryptophan residues as intrinsic fluorescence probes of the microenvironment of ACP, it was further revealed that the polarity of positions 46, 50, 72 changed from hydrophilic in unfolded holo-ACP to increasingly hydrophobic with increasing length of covalently attached acyl group, and was the least polar in the presence of Mg^{2+}. Thus, acylation

progressively stabilizes folded ACP conformation with increasing chain length, whereas Mg^{2+} causes additional conformational changes of acyl-ACP.

v) *Binding of a natural partner enzyme can shift the conformational equilibrium of ACP to the folded state.* The investigation of fluorescent properties of Trp mutants of *V. harveyi* ACP in the presence of LpxA has provided the first evidence that ACP adopts an ordered structure upon enzyme binding, independent of divalent cation binding or fatty acylation. More recent studies from our lab suggest that ACPS from *V. fisheri* induces folding of apo-ACP (D. Byers, personal communication). These results support the membership of ACP in the growing family of natively unfolded proteins, which are thought to achieve interaction specificity with many binding partners through binding coupled with folding.

My work has shed considerable light on the mechanism of ACP interaction with partner enzymes and will have an impact on both theoretical and applied research with this protein. An estimated 30% of eukaryotic proteomes contain long stretches of natively unfolded segments. These proteins are often involved in regulation and signalling. However, lack of knowledge persists because protein intrinsic disorder is difficult to characterize. In order to better understand interaction of natively unfolded proteins with their partners, *V. harveyi* ACP and mutants can be used to dissect energetic differences of binding vs folding and to study the effect of ACP conformational stability on reaction equilibria employing calorimetric tools. Other biophysical analyses can be used to define critical regions and mechanisms of enzyme interaction. For example, extrinsic fluorescent probes or chemical shift perturbation NMR can be used to study enzyme binding, ACP conformational changes upon enzyme binding, and prosthetic group dynamics.

Advanced knowledge of ACP-enzyme interactions will assist the design of chemical or genetic approaches to manipulate ACP-dependent processes. Given the discovery that different enzymes recognize distinct features of ACP, it may be possible to exert control over certain aspects of ACP function without affecting other essential cellular activities, or impacting ACP-dependent processes in host type I FAS systems. Practical applications include design of novel antibiotics against ACP-dependent drug targets (e.g. FAS, ACPS, and LpxA) and engineering of plant lipids and secondary metabolites. Conversely, ACP derivatives of high enzyme affinity could be developed to protect the enzyme active sites from the attack of drugs or to inhibit the binding of cofactors. Thus, further knowledge of

the mechanisms of the interactions between ACP and partner enzymes will have significant implications for both basic science and human life.

References

Abbadi A, Brummel M, and Spener F. (2000) Knockout of the regulatory site of 3-ketoacyl-ACP synthase III enhances short- and medium-chain acyl-ACP synthesis. Plant J 24:1-9.

Abita JP, Lazdunski M, and Ailhaud G. (1971) Structure-function relationships of the acyl-carrier protein of *Escherichia coli.* Eur J Biochem 23:412-20.

Aguilar PS, Cronan JE Jr, and de Mendoza D. (1998) A *Bacillus subtilis* gene induced by cold shock encodes a membrane phospholipid desaturase. J Bacteriol 180:2194-200.

Alberts AW, Majerus PW, and Vagelos PR. (1969) Acetyl-CoA acyl carrier protein transacylase. Methods Enzymol 14:50-3.

Anderson MS, and Raetz CR. (1987) Biosynthesis of lipid A precursors in *Escherichia coli.* A cytoplasmic acyltransferase that converts UDP-N-acetylglucosamine to UDP-3-O-(R-3-hydroxymyristoyl)-N-acetylglucosamine. J Biol Chem 262:5159-69.

Anderson MS, Bull HG, Galloway SM, Kelly TM, Mohan S, Radika K, and Raetz CRH. (1993) UDP-N-acetylglucosamine acyltransferase of *Escherichia coli.* The first step of endotoxin biosynthesis is thermodynamically unfavorable. J Biol Chem 268:19858-65.

Andrade MA, Chacon P, Merelo JJ, and Moran F. (1993) Evaluation of secondary structure of proteins from UV circular dichroism spectra using an unsupervised learning neural network. Protein Eng 6:383-90.

Andrec M, Hill RB, and Prestegard JH. (1995) Amide exchange rates in *Escherichia coli* acyl carrier protein: correlation with protein structure and dynamics. Protein Sci 4:983-93.

Aparicio JF, Molnar I, Schwecke T, Konig A, Haydock SF, Khaw LE, Staunton J, and Leadlay PF. (1996) Organization of the biosynthetic gene cluster for rapamycin in *Streptomyces hygroscopicus*: analysis of the enzymatic domains in the modular polyketide synthase. Gene 169:9-16.

Arthur CJ, Szafranska A, Evans SE, Findlow SC, Burston SG, Owen P, Clark-Lewis I, Simpson TJ, Crosby J, and Crump MP. (2005) Self-malonylation is an intrinsic property of a chemically synthesized type II polyketide synthase acyl carrier protein. Biochemistry 44:15414-21.

Asturias FJ, Chadick JZ, Cheung IK, Stark H, Witkowski A, Joshi AK, and Smith S. (2005) Structure and molecular organization of mammalian fatty acid synthase. Nat Struct Mol Biol 12:225-32.

Austin MB and Noel JP. (2003) The chalcone synthase superfamily of type III polyketide synthases. Nat Prod Rep 20:79-110.

Baldock C, Rafferty JB, Sedelnikova SE, Baker PJ, Stuitje AR, Slabas AR, Hawkes TR, and Rice DW. (1996) A mechanism of drug action revealed by structural studies of enoyl reductase. Science 274:2107-10.

Banerjee A, Dubnau E, Quemard A, Balasubramanian V, Um KS, Wilson T, Collins D, de Lisle G, and Jacobs WR Jr. (1994) *inhA*, a gene encoding a target for isoniazid and ethionamide in *Mycobacterium tuberculosis.* Science 263:227-30.

Barekzi N, Joshi S, Irwin S, Ontl T, and Schweizer HP. (2004) Genetic characterization of *pcpS*, encoding the multifunctional phosphopantetheinyl transferase of *Pseudomonas aeruginosa.* Microbiology 150:795-803.

Bayan N and Therisod H. (1989) Evidence of interactions of acyl carrier protein with glycerol-3-phosphate acyltransferase, an inner membrane protein of *Escherichia coli.* FEBS Lett 255:330-4.

Berg M, Hilbi H, and Dimroth P. (1996) The acyl carrier protein of malonate decarboxylase of *Malonomonas rubra* contains 2'-(5"-phosphoribosyl)-3'-dephosphocoenzyme A as a prosthetic group. Biochemistry 35:4689-96.

Bergler H, Wallner P, Ebeling A, Leitinger B, Fuchsbichler S, Aschauer H, Kollenz G, Hogenauer G, and Turnowsky F. (1994) Protein EnvM is the NADH-dependent enoyl-ACP reductase (FabI) of *Escherichia coli.* J Biol Chem 269:5493-6.

Bhat UR, Mayer H, Yokota A, Hollingsworth RI, and Carlson RW. (1991) Occurrence of lipid A variants with 27-hydroxyoctacosanoic acid in lipopolysaccharides from members of the family *Rhizobiaceae.* J Bacteriol 173:2155-9.

Bibb MJ, Sherman DH, Omura S, and Hopwood DA. (1994) Cloning, sequencing and deduced functions of a cluster of *Streptomyces* genes probably encoding biosynthesis of the polyketide antibiotic frenolicin. Gene 142:31-9.

Bisang C, Long PF, Cortes J, Westcott J, Crosby J, Matharu AL, Cox RJ, Simpson TJ, Staunton J, and Leadlay PF. (1999) A chain initiation factor common to both modular and aromatic polyketide synthases. Nature 401:502-5.

Brennan PJ and Nikaido H. (1995) The envelope of mycobacteria. Annu Rev Biochem 64:29-63.

Brody S and Mikolajczyk S. (1988) *Neurospora* mitochondria contain an acyl-carrier protein. Eur J Biochem 173:353-9.

Brody S, Oh C, Hoja U, and Schweizer E. (1997) Mitochondrial acyl carrier protein is involved in lipoic acid synthesis in *Saccharomyces cerevisiae.* FEBS Lett 408:217-20.

Broun P, Shanklin J, Whittle E, and Somerville C. (1998) Catalytic plasticity of fatty acid modification enzymes underlying chemical diversity of plant lipids. Science 282:1315-7.

Brown MR, Omar S, Raubach RA, and Schleich T. (1977) Quenching of the tyrosyl and tryptophyl fluorescence of subtilisins Carlsberg and Novo by iodide. Biochemistry 16:987-92.

Brown AP, Carnaby S, Brough C, Brazier M, and Slabas AR. (2002) *Limnanthes douglasii* lysophosphatidic acid acyltransferases: immunological quantification, acyl selectivity and functional replacement of the *Escherichia coli plsC* gene. Biochem J 364:795-805.

Brozek KA, Carlson RW, and Raetz CRH. (1996) A special acyl carrier protein for transferring long hydroxylated fatty acids to lipid A in *Rhizobium.* J Biol Chem 271:32126-36.

Buckel W and Bobi A. (1976) The enzyme complex citramalate lyase from *Clostridium tetanomorphum.* Eur J Biochem 64:255-62.

Burstein EA, Vedenkina NS, and Ivkova MN. (1973) Fluorescence and the location of tryptophan residues in protein molecules. Photochem Photobiol 18:263-79.

Butland G, Peregrin-Alvarez JM, Li J, Yang W, Yang X, Canadien V, Starostine A, Richards D, Beattie B, Krogan N, Davey M, Parkinson J, Greenblatt J, and Emili A. (2005) Interaction network containing conserved and essential protein complexes in *Escherichia coli.* Nature 433:531-7.

Butler MJ, Friend EJ, Hunter IS, Kaczmarek FS, Sugden DA, and Warren M. (1989) Molecular cloning of resistance genes and architecture of a linked gene cluster involved in biosynthesis of oxytetracycline by *Streptomyces rimosus.* Mol Gen Genet 215:231-8.

Butterworth PHW and Bloch K. (1970) Comparative aspects of fatty acid synthesis in *Bacillus subtilis* and *Escherichia coli.* Eur J Biochem 12:496-501.

Byers DM. (1988) Luminescence-specific synthesis of myristic acid in the bioluminescent bacterium *Vibrio harveyi.* Biochem Cell Biol 66:741-9.

Byers DM. (1989) Elongation of exogenous fatty acids by the bioluminescent bacterium *Vibrio harveyi.* J Bacteriol 171:59-64.

Byers DM and Meighen EA. (1985) Acyl-acyl carrier protein as a source of fatty acids for bacterial bioluminescence. Proc Natl Acad Sci USA 82:6085-9.

Calhoun DB, Vanderkooi JM, and Englander SW. (1983) Penetration of small molecules into proteins studied by quenching of phosphorescence and fluorescence. Biochemistry 22:1533-9.

Campbell JW and Cronan JE Jr. (2001) Bacterial fatty acid biosynthesis: targets for antibacterial drug discovery. Annu Rev Microbiol 55:305-32.

Cane DE. (1997) Introduction: polyketide and nonribosomal polypeptide biosynthesis. From Collie to *coli.* Chem Rev 97:2463-4.

Cane DE and Walsh CT. (1999) The parallel and convergent universes of polyketide synthases and nonribosomal peptide synthetases. Chem Biol 6:R319-25.

Cane DE, Walsh CT, and Khosla C. (1998) Harnessing the biosynthetic code: combinations, permutations, and mutations. Science 282:63-8.

Cao JG and Meighen EA. (1989) Purification and structural identification of an autoinducer for the luminescence system of *Vibrio harveyi.* J Biol Chem 264:21670-6.

Carreras CW and Khosla C. (1998) Purification and in vitro reconstitution of the essential protein components of an aromatic polyketide synthase. Biochemistry 37:2084-8.

Chen Y and Barkley MD. (1998) Toward understanding tryptophan fluorescence in proteins. Biochemistry 37:9976-82.

Chen Y, Liu B, Yu HT, and Barkley MD. (1996) The peptide bond quenches indole fluorescence. J Am Chem Soc 118:9271-8.

Chirgadze NY, Briggs SL, McAllister KA, Fischl AS, and Zhao G. (2000) Crystal structure of *Streptococcus pneumoniae* acyl carrier protein synthase: an essential enzyme in bacterial fatty acid biosynthesis. EMBO J 19:5281-7.

Choi KH, Kremer L, Besra GS, and Rock CO. (2000) Identification and substrate specificity of beta-ketoacyl (acyl carrier protein) synthase III (mtFabH) from *Mycobacterium tuberculosis.* J Biol Chem 275:28201-7.

Chu M, Mierzwa R, Xu L, Yang SW, He L, Patel M, Stafford J, Macinga D, Black T, Chan TM, and Gullo V. (2003) Structure elucidation of Sch 538415, a novel acyl carrier protein synthase inhibitor from a microorganism. Bioorg Med Chem Lett 13:3827-9.

Coleman J. (1990) Characterization of *Escherichia coli* cells deficient in 1-acyl-sn-glycerol-3-phosphate acyltransferase activity. J Biol Chem 265:17215-21.

Collins LV, Kristian SA, Weidenmaier C, Faigle M, Van Kessel KP, Van Strijp JA, Gotz F, Neumeister B, and Peschel A. (2002) *Staphylococcus aureus* strains lacking D-alanine modifications of teichoic acids are highly susceptible to human neutrophil killing and are virulence attenuated in mice. J Infect Dis 186:214-9.

Cooper CL, Hsu L, Jackowski S, and Rock CO. (1989) 2-Acylglycerolphosphoethanolamine acyltransferase/acyl-acyl carrier protein synthetase is a membrane-associated acyl carrier protein binding protein. J Biol Chem 264:7384-9.

Cortes J, Haydock SF, Roberts GA, Bevitt DJ, and Leadlay PF. (1990) An unusually large multifunctional polypeptide in the erythromycin-producing polyketide synthase of *Saccharopolyspora erythraea.* Nature 348:176-8.

Cox RJ, Hitchman TS, Byrom KJ, Findlow IS, Tanner JA, Crosby J, and Simpson TJ. (1997) Post-translational modification of heterologously expressed *Streptomyces* type II polyketide synthase acyl carrier proteins. FEBS Lett 405:267-72.

Cronan JE Jr. (1982) Molecular properties of short chain acyl thioesters of acyl carrier protein. J Biol Chem 257:5013-7.

Cronan JE Jr and Waldrop GL. (2002) Multi-subunit acetyl-CoA carboxylases. Prog Lipid Res 41:407-35.

Cronan JE Jr, Birge CH, and Vagelos PR. (1969) Evidence for two genes specifically involved in unsaturated fatty acid biosynthesis in *Escherichia coli.* J Bacteriol 100:601-4.

Cronan JE Jr, Weisberg LJ, and Allen RG. (1975) Regulation of membrane lipid synthesis in *Escherichia coli.* Accumulation of free fatty acids of abnormal length during inhibition of phospholipid synthesis. J Biol Chem 250:5835-40.

Cronan JE, Fearnley IM, and Walker JE. (2005) Mammalian mitochondria contain a soluble acyl carrier protein. FEBS Lett 579:4892-6.

Crosby J, Byrom KJ, Hitchman TS, Cox RJ, Crump MP, Findlow IS, Bibb MJ, and Simpson TJ. (1998) Acylation of *Streptomyces* type II polyketide synthase acyl carrier proteins. FEBS Lett 433:132-8.

Crump MP, Crosby J, Dempsey CE, Murray M, Hopwood DA, and Simpson TJ. (1996) Conserved secondary structure in the actinorhodin polyketide synthase acyl carrier protein from *Streptomyces coelicolor* A3(2) and the fatty acid synthase acyl carrier protein from *Escherichia coli.* FEBS Lett 391:302-6.

Crump MP, Crosby J, Dempsey CE, Parkinson JA, Murray M, Hopwood DA, and Simpson TJ. (1997) Solution structure of the actinorhodin polyketide synthase acyl carrier protein from *Streptomyces coelicolor* A3(2). Biochemistry 36:6000-8.

Daines RA, Pendrak I, Sham K, Van Aller GS, Konstantinidis AK, Lonsdale JT, Janson CA, Qiu X, brandt M, Khandekar SS, Silverman C, and Head MS. (2003) First X-ray cocrystal structure of a bacterial FabH condensing enzyme and a small molecule inhibitor achieved using rational design and homology modeling. J Med Chem 46:5-8.

David SA. (2001) Towards a rational development of anti-endotoxin agents: novel approaches to sequestration of bacterial endotoxins with small molecules. J Mol Recognit 14:370-87.

Davies C, Heath RJ, White SW, and Rock CO. (2000) The 1.8 angstrom crystal structure and active-site architecture of β-ketoacyl-acyl carrier protein synthase III (FabH) from *Escherichia coli*. Struct Fold Des 8:185-95.

Davis MS and Cronan JE Jr. (2001) Inhibition of *Escherichia coli* acetyl coenzyme A carboxylase by acyl-acyl carrier protein. J Bacteriol 183:1499-503.

Davis MS, Solbiati J, and Cronan JE Jr. (2000) Overproduction of acetyl-CoA carboxylase activity increases the rate of fatty acid biosynthesis in *Escherichia coli*. J Biol Chem 275:28593-8.

De Lay NR and Cronan JE. (2006) A genome rearrangement has orphaned the *Escherichia coli* K-12 AcpT phosphopantetheinyl transferase from its cognate *Escherichia coli* O157:H7 substrates. Mol Microbiol 61:232-42.

Debabov DV, Heaton MP, Zhong Q, Stewart KD, Lambalot RH, and Neuhaus FC. (1996) The D-alanyl carrier protein in *Lactobacillus casei*: cloning, sequencing, and expression of *dltC*. J Bacteriol 178:3869-76.

Demont N, Debelle F, Aurelle H, Denarie J, and Prome JC. (1993) Role of the *Rhizobium meliloti nodF* and *nodE* genes in the biosynthesis of lipo-oligosaccharidic nodulation factors. J Biol Chem 268:20134-42.

Demont N, Ardourel M, Maillet F, Prome D, Ferro M, Prome JC, and Denarie J. (1994) The *Rhizobium meliloti* regulatory *nodD3* and *syrM* genes control the synthesis of a particular class of nodulation factors N-acylated by (omega-1)-hydroxylated fatty acids. EMBO J 13:2139-49.

Dillon SC and Bateman A. (2004) The Hotdog fold: wrapping up a superfamily of thioesterases and dehydratases. BMC Bioinformatics 5:109.

Dimroth P. (1976) The prosthetic group of citrate-lyase acyl-carrier protein. Eur J Biochem 64:269-81.

Dimroth P and Eggerer H. (1975) Isolation of subunits of citrate lyase and characterization of their function in the enzyme complex. Proc Natl Acad Sci USA 72:3458-62.

Dimroth P and Hilbi H. (1997) Enzymic and genetic basis for bacterial growth on malonate. Mol Microbiol 25:3-10.

Dimroth P, Buckel W, Loyal R, and Eggerer H. (1977a) Isolation and function of the subunits of citramalate lyase and formation of hybrids with the subunits of citrate lyase. Eur J Biochem 80:469-77.

Dimroth P, Loyal R, and Eggerer H. (1977b) Characterization of the isolated transferase subunit of citrate lyase as a CoA-Transferase. Evidence against a covalent enzyme-substrate intermediate. Eur J Biochem 80:479-88.

Dittmann E, Neilan BA, and Borner T. (2001) Molecular biology of peptide and polyketide biosynthesis in cyanobacteria. Appl Microbiol Biotechnol 57:467-73.

Dobryszycki P, Rymarczuk M, Bulaj G, and Kochman M. (1999) Effect of acrylamide on aldolase structure. I. Induction of intermediate states. Biochim Biophys Acta 1431:338-50.

Dong YH, Wang LH, Xu JL, Zhang HB, Zhang XF, and Zhang LH. (2001) Quenching quorum-sensing-dependent bacterial infection by an N-acyl homoserine lactonase. Nature 411:813-7.

Dormann P, Voelker TA, and Ohlrogge JB. (1995) Cloning and expression in *Escherichia coli* of a novel thioesterase from *Arabidopsis thaliana* specific for long-chain acyl-acyl carrier proteins. Arch Biochem Biophys 316:612-8.

Dyson HJ and Wright PE. (2002) Coupling of folding and binding for unstructured proteins. Curr Opin Struct Biol 12:54-60.

Dyson HJ and Wright PE. (2005) Intrinsically unstructured proteins and their functions. Nat Rev Mol Cell Biol 6:197-208.

Engebrecht J and Silverman M. (1984) Identification of genes and gene products necessary for bacterial bioluminescence. Proc Natl Acad Sci USA 81:4154-8.

Eftink MR. (1997) Fluorescence methods for studying equilibrium macromolecule-ligand interactions. Methods Enzymol 278:221-57.

Eftink MR and Ghiron CA. (1976) Exposure of tryptophanyl residues in proteins. Quantitative determination by fluorescence quenching studies. Biochemistry 15:672-80.

Eftink MR and Ghiron CA. (1977) Exposure of tryptophanyl residues and protein dynamics. Biochemistry 16:5546-51.

Eftink MR and Ghiron CA. (1981) Fluorescence quenching studies with proteins. Anal Biochem 114:199-227.

Eftink MR and Ghiron CA. (1987) Does the fluorescence quencher acrylamide bind to proteins? Biochim Biophys Acta 916:343-9.

Ernst-Fonberg ML, Williams SG, and Worsham LMS. (1990) Acyl carrier protein interacts with melittin. Biochim Biophys Acta 1046:111-9.

Fernandez-Moreno MA, Martinez E, Boto L, Hopwood DA, and Malpartida F. (1992) Nucleotide sequence and deduced functions of a set of cotranscribed genes of *Streptomyces coelicolor* A3(2) including the polyketide synthase for the antibiotic actinorhodin. J Biol Chem 267:19278-90.

Ferri SR and Meighen EA. (1994) An essential histidine residue required for fatty acylation and acyl transfer by myristoyltransferase from luminescent bacteria. J Biol Chem 269:6683-8.

Fice D, Shen Z, and Byers DM. (1993) Purification and characterization of fatty acyl-acyl carrier protein synthetase from *Vibrio harveyi*. J Bacteriol 175:1865-70.

Fichtlscherer F, Wellein C, Mittag M, and Schweizer E. (2000) A novel function of yeast fatty acid synthase. Eur J Biochem 267:2666-71.

Findlow SC, Winsor C, Simpson TJ, Crosby J, and Crump MP. (2003) Solution structure and dynamics of oxytetracycline polyketide synthase acyl carrier protein from *Streptomyces rimosus*. Biochemistry 42:8423-33.

Finking R, Mofid MR, and Marahiel MA. (2004) Mutational analysis of peptidyl carrier protein and acyl carrier protein synthase unveils residues involved in protein-protein recognition. Biochemistry 43:8946-56.

Fischer W. (1988) Physiology of lipoteichoic acids in bacteria. Adv Microb Physiol 29:233-302.

Fischl AS and Kennedy EP. (1990) Isolation and properties of acyl carrier protein phosphodiesterase of *Escherichia coli*. J Bacteriol 172:5445-9.

Flaman AS, Chen JM, Van Iderstine SC, and Byers DM. (2001) Site-directed mutagenesis of acyl carrier protein (ACP) reveals amino acid residues involved in ACP structure and acyl-ACP synthetase activity. J Biol Chem 276:35934-9.

Flint DH. (1996) *Escherichia coli* contains a protein that is homologous in function and N-terminal sequence to the protein encoded by the *nifS* gene of *Azotobacter vinelandii* and that can participate in the synthesis of the Fe-S cluster of dihydroxy-acid dehydratase. J Biol Chem 271:16068-74.

Florova G, Kazanina G, and Reynolds KA. (2002) Enzymes involved in fatty acid and polyketide biosynthesis in *Streptomyces glaucescens*: role of FabH and FabD and their acyl carrier protein specificity. Biochemistry 41:10462-71.

Flugel RS, Hwangbo Y, Lambalot RH, Cronan JE Jr, and Walsh CT. (2000) Holo-(acyl carrier protein) synthase and phosphopantetheinyl transfer in *Escherichia coli*. J Biol Chem 275:959-68.

Fray RG, Throup JP, Daykin M, Wallace A, Willams P, Stewart GS, and Grierson D. (1999) Plants genetically modified to produce N-acylhomoserine lactones communicate with bacteria. Nat Biotechnol 171:1017-20.

Frederick AF, Kay LE, and Prestegard JH. (1988) Location of divalent ion sites in acyl carrier protein using relaxation perturbed 2D NMR. FEBS Lett 238:43-8.

Funa N, Ohnishi Y, Fujii I, Shibuya M, Ebizuka Y, and Horinouchi S. (1999) A new pathway for polyketide synthesis in microorganisms. Nature 400:897-9.

Fuqua C and Greenberg EP. (1998) Self perception in bacteria: quorum sensing with acylated homoserine lactones. Curr Opin Microbiol 1:183-9.

Galloway SM and Raetz CRH. (1990) A mutant of *Escherichia coli* defective in the first step of endotoxin biosynthesis. J Biol Chem 265:6394-402.

Gally HU, Spencer AK, Armitage IM, Prestegard JH, and Cronan JE Jr. (1978) Acyl carrier protein from *Escherichia coli*: characterization by proton and fluorine-19 nuclear magnetic resonance and evidence for restricted mobility of the fatty acid chain in tetradecanoyl-acyl-carrier protein. Biochemistry 17:5377-5382.

Gangar A, Karande AA, and Rajasekharan R. (2001) Purification and characterization of acyl-acyl carrier protein synthetase from oleaginous yeast and its role in triacylglycerol biosynthesis. Biochem J 360:471-9.

Garwin JL, Klages AL, and Cronan JE Jr. (1980) Structural, enzymatic, and genetic studies of beta-ketoacyl-acyl carrier protein synthases I and II of *Escherichia coli.* J Biol Chem 255:11949-56.

Gehring AM, Lambalot RH, Vogel KW, Drueckhammer DG, and Walsh CT. (1997) Ability of *Streptomyces* spp. acyl carrier proteins and coenzyme A analogs to serve as substrates in vitro for *E. coli* holo-ACP synthase. Chem Biol 4:17-24.

Geiger O and Lopez-Lara IM. (2002) Rhizobial acyl carrier proteins and their roles in the formation of bacterial cell-surface components that are required for the development of nitrogen-fixing root nodules on legume hosts. FEMS Microbiol Lett 208:153-62.

Geiger O, Spaink HP, and Kennedy EP. (1991) Isolation of the *Rhizobium leguminosarum* NodF nodulation protein: NodF carries a 4'-phosphopantetheine prosthetic group. J Bacteriol 173:2872-8.

Gilbert AM, Kirisits M, Toy P, Nunn DS, Failli A, Dushin EG, Novikova E, Petersen PJ, Joseph-McCarthy D, McFadyen I, and Fritz CC. (2004) Anthranilate 4H-oxazol-5-ones: novel small molecule antibacterial acyl carrier protein synthase (AcpS) inhibitors. Bioorg Med Chem Lett 14:37-41.

Gong H and Byers DM. (2003) Glutamate-41 of *Vibrio harveyi* acyl carrier protein is essential for fatty acid synthase but not acyl-ACP synthetase activity. Biochem Biophys Res Commun 302:35-40.

Gong H, Murphy A, McMaster CR, and Byers DM. (2006) Neutralization of acidic residues in helix II stabilizes the folded conformation of acyl carrier protein and variably alters its function with different enzymes. J Biol Chem in press.

Graumann PL. (2001) SMC proteins in bacteria: condensation motors for chromosome segregation? Biochimie 83:53-9.

Green PR, Merrill AH Jr, and Bell RM. (1981) Membrane phospholipid synthesis in *Escherichia coli.* Purification, reconstitution, and characterization of sn-glycerol-3-phosphate acyltransferase. J Biol Chem 256:11151-9.

Griffiths GL, Sigel SP, Payne SM, and Neilands JB. (1984) Vibriobactin, a siderophore from *Vibrio cholerae.* J Biol Chem 259:383-5.

Gross M, Cramton SE, Gotz F, and Peschel A. (2001) Key role of teichoic acid net charge in *Staphylococcus aureus* colonization of artificial surfaces. Infect Immun 69:3423-6.

Grossman TH, Tuckman M, Ellestad S, and Osburne MS. (1993) Isolation and characterization of *Bacillus subtilis* genes involved in siderophore biosynthesis: relationship between *B. subtilis sfpO* and *Escherichia coli entD* genes. J Bacteriol 175:6203-11.

Gueguen V, Macherel D, Jaquinod M, Douce R, and Bourguignon J. (2000) Fatty acid and lipoic acid biosynthesis in higher plant mitochondria. J Biol Chem 275:5016-25.

Guex N and Peitsch MC. (1997) SWISS-MODEL and the Swiss-PdbViewer: an environment for comparative protein modeling. Electrophoresis 18:2714-23.

Gully D, Moinier D, Loiseau L, and Bouveret E. (2003) New partners of acyl carrier protein detected in *Escherichia coli* by tandem affinity purification. FEBS Lett 548:90-6.

Hadfield AT, Limpkin C, Teartasin W, Simpson TJ, Crosby J, and Crump MP. (2004) The crystal structure of the *actIII* actinorhodin polyketide reductase: proposed mechanism for ACP and polyketide binding. Structure 12:1865-75.

Hanke C, Wolter FP, Coleman J, Peterek G, and Frentzen M. (1995) A plant acyltransferase involved in triacylglycerol biosynthesis complements an *Escherichia coli* sn-1-acylglycerol-3-phosphate acyltransferase mutant. Eur J Biochem 232:806-10.

Hanzelka BL, Stevens AM, Parsek MR, Crone TJ, and Greenberg EP. (1997) Mutational analysis of the *Vibrio fischeri* LuxI polypeptide: critical regions of an autoinducer synthase. J Bacteriol 179:4882-7.

Hanzelka BL, Parsek MR, Val DL, Dunlap PV, Cronan JE Jr, and Greenberg EP. (1999) Acylhomoserine lactone synthase activity of the *Vibrio fischeri* AinS protein. J Bacteriol 181:5766-70.

Harder ME, Ladenson RC, Schimmel SD, and Silbert DF. (1974) Mutants of *Escherichia coli* with temperature-sensitive malonyl coenzyme A-acyl carrier protein transacylase. J Biol Chem 249:7468-75.

Harington A, Herbert CJ, Tung B, Getz GS, and Slonimski PP. (1993) Identification of a new nuclear gene (CEM1) encoding a protein homologous to a beta-keto-acyl synthase which is essential for mitochondrial respiration in *Saccharomyces cerevisiae.* Mol Microbiol 9:545-55.

Harris DL and Hudson BS. (1990) Photophysics of tryptophan in bacteriophage T4 lysozymes. Biochemistry 29:5276-85.

Heath RJ and Rock CO. (1995) Enoyl-acyl carrier protein reductase (*fabI*) plays a determinant role in completing cycles of fatty acid elongation in *Escherichia coli.* J Biol Chem 270:26538-42.

Heath RJ and Rock CO. (1996a) Inhibition of beta-ketoacyl-acyl carrier protein synthase III (FabH) by acyl-acyl carrier protein in *Escherichia coli.* J Biol Chem 271:10996-1000.

Heath RJ and Rock CO. (1996b) Regulation of fatty acid elongation and initiation by acyl-acyl carrier protein in *Escherichia coli.* J Biol Chem 271:1833-6.

Heath RJ and Rock CO. (1996c) Roles of the FabA and FabZ beta-hydroxyacyl-acyl carrier protein dehydratases in *Escherichia coli* fatty acid biosynthesis. J Biol Chem 271:27795-801.

Heath RJ and Rock CO. (1998) A conserved histidine is essential for glycerolipid acyltransferase catalysis. J Bacteriol 180:1425-30.

Heath RJ and Rock CO. (1999) A missense mutation accounts for the defect in the glycerol-3-phosphate acyltransferase expressed in the *plsB26* mutant. J Bacteriol 181:1944-6.

Heath RJ and Rock CO. (2000) A triclosan-resistant bacterial enzyme. Nature 406:145-6.

Heath RJ, Jackowski S, and Rock CO. (1994) Guanosine tetraphosphate inhibition of fatty acid and phospholipid synthesis in *Escherichia coli* is relieved by overexpression of glycerol-3-phosphate acyltransferase (*plsB*). J Biol Chem 269:26584-90.

Heath RJ, Su N, Murphy CK, and Rock CO. (2000) The enoyl-[acyl-carrier-protein] reductases FabI and FabL from *Bacillus subtilis*. J Biol Chem 275:40128-33.

Heath RJ, White SW, and Rock CO. (2002) Inhibitors of fatty acid synthesis as antimicrobial chemotherapeutics. Appl Microbiol Biotechnol 58:695-703.

Heaton MP and Neuhaus FC. (1994) Role of the D-alanyl carrier protein in the biosynthesis of D-alanyl-lipoteichoic acid. J Bacteriol 176:681-90.

Herald VL, Heazlewood JL, Day DA, and Millar AH. (2003) Proteomic identification of divalent metal cation binding proteins in plant mitochondria. FEBS Lett 537:96-100.

Hilbi H and Dimroth P. (1994) Purification and characterization of a cytoplasmic enzyme component of the Na^+-activated malonate decarboxylase system of *Malonomonas rubra*: acetyl-S-acyl carrier protein: malonate acyl carrier protein-SH transferase. Arch Microbiol 162:48-52.

Hitchman TS, Crosby J, Byrom KJ, Cox RJ, and Simpson TJ. (1998) Catalytic self-acylation of type II polyketide synthase acyl carrier proteins. Chem Biol 5:35-47.

Holak TA, Nilges M, Prestegard JH, Gronenborn AM, and Clore GM. (1988) Three-dimensional structure of acyl carrier protein in solution determined by nuclear magnetic resonance and the combined use of dynamical simulated annealing and distance geometry. Eur J Biochem 175:9-15.

Hopwood DA. (1997) Genetic contributions to understanding polyketide synthases. Chem Rev 97:2465-97.

Hopwood DA and Sherman DH. (1990) Molecular genetics of polyketides and its comparison to fatty acid biosynthesis. Annu Rev Genet 24:37-66.

Horvath LA, Sturtevant JM, and Prestegard JH. (1994) Kinetics and thermodynamics of thermal denaturation in acyl carrier protein. Protein Sci 3:103-8.

Hsu L, Jackowski S, and Rock CO. (1989) Uptake and acylation of 2-acyl-lysophospholipids by *Escherichia coli*. J Bacteriol 171:1203-5.

Issartel JP, Koronakis V, and Hughes C. (1991) Activation of *Escherichia coli* prohaemolysin to the mature toxin by acyl carrier protein-dependent fatty acylation. Nature 351:759-61.

Jackowski S and Rock CO. (1983) Ratio of active to inactive forms of acyl carrier protein in *Escherichia coli*. J Biol Chem 258:15186-91.

Jackowski S and Rock CO. (1987) Acetoacetyl-acyl carrier protein synthase, a potential regulator of fatty acid biosynthesis in bacteria. J Biol Chem 262:7927-31.

Jain NU, Wyckoff TJO, Raetz CRH, and Prestegard JH. (2004) Rapid analysis of large protein-protein complexes using NMR-derived orientational constraints: the 95 kDa complex of LpxA with acyl carrier protein. J Mol Biol 343:1379-89.

Jenni S, Leibundgut M, Maier T, and Ban N. (2006) Architecture of a fungal fatty acid synthase at 5 angstrom resolution. Science 311:1263-7.

Jez JM, Austin MB, Ferrer JL, Bowman ME, Schroder J, and Noel JP. (2000) Structural control of polyketide formation in plant-specific polyketide synthases. Chem Biol 7:919-30.

Jiang Y, Chan CH, and Cronan JE. (2006) The soluble acyl-acyl carrier protein synthetase of *Vibrio harveyi* B392 is a member of the medium chain acyl-CoA synthetase family. Biochemistry 45:10008-19.

John M, Rohrig H, Schmidt J, Wieneke U, and Schell J. (1993) *Rhizobium* NodB protein involved in nodulation signal synthesis is a chitooligosaccharide deacetylase. Proc Natl Acad Sci USA 90:625-9.

Johnson K, King DS, and Schultz PG. (1995) Studies on the mechanism of action of isoniazid and ethionamide in the Chemotherapy of tuberculosis. J Am Chem Soc 117:5009-10.

Jones PJ, Cioffi EA, and Prestegard JH. (1987a) [19F]-1H heteronuclear nuclear overhauser effect studies of the acyl chain-binding site of acyl carrier protein. J Biol Chem 262:8963-5.

Jones PJ, Holak TA, and Prestegard JH. (1987b) Structural comparison of acyl carrier protein in acylated and sulfhydryl forms by two-dimensional 1H NMR spectroscopy. Biochemistry 26:3493-500.

Jordan SW and Cronan JE Jr. (1997) A new metabolic link. The acyl carrier protein of lipid synthesis donates lipoic acid to the pyruvate dehydrogenase complex in *Escherichia coli* and mitochondria. J Biol Chem 272:17903-6.

Joseph-McCarthy D, Parris K, Huang A, Failli A, Quagliato D, Dushin EG, Novikova E, Severina E, Tuckman M, Petersen PJ, Dean C, Fritz CC, Meshulam T, DeCenzo M, Dick L, McFadyen IJ, Somers WS, Lovering F, and Gilbert AM. (2005) Use of structure-based drug design approaches to obtain novel anthranilic acid acyl carrier protein synthase inhibitors. J Med Chem 48:7960-9.

Joshi AK, Zhang L, Rangan VS, and Smith S. (2003) Cloning, expression, and characterization of a human 4'-phosphopantetheinyl transferase with broad substrate specificity. J Biol Chem 278:33142-9.

Kamst E, Spaink HP, and Kafetzopoulos D. (1998) Biosynthesis and secretion of rhizobial lipochitin-oligosaccharide signal molecules. Subcell Biochem 29:29-71.

Kass LR. (1968) The antibacterial activity of 3-decynoyl-n-acetylcysteamine. Inhibition in vivo of beta-hydroxydecanoyl thioester dehydrase. J Biol Chem 243:3223-8.

Keating DH and Cronan JE Jr. (1996) An isoleucine to valine substitution in *Escherichia coli* acyl carrier protein results in a functional protein of decreased molecular radius at elevated pH. J Biol Chem 271:15905-10.

Keating DH, Carey MR, and Cronan JE Jr. (1995) The unmodified (apo) form of *Escherichia coli* acyl carrier protein is a potent inhibitor of cell growth. J Biol Chem 270:22229-35.

Keating MM, Gong H, and Byers DM. (2002) Identification of a key residue in the conformational stability of acyl carrier protein. Biochim Biophys Acta 1601:208-14.

Keatinge-Clay AT, Shelat AA, Savage DF, Tsai SC, Miercke LJW, O'Connell JD III, Khosla C, and Stroud RM. (2003) Catalysis, specificity, and ACP docking site of *Streptomyces coelicolor* malonyl-CoA:ACP transacylase. Structure (Camb) 11:147-54.

Kelly TM, Stachula SA, Raetz CRH, and Anderson MS. (1993) The firA gene of *Escherichia coli* encodes UDP-3-O-(R-3-hydroxymyristoyl)-glucosamine N-acyltransferase. The third step of endotoxin biosynthesis. J Biol Chem 268:19866-74.

Kennedy EP. (1982) Osmotic regulation and the biosynthesis of membrane-derived oligosaccharides in *Escherichia coli.* Proc Natl Acad Sci USA 79:1092–5.

Khosla C, Ebert-Khosla S, and Hopwood DA. (1992) Targeted gene replacements in a *Streptomyces* polyketide synthase gene cluster: role for the acyl carrier protein. Mol Microbiol 6:3237-49.

Kim Y and Prestegard JH. (1989) A dynamic model for the structure of acyl carrier protein in solution. Biochemistry 28:8792-7.

Kim Y and Prestegard JH. (1990a) Demonstration of a conformational equilibrium in acyl carrier protein from spinach using rotating frame nuclear magnetic resonance spectroscopy. J Am Chem Soc 112:3707-9.

Kim Y and Prestegard JH. (1990b) Refinement of the NMR structures for acyl carrier protein with scalar coupling data. Proteins 8:377-85.

Kim Y, Kovrigin EL, and Eletr Z. (2006) NMR studies of *Escherichia coli* acyl carrier protein: Dynamic and structural differences of the apo- and holo-forms. Biochem Biophys Res Commun 341:776-83.

Kimber MS, Martin F, Lu Y, Houston S, Vedadi M, Dharamsi A, Fiebig KM, Schmid M, and Rock CO. (2004) The structure of (3R)-hydroxyacyl-acyl carrier protein dehydratase (FabZ) from *Pseudomonas aeruginosa.* J Biol Chem 279:52593-602.

Kiriukhin MY and Neuhaus FC. (2001) D-alanylation of lipoteichoic acid: role of the D-alanyl carrier protein in acylation. J Bacteriol 183:2051-8.

Kitamoto T, Nishigai M, Sasaki T, and Ikai A. (1988) Structure of fatty acid synthetase from the Harderian gland of guinea pig. Proteolytic dissection and electron microscopic studies. J Mol Biol 203:183-95.

Koch B, Liljefors T, Persson T, Nielsen J, Kjelleberg S, and Givskov M. (2005) The LuxR receptor: the sites of interaction with quorum-sensing signals and inhibitors. Microbiology 151:3589-602.

Kolattukudy PE, Fernandes ND, Azad AK, Fitzmaurice AM, and Sirakova TD. (1997) Biochemistry and molecular genetics of cell-wall lipid biosynthesis in *Mycobacteria.* Mol Microbiol 24:263-70.

Kolodziej SJ, Penczek PA, Schroeter JP, and Stoops JK. (1996) Structure-function relationships of the *Saccharomyces cerevisiae* fatty acid synthase. Three-dimensional structure. J Biol Chem 271:28422-9.

Kuo A, Blough NV, and Dunlap PV. (1994) Multiple N-acyl-L-homoserine lactone autoinducers of luminescence in the marine symbiotic bacterium *Vibrio fischeri.* J Bacteriol 176:7558-65.

Lakowicz JR. (1983) Principles of Fluorescence Spectroscopy. Plenum Press, New York.

Lakowicz JR. (2000) On spectral relaxation in proteins. Photochem Photobiol 72:421-37.

Lambalot RH, and Walsh CT. (1995) Cloning, overproduction, and characterization of the *Escherichia coli* holo-acyl carrier protein synthase. J Biol Chem 270:24658-61.

Lambalot RH and Walsh CT. (1997) Holo-[acyl-carrier-protein] synthase of *Escherichia coli.* Methods Enzymol 279: 254-62.

Lambalot RH, Gehring AM, Flugel RS, Zuber P, LaCelle M, Marahiel MA, Reid R, Khosla C, and Walsh CT. (1996) A new enzyme superfamily - the phosphopantetheinyl transferases. Chem Biol 3:923-36.

Larsen TA, Olson AJ, and Goodsell DS. (1998) Morphology of protein-protein interfaces. Structure 6:421-7.

Lautru S and Challis GL. (2004) Substrate recognition by nonribosomal peptide synthetase multi-enzymes. Microbiology 150:1629-36.

Lawson DM, Derewenda U, Serre L, Ferri S, Szittner R, Wei Y, Meighen EA, and Derewenda ZS. (1994) Structure of a myristoyl-ACP-specific thioesterase from *Vibrio harveyi.* Biochemistry 33:9382-8.

Lee BI and Suh SW. (2003) Crystal structure of UDP-N-acetylglucosamine acyltransferase from *Helicobacter pylori.* Proteins: Struct Funct Genet 53:772-4.

Lee CY and Meighen EA. (1997) Cysteine-286 as the site of acylation of the Lux-specific fatty acyl-CoA reductase. Biochim Biophys Acta 1338:215-22.

Lee CY, Szittner RB, and Meighen EA. (1991) The *lux* genes of the luminous bacterial symbiont, *Photobacterium leiognathi*, of the ponyfish. Nucleotide sequence, difference in gene organization, and high expression in mutant *Escherichia coli.* Eur J Biochem 201:161-7.

Leesong M, Henderson BS, Gillig JR, Schwab JM, and Smith JL. (1996) Structure of a dehydratase-isomerase from the bacterial pathway for biosynthesis of unsaturated fatty acids: two catalytic activities in one active site. Structure 4:253-64.

Lehrer SS. (1971) Solute perturbation of protein fluorescence. The quenching of the tryptophyl fluorescence of model compounds and of lysozyme by iodide ion. Biochemistry 10:3254-63.

Levy CW, Roujeinikova A, Sedelnikova S, Baker PJ, Stuitje AR, Slabas AR, Rice DW, and Rafferty JB. (1999) Molecular basis of triclosan activity. Nature 398:383-4.

Li BH, Ma XF, Wu XD, and Tian WX. (2006) Inhibitory activity of chlorogenic acid on enzymes involved in the fatty acid synthesis in animals and bacteria. IUBMB Life 58:39-46.

Li Q, Khosla C, Puglisi JD, Liu CW. (2003) Solution structure and backbone dynamics of the holo form of the frenolicin acyl carrier protein. Biochemistry 42:4648-57.

Li Z and Meighen EA. (1995) Tryptophan 250 on the alpha subunit plays an important role in flavin and aldehyde binding to bacterial luciferase. Effects of W->Y mutations on catalytic function. Biochemistry 34:15084-90.

Lilley BN and Bassler BL. (2000) Regulation of quorum sensing in *Vibrio harveyi* by LuxO and sigma-54. Mol Microbiol 36:940-54.

Loubens I, Debarbieux L, Bohin A, Lacroix JM, and Bohin JP. (1993) Homology between a genetic locus (*mdoA*) involved in the osmoregulated biosynthesis of periplasmic glucans in *Escherichia coli* and a genetic locus (*hrpM*) controlling pathogenicity of *Pseudomonas syringae*. Mol Microbiol 10:329–40.

Lu JZ, Lee PJ, Waters NC, and Prigge ST. (2005) Fatty acid synthesis as a target for antimalarial drug discovery. Comb Chem High Throughput Screen 8:15-26.

Lu YJ and Rock CO. (2006) Transcriptional regulation of fatty acid biosynthesis in *Streptococcus pneumoniae*. Mol Microbiol 59:551-66.

Ludwig A, Vogel M, and Goebel W. (1987) Mutations affecting activity and transport of haemolysin in *Escherichia coli*. Mol Gen Genet 206:238-45.

Lupp C and Ruby EG. (2005) *Vibrio fischeri* uses two quorum-sensing systems for the regulation of early and late colonization factors. J Bacteriol 187:3620-9.

Maekawa T, Yanagihara K, and Ohtsubo E. (1996) Specific nicking at the 3' ends of the terminal inverted repeat sequences in transposon Tn3 by transposase and an *E. coli* protein ACP. Genes Cells 1:1017-30.

Maier T, Jenni S, and Ban N. (2006) Architecture of mammalian fatty acid synthase at 4.5 A resolution. Science 311:1258-62.

Malpartida F and Hopwood DA. (1984) Molecular cloning of the whole biosynthetic pathway of a *Streptomyces* antibiotic and its expression in a heterologous host. Nature 309:462-4.

Manefield M, de Nys R, Kumar N, Read R, Givskov M, Steinberg P, Kjelleberg S. (1999) Evidence that halogenated furanones from *Delisea pulchra* inhibit acylated homoserine lactone (AHL)-mediated gene expression by displacing the AHL signal from its receptor protein. Microbiology 145:283-91.

Marahiel MA, Stachelhaus T, Mootz HD. (1997) Modular peptide synthetases involved in peptide synthesis. Chem Rev 97:2651-74.

Matharu AL, Cox RJ, Crosby J, Byrom KJ, and Simpson TJ. (1998) MCAT is not required for in vitro polyketide synthesis in a minimal actinorhodin polyketide synthase from *Streptomyces coelicolor*. Chem Biol 5:699-711.

Mathieu M, Modis Y, Zeelen JP, Engel CK, Abagyan RA, Ahlberg A, Rasmussen B, Lamzin VS, Kunau WH, and Wierenga RK. (1997) The 1.8 angstrom crystal structure of the dimeric peroxisomal 3-ketoacyl-CoA thiolase of *Saccharomyces cerevisiae*: implications for substrate binding and reaction mechanism. J Mol Biol 273:714-28.

Mayo KH and Prestegard JH. (1985) Acyl carrier protein from *Escherichia coli*. Structural characterization of short-chain acylated acyl carrier proteins by NMR. Biochemistry 24:7834-8.

McAllister KA, Peery RB, and Zhao G. (2006) Acyl carrier protein synthases from gram-negative, gram-positive, and atypical bacterial species: Biochemical and structural properties and physiological implications. J Bacteriol 188:4737-48.

McDaniel R, Ebert-Khosla S, Hopwood DA, and Khosla C. (1993) Engineered biosynthesis of novel polyketides. Science 262:1546-50.

McLellan T. (1982) Electrophoresis buffers for polyacrylamide gels at various pH. Anal Chem 126:94-9.

Meighen EA. (1988) Enzymes and genes from the *lux* operons of bioluminescent bacteria. Ann Rev Microbiol 42:151-76.

Meighen EA. (1991) Molecular biology of bacterial bioluminescence. Microbiol Rev 55:123-42.

Meighen EA. (1993) Bacterial bioluminescence: organization, regulation, and application of the *lux* genes. FASEB J 7:1016-22.

Mihara H and Esaki N. (2002) Bacterial cysteine desulfurases: their function and mechanisms. Appl Microbiol Biotechnol 60:12-23.

Miller KG and Bhattacharjee JK. (1996) The *LYS5* gene of *Saccharomyces cerevisiae*. Gene 172:167-8.

Moche M, Dehesh K, Edwards, and Lindqvist Y. (2001) The crystal structure of beta-ketoacyl-acyl carrier protein synthase II from *Synechocystis sp.* At 1.54 angstrom resolution and its relationship to other condensing enzymes. J Mol Biol 305:491-503.

Mofid MR, Finking R, and Marahiel MA. (2002) Recognition of hybrid peptidyl carrier proteins/acyl carrier proteins in nonribosomal peptide synthetase modules by the 4'-phosphopantetheinyl transferases AcpS and Sfp. J Biol Chem 277:17023-31.

Mofid MR, Finking R, Essen LO, and Marahiel MA. (2004) Structure-based mutational analysis of the 4'-phosphopantetheinyl transferases Sfp from *Bacillus subtilis*: carrier protein recognition and reaction mechanism. Biochemistry 43:4128-36.

Mohan S, Kelly TM, Eveland SS, Raetz CRH, and Anderson MS. (1994) An *Escherichia coli* gene (*fabZ*) encoding (3R)-hydroxymyristoyl acyl carrier protein dehydrase. Relation to *fabA* and suppression of mutations in lipid A biosynthesis. J Biol Chem 269:32896-903.

Moir DT. (2005) Identification of inhibitors of bacterial enoyl-acyl carrier protein reductase. Curr Drug Targets Infect Disord 5:297-305.

Mootz HD and Marahiel MA. (1997) The tyrocidine biosynthesis operon of *Bacillus brevis*: complete nucleotide sequence and biochemical characterization of functional internal adenylation domains. J Bacteriol 179:6843-50.

Mootz HD, Finking R, and Marahiel MA. (2001) 4'-Phosphopantetheine transfer in primary and secondary metabolism of *Bacillus subtilis*. J Biol Chem 276:37289-98.

More MI, Finger LD, Stryker JL, Fuqua C, Eberhard A, and Winans SC. (1996) Enzymatic synthesis of a quorum-sensing autoinducer through use of defined substrates. Science 272:1655-8.

Morikawa T, Yasuno R, and Wada H. (2001) Do mammalian cells synthesize lipoic acid? Identification of a mouse cDNA encoding a lipoic acid synthase located in mitochondria. FEBS Lett 498:16-21.

Morris ME and Jinks-Robertson S. (1991) Nucleotide sequence of the LYS2 gene of *Saccharomyces cerevisiae*: homology to *Bacillus brevis* tyrocidine synthetase 1. Gene 98:141-5.

Murata N and Tasaka Y. (1997) Glycerol-3-phosphate acyltransferase in plants. Biochim Biophys Acta 1348:10-6.

Nagai J and Bloch K. (1967) Elongation of acyl carrier protein derivatives by bacterial and plant extracts. J Biol Chem 242:357-62.

Naggert J, Narasimhan ML, DeVeaux L, Cho H, Randhawa ZI, Cronan JE Jr, Green BN, and Smith S. (1991) Cloning, sequencing, and characterization of *Escherichia coli* thioesterase II. J Biol Chem 266:11044-50.

Nakano MM, Corbell N, Besson J, and Zuber P. (1992) Isolation and characterization of *sfp*: a gene that functions in the production of the lipopeptide biosurfactant, surfactin, in *Bacillus subtilis*. Mol Gen Genet 232:313-21.

Neilands JB. (1976) Siderophores: diverse roles in microbial and human physiology. Ciba Found Symp 51:107-24.

Neuhaus FC and Baddiley J. (2003) A continuum of anionic charge: structures and functions of D-alanyl-teichoic acids in gram-positive bacteria. Microbiol Mol Biol Rev 67:686-723.

Niki H, Imamura R, Kitaoka M, Yamanaka K, Ogura T, and Hiraga S. (1992) *E. coli* MukB protein involved in chromosome partition forms a homodimer with a rod-and-hinge structure having DNA binding and ATP/GTP binding activities. EMBO J 11:5101-9.

Odegaard TJ, Kaltashov IA, Cotter RJ, Steeghs L, van der Ley P, Khan S, Maskell DJ, and Raetz CR. (1997) Shortened hydroxyacyl chains on lipid A of *Escherichia coli* cells expressing a foreign UDP-N-acetylglucosamine O-acyltransferase. J Biol Chem 272:19688-96.

Olsen JG, Kadziola A, von Wettstein-Knowles P, Siggaard-Andersen M, Lindquist Y, and Larsen S. (1999) The X-ray crystal structure of beta-ketoacyl [acyl carrier protein] synthase I. FEBS Lett 460:46-52.

Onishi HR, Pelak BA, Gerckens LS, Silver LL, Kahan FM, Chen MH, Patchett AA, Galloway SM, Hyland SA, Anderson MS, and Raetz CRH. (1996) Antibacterial agents that inhibit lipid A biosynthesis. Science 274:980-2.

Oppermann U, Filling C, Hult M, Shafqat N, Wu X, Lindh M, Shafqat J, Nordling E, Kallberg Y, Persson B, and Jornvall H. (2003) Short-chain dehydrogenases/reductases (SDR): the 2002 update. Chem Biol Interact 143-144:247-53.

Pace CN. (1986) Determination and analysis of urea and guanidine hydrochloride denaturation curves. Methods Enzymol 131:266-80.

Pace CN and Scholtz JM. (1997) Measuring the conformational stability of a protein. In Protein structure: a practical approach (ed. Creighton TE), Chapter 12. Oxford University Press.

Parisi G and Echave J. (2004) The structurally constrained protein evolution model accounts for sequence patterns of the LbetaH superfamily. BMC Evol Biol 4:41.

Park SJ, Kim JS, Son WS, and Lee BJ. (2004) pH-Induced conformational transition of *H. pylori* acyl carrier protein: insight into the unfolding of local structure. J Biochem 135:337-46.

Parris KD, Lin L, Tam A, Mathew R, Hixon J, Stahl M, Fritz CC, Seehra J, and Somers WS. (2000) Crystal structures of substrate binding to *Bacillus subtilis* holo-(acyl carrier protein) synthase reveal a novel trimeric arrangement of molecules resulting in three active sites. Structure Fold Des 8:883-95.

Parsek MR, Val DL, Hanzelka BL, Cronan JE Jr, and Greenberg EP. (1999) Acyl homoserine-lactone quorum-sensing signal generation. Proc Natl Acad Sci U S A 96:4360-5.

Pearson JP, Gray KM, Passador L, Tucker KD, Eberhard A, Iglewski BH, and Greenberg EP. (1994) Structure of the autoinducer required for expression of *Pseudomonas aeruginosa* virulence genes. Proc Natl Acad Sci USA 91:197-201.

Perham RN. (2000) Swinging arms and swinging domains in multifunctional enzymes: catalytic machines for multistep reactions. Annu Rev Biochem 69:961-1004.

Peschel A, Vuong C, Otto M, and Gotz F. (2000) The D-alanine residues of *Staphylococcus aureus* teichoic acids alter the susceptibility to vancomycin and the activity of autolytic enzymes. Antimicrob Agents Chemother 44:2845-7.

Pettersen EF, Goddard TD, Huang CC, Couch GS, Greenblatt DM, Meng EC, and Ferrin TE. (2004) UCSF Chimera - a visualization system for exploratory research and analysis. J Comput Chem 25:1605-12.

Pfitzner U, Raetz CR, and Roderick SL. (1995) Crystallization of UDP-N-acetylglucosamine O-acyltransferase from *Escherichia coli*. Proteins 22:191-2.

Post-Beittenmiller D, Jaworski JG, and Ohlrogge JB. (1991) *In vivo* pools of free and acylated acyl carrier proteins in spinach. Evidence for sites of regulation of fatty acid biosynthesis. J Biol Chem 266:1858-65.

Praphanphoj V, Sacksteder KA, Gould SJ, Thomas GH, and Geraghty MT. (2001) Identification of the alpha-aminoadipic semialdehyde dehydrogenase-phosphopantetheinyl transferase gene, the human ortholog of the yeast LYS5 gene. Mol Genet Metab 72:336-42.

Prescott DJ and Vagelos PR. (1972) Acyl carrier protein. Adv Enzymol Relat Areas Mol Biol 36:269-311.

Price AC, Choi KH, Heath RJ, Li Z, White SW, and Rock CO. (2001a) Inhibition of beta-ketoacyl-acyl carrier protein synthases by thiolactomycin and cerulenin. Structure and mechanism. J Biol Chem 276:6551-9.

Price AC, Zhang YM, Rock CO, and White SW. (2001b) Structure of beta-ketoacyl-[acyl carrier protein] reductase from *Escherichia coli*: negative cooperativity and its structural basis. Biochemistry 40:12772-81.

Price AC, Rock CO, and White SW. (2003) The 1.3-angstrom-resolution crystal structure of beta-ketoacyl-acyl carrier protein synthase II from *Streptococcus pneumoniae*. J Bacteriol 185:4136-43.

Price AC, Zhang YM, Rock CO, and White SW. (2004) Cofactor-induced conformational rearrangements establish a catalytically competent active site and a proton relay conduit in FabG. Structure (Camb) 12:417-28.

Qiu X and Janson CA. (2004) Structure of apo acyl carrier protein and a proposal to engineer protein crystallization through metal ions. Acta Crystallogr D Biol crystallogr 60:1545-54.

Qiu X, Janson CA, Konstantinidis AK, Nwagwu S, Silverman C, Smith WW, Khandekar S, Lonsdale J, and Abdel-Meguid SS. (1999) Crystal structure of beta-ketoacyl-acyl carrier protein synthase III. J Biol Chem 274:36465-71.

Que NLS, Ribeiro AA, and Raetz CRH. (2000) Two-dimensional NMR spectroscopy and structures of six lipid A species from *Rhizobium etli* CE3. Detection of an acyloxyacyl residue in each component and origin of the aminogluconate moiety. J Biol Chem 275:28017-27.

Raetz CRH. (1993) Bacterial endotoxins: extraordinary lipids that activate eukaryotic signal transduction. J Bacteriol 175:5745-53.

Raetz CRH and Roderick SL. (1995) A left-handed parallel beta helix in the structure of UDP-N-acetylglucosamine acyltransferase. Science 270:997-1000.

Rafi S, Novichenok P, Kolappan S, Zhang X, Stratton CF, Rawat R, Kisker C, Simmerling C, and Tonge PJ. (2006) Structure of acyl carrier protein bound to FabI, the FASII enoyl reductase from *Escherichia coli*. J Biol Chem 281:39285-93.

Rangan VS, Joshi AK, and Smith S. (2001) Mapping the functional topology of the animal fatty acid synthase by mutant complementation *in vitro*. Biochemistry 40:10792-9.

Reed MAC, Schweizer M, Szafranska AE, Arthur C, Nicholson TP, Cox RJ, Crosby J, Crump MP, and Simpson TJ. (2003) The type I rat fatty acid synthase ACP shows structural homology and analogous biochemical properties to type II ACPs. Org Biomol Chem 1:463-71.

Reimold U, Kroeger M, Kreuzaler F, and Hahlbrock K. (1983) Coding and 3' non-coding nucleotide sequence of chalcone synthase mRNA and assignment of amino acid sequence of the enzyme. EMBO J 2:1801-5.

Reisser D, Pance A, and Jeannin JF. (2002) Mechanisms of the antitumoral effect of lipid A. Bioessays 24:284-9.

Reuhs BL, Carlson RW, and Kim JS. (1993) *Rhizobium fredii* and *Rhizobium meliloti* produce 3-deoxy-D-manno-2-octulosonic acid-containing polysaccharides that are structurally analogous to group II K antigens (capsular polysaccharides) found in *Escherichia coli*. J Bacteriol 175:3570-80.

Reuter K, Mofid MR, Marahiel MA, and Ficner R. (1999) Crystal structure of the surfactin synthetase-activating enzyme Sfp: a prototype of the 4'-phosphopantetheinyl transferase superfamily. EMBO J 18:6823-31.

Revill WP, Bibb MJ, Scheu AK, Kieser HJ, and Hopwood DA. (2001) Beta-ketoacyl acyl carrier protein synthase III (FabH) is essential for fatty acid biosynthesis in *Streptomyces coelicolor* A3(2). J Bacteriol 183:3526-30.

Rietschel ET, Kirikae T, Schade FU, Ulmer AJ, Holst O, Brade H, Schmidt G, Mamat U, Grimmecke HD, Kusumoto S, and Zahringer U. (1993) The chemical structure of bacterial endotoxin in relation to bioactivity. Immunobiology 187:169-90.

Ritsema T, Gehring AM, Stuitje AR, van der Drift KMGM, Dandal I, Lambalot RH, Walsh CT, Thomas-Oates JE, Lugtenberg BJJ, and Spaink HP. (1998) Functional analysis of an interspecies chimera of acyl carrier proteins indicates a specialized domain for protein recognition. Mol Gen Genet 257:641-8.

Rock CO. (1983) Environment of the aromatic chromophores of acyl carrier protein. Arch Biochem Biophys 225:122-9.

Rock CO. (1984) Turnover of fatty acids in the 1-position of phosphatidylethanolamine in *Escherichia coli.* J Biol Chem 259:6188-94.

Rock CO and Cronan JE Jr. (1979) Re-evaluation of the solution structure of acyl carrier protein. J Biol Chem 254:9778-85.

Rock CO and Cronan JE Jr. (1996) *Escherichia coli* as a model for the regulation of dissociable (type II) fatty acid biosynthesis. Biochim Biophys Acta 1302:1-16.

Rock CO and Garwin JL. (1979) Preparative enzymatic synthesis and hydrophobic chromatography of acyl-acyl carrier protein. J Biol Chem 254:7123-8.

Rock CO and Jackowski S. (1982) Regulation of phospholipid synthesis in *Escherichia coli.* Composition of the acyl-acyl carrier protein pool *in vivo.* J Biol Chem 257:10759-65.

Rock CO, Cronan JE Jr, and Armitage IM. (1981) Molecular properties of acyl carrier protein derivatives. J Biol Chem 256:2669-74.

Rodriguez A, Wall L, Riendeau D, and Meighen EA. (1983) Fatty acid acylation of proteins in bioluminescent bacteria. Biochemistry 22:5604-11.

Romero P, Obradovic Z, Li X, Garner EC, Brown CJ, and Dunker AK. (2001) Sequence complexity of disordered protein. Proteins 42:38-48.

Rosenfeld IS, D'Agnolo G, and Vagelos PR. (1973) Synthesis of unsaturated fatty acids and the lesion in *fabB* mutants. J Biol Chem 248:2452-60.

Roughan PG and Ohlrogge JB. (1996) Evidence that isolated chloroplasts contain an integrated lipid-synthesizing assembly that channels acetate into long-chain fatty acids. Plant Physiol 110:1239-47.

Roujeinikova A, Levy CW, Rowsell S, Sedelnikova S, Baker PJ, Minshull CA, Mistry A, Colls JG, Camble R, Stuitje AR, Slabas AR, Rafferty JB, Pauptit RA, Viner R, and Rice DW. (1999) Crystallographic analysis of triclosan bound to enoyl reductase. J Mol Biol 294:527-35.

Roujeinikova A, Baldock C, Simon WJ, Gilroy J, Baker PJ, Stuitje AR, Rice DW, Slabas AR, and Rafferty JB. (2002) X-ray crystallographic studies on butyryl-ACP reveal flexibility of the structure around a putative acyl chain binding site. Structure (Camb) 10:825-35.

Royer CA. (1995) Fluorescence spectroscopy. Methods Mol Biol 40:65-89.

Rozwarski DA, Grant GA, Barton DH, Jacobs WR Jr, and Sacchettini JC. (1998) Modification of the NADH of the isoniazid target (InhA) from *Mycobacterium tuberculosis.* Science 279:98-102.

Scarsdale JN, Kazanina G, He X, Raynolds KA, and Wright HT. (2001) Crystal structure of the *Mycobacterium tuberculosis* beta-ketoacyl-acyl carrier protein synthase III. J Biol Chem 276:20516-22.

Scheideler MA and Bell RM. (1986) Efficiency of reconstitution of the membrane-associated sn-glycerol-3-phosphate acyltransferase of *Escherichia coli.* J Biol Chem 261:10990-5.

Schmid FX. (1997) Optical spectroscopy to characterize protein conformation and conformational changes. In Protein structure: a practical approach (ed. Creighton TE). Oxford University Press.

Schneider R, Brors B, Massow M, and Weiss H. (1997) Mitochondrial fatty acid synthesis: a relic of endosymbiontic origin and a specialized means for respiration. FEBS Lett 407:249-52.

Schroder J, Raiber S, Berger T, Schmidt A, Schmidt J, Soares-Sello AM, Bardshiri E, Strack D, Simpson TJ, Veit M, and Schroder G. (1998) Plant polyketide synthases: a chalcone synthase-type enzyme which performs a condensation reaction with methylmalonyl-CoA in the biosynthesis of C-methylated chalcones. Biochemistry 37:8417-25.

Schulman H and Kennedy EP. (1979) Localization of membrane-derived oligosaccharides in the outer envelope of *Escherichia coli* and their occurrence in other Gram-negative bacteria. J Bacteriol 137:686–8.

Schulz H. (1975) On the structure-function relationship of acyl carrier protein of *Escherichia coli.* J Biol Chem 250: 2299-304.

Schulz H, Weeks G, Toomey RE, Shapiro M, and Wakil SJ. (1969) Studies on the mechanism of fatty acid synthesis. XXII. Salt activation of the fatty acid-synthesizing enzymes of *Escherichia coli.* J Biol Chem 244:6577-83.

Schweizer E and Hofmann J. (2004) Microbial type I fatty acid synthases (FAS): major players in a network of cellular FAS systems. Microbiol Mol Biol Rev 68:501-17.

Seidle HF, Couch RD, and Parry RJ. (2006) Characterization of a nonspecific phosphopantetheinyl transferase from *Pseudomonas syringae* pv. syringae FF5. Arch Biochem Biophys 446:167-74.

Seo DW, Moon HI, Han JW, Hong SY, Lee HY, Kim S, Paik WK, and Lee HW. (2000) An endogenous proteinacious inhibitor in porcine liver for S-adenosyl-L-methionine dependent methylation reactions: identification as oligosaccharide-linked acyl carrier protein. Int J Biochem Cell Biol 32:455-64.

Seo DW, Kim YK, Cho EJ, Han JW, Lee HY, Hong S, and Lee HW. (2002) Oligosaccharide-linked acyl carrier protein, a novel transmethylase inhibitor, from porcine liver inhibits cell growth. Arch Pharm Res 25:463-8.

Serre L, Verbree EC, Dauter Z, Stuitje AR, and Derewenda ZS. (1995) The *Escherichia coli* malonyl-CoA:acyl carrier protein transacylase at 1.5-angstrom resolution. J Biol Chem 270:12961-4.

Seyfzadeh M, Keener J, and Nomura M. (1993) SpoT-dependent accumulation of guanosine tetraphosphate in response to fatty acid starvation in *Escherichia coli.* Proc Natl Acad Sci USA 90:11004-8.

Sharma SK, Kapoor M, Ramya TN, Kumar S, Kumar G, Modak R, Sharma S, Surolia N, and Surolia A. (2003) Identification, characterization, and inhibition of *Plasmodium falciparum* beta-hydroxyacyl-acyl carrier protein dehydratase (FabZ). J Biol Chem 278:45661-71.

Sharma AK, Sharma SK, Surolia A, Surolia N, and Sarma SP. (2006) Solution structures of conformationally equilibrium forms of holo-acyl carrier protein (PfACP) from *Plasmodium falciparum* provides insight into the mechanism of activation of ACPs. Biochemistry 45:6904-16.

Sharpe PL and Craig NL. (1998) Host proteins can stimulate Tn7 transposition: a novel role for the ribosomal protein L29 and the acyl carrier protein. EMBO J 17:5822-31.

Shearman CA, Rossen L, Johnston AW, and Downie JA. (1986) The *Rhizobium leguminosarum* nodulation gene *nodF* encodes a polypeptide similar to acyl-carrier protein and is regulated by *nodD* plus a factor in pea root exudate. EMBO J 5:647-652.

Shen B and Kwon HJ. (2002) Macrotetrolide biosynthesis: a novel type II polyketide synthase. Chem Rec 2:389-96.

Shen Z and Byers DM. (1996) Isolation of *Vibrio harveyi* acyl carrier protein and the *fabG*, *acpP*, and *fabF* genes involved in fatty acid biosynthesis. J Bacteriol 178:571-3.

Sieber SA, Linne U, Hillson NJ, Roche E, Walsh CT, and Marahiel MA. (2002) Evidence for a monomeric structure of nonribosomal peptide synthetases. Chem Biol 9:997-1008.

Silbert DF and Vagelos PR. (1967) Fatty acid mutant of *E. coli* lacking a beta-hydroxydecanoyl thioester dehydrase. Proc Natl Acad Sci USA 58:1579-86.

Singh V, Shi W, Almo SC, Evans GB, Furneaux RH, Tyler PC, Painter GF, Lenz DH, Mee S, Zheng R, and Schramm VL. (2006) Structure and inhibition of a quorum sensing target from *Streptococcus pneumoniae*. Biochemistry 45:12929-41.

Smith S, Witkowski A, and Joshi AK. (2003) Structural and functional organization of the animal fatty acid synthase. Prog Lipid Res 42:289-317.

Spaink HP. (2000) Root nodulation and infection factors produced by rhizobial bacteria. Annu Rev Microbiol 54:257-88.

Spoering AL, Vulie M, and Lewis K. (2006) GlpD and PlsB participate in persister cell formation in *Escherichia coli*. J Bacteriol 188:5136-44.

Stanley P, Packman LC, Koronakis V, and Hughes C. (1994) Fatty acylation of two internal lysine residues required for the toxic activity of *Escherichia coli* hemolysin. Science 266:1992-6.

Stanley P, Hyland C, Koronakis V, and Hughes C. (1999) An ordered reaction mechanism for bacterial toxin acylation by the specialized acyltransferase HlyC: formation of a ternary complex with acylACP and protoxin substrates. Mol Microbiol 34:887-901.

Staunton J and Weissman KJ. (2001) Polyketide biosynthesis: a millennium review. Nat Prod Rep 18:380-416.

Staunton J, Caffrey P, Aparicio JF, Roberts GA, Bethell SS, and Leadlay PF. (1996) Evidence for a double-helical structure for modular polyketide synthases. Nat Struct Biol 3:188-92.

Stewart MJ, Parikh S, Xiao G, Tonge PJ, and Kisker C. (1999) Structural basis and mechanism of enoyl reductase inhibition by triclosan. J Mol Biol 290:859-65.

Stoops JK, Awad ES, Arslanian MJ, Gunsberg S, Wakil SJ, and Oliver RM. (1978) Studies on the yeast fatty acid synthetase. Subunit composition and structural organization of a large multifunctional enzyme complex. J Biol Chem 253:4464-75.

Stuible HP, Meier S, Wagner C, Hannappel E, and Schweizer E. (1998) A novel phosphopantetheine:protein transferase activating yeast mitochondrial acyl carrier protein. J Biol Chem 273:22334-9.

Suvarna K, Seah L, Bhattacharjee V, and Bhattacharjee JK. (1998) Molecular analysis of the LYS2 gene of *Candida albicans*: homology to peptide antibiotic synthetases and the regulation of the alpha-aminoadipate reductase. Curr Genet 33:268-75.

Sweet CR, Lin S, Cotter RJ, and Raetz CRH. (2001) A *Chlamydia trachomatis* UDP-N-acetylglucosamine acyltransferase selective for myristoyl-acyl carrier protein. Expression in *Escherichia coli* and formation of hybrid lipid A species. J Biol Chem 276:19565-74.

Sweet CR, Preston A, Toland E, Ramirez SM, Cotter RJ, Maskell DJ, and Raetz CR. (2002) Relaxed acyl chain specificity of *Bordetella* UDP-N-acetylglucosamine acyltransferases. J Biol Chem 277:18281-90.

Sweet CR, Williams AH, Karbarz MJ, Werts C, Kalb SR, Cotter RJ, and Raetz CR. (2004) Enzymatic synthesis of lipid A molecules with four amide-linked acyl chains. LpxA acyltransferases selective for an analog of UDP-N-acetylglucosamine in which an amine replaces the 3"-hydroxyl group. J Biol Chem 279:25411-9.

Takagi T and Tanford C. (1968) Gross conformation of *Escherichia coli* acyl carrier protein. J Biol Chem 243:6432-5.

Tang L, Weissborn AC, and Kennedy EP. (1997) Domains of *Escherichia coli* acyl carrier protein important for membrane-derived-oligosaccharide biosynthesis. J Bacteriol 179:3697-705.

Tener DM and Mayo KH. (1990) Divalent cation binding to reduced and octanoyl acyl-carrier protein. Eur J Biochem 189:559-65.

Therisod H and Kennedy EP. (1987) The function of acyl carrier protein in the synthesis of membrane-derived oligosaccharides does not require its phosphopantetheine prosthetic group. Proc Natl Acad Sci USA 84:8235-8.

Therisod H, Weissborn AC, and Kennedy EP. (1986) An essential function for acyl carrier protein in the biosynthesis of membrane-derived oligosaccharides of *Escherichia coli*. Proc Natl Acad Sci USA 83:7236-40.

Thomas J and Cronan JE. (2005) The enigmatic acyl carrier protein phosphodiesterase of *Escherichia coli*: genetic and enzymological characterization. J Biol Chem 280:34675-83.

Tian WX, Hsu RY, and Wang YS. (1985) Studies on the reactivity of the essential sulfhydryl groups as a conformational probe for the fatty acid synthetase of chicken liver. Inactivation by 5,5'-dithiobis-(2-nitrobenzoic acid) and intersubunit cross-linking of the inactivated enzyme. J Biol Chem 260:11375-87.

Tokuhisa J and Browse J. (1999) Genetic engineering of plant chilling tolerance. Genet Eng (N Y) 21:79-93.

Trivedi OA, Arora P, Sridharan V, Tickoo R, Mohanty D, and Gokhale RS. (2004) Enzymic activation and transfer of fatty acids as acyl-adenylates in mycobacteria. Nature 428:441-5.

Tsai CJ, Xu D, and Nussinov R. (1998) Protein folding via binding and vice versa. Fold Des 3:R71-80.

Tsai CJ, Ma B, Sham YY, Kumar S, and Nussinov R. (2001) Structured disorder and conformational selection. Proteins 44:418-27.

Tsay JT, Rock CO and Jackowski S. (1992) Overproduction of beta-ketoacyl-acyl carrier protein synthase I imparts thiolactomycin resistance to *Escherichia coli* K-12. J Bacteriol 174:508-13.

Tsuji SY, Wu N, and Khosla C. (2001) Intermodular communication in polyketide synthases: comparing the role of protein-protein interactions to those in other multidomain proteins. Biochemistry 40:2317-25.

Turnbull AP, Rafferty JB, Sedelnikova SE, Slabas AR, Schierer TP, Kroon JTM, Simon JW, Fawcett T, Nishida I, Murata N, and Rice DW. (2001) Analysis of the structure, substrate specificity and mechanism of squash glycerol-3-phosphate (1)-acyltransferase. Structure (Camb) 9:347-53.

Ulevitch RJ and Tobias PS. (1995) Receptor-dependent mechanisms of cell stimulation by bacterial endotoxin. Annu Rev Immunol 13:437-57.

Uversky VN, Gillespie JR, and Fink AL. (2000) Why are "natively unfolded" proteins unstructured under physiologic conditions? Proteins 41:415-27.

Vaara M. (1993) Antibiotic-supersusceptible mutants of *Escherichia coli* and *Salmonella typhimurium*. Antimicrob Agents Chemother 37:2255-60.

Vagelos PR and Larrabes AR. (1967) Acyl carrier protein. IX. Acyl carrier protein hydrolase. J Biol Chem 242:1776-81.

Val DL and Cronan JE Jr. (1998) In vivo evidence that S-adenosylmethionine and fatty acid synthesis intermediates are the substrates for the LuxI family of autoinducer synthases. J Bacteriol 180:2644-51.

Vivian JT and Callis PR. (2001) Mechanisms of tryptophan fluorescence shifts in proteins. Biophys J 80:2093-109.

Voelker TA and Davies HM. (1994) Alteration of the specificity and regulation of fatty acid synthesis of *Escherichia coli* by expression of a plant medium-chain acyl-acyl carrier protein thioesterase. J Bacteriol 176:7320-7.

Volkman BF, Zhang Q, Debabov DV, Rivera E, Kresheck GC, and Neuhaus FC. (2001) Biosynthesis of D-alanyl-lipoteichoic acid: the tertiary structure of apo-D-alanyl carrier protein. Biochemistry 40:7964-72.

Vuorio R, Harkonen T, Tolvanen M, and Vaara M. (1994) The novel hexapeptide motif found in the acyltransferases LpxA and LpxD of lipid A biosynthesis is conserved in various bacteria. FEBS Lett 337:289-92.

Wakil SJ. (1989) Fatty acid synthase, a proficient multifunctional enzyme. Biochemistry 28:4523-30.

Walker TA and Ernst-Fonberg ML. (1982) Relatedness of acyl carrier proteins shown by amino acid compositions. Int J Biochem 14:879-82.

Wall L, Rodriguez A, and Meighen EA. (1986) Intersubunit transfer of fatty acyl groups during fatty acid reduction. J Biol Chem 261:15981-8.

Walsh CT, Gehring AM, Weinreb PH, Quadri LE, and Flugel RS. (1997) Post-translational modification of polyketide and nonribosomal peptide synthases. Curr Opin Chem Biol 1:309-15.

Ward JJ, Sodhi JS, McGuffin LJ, Buxton BF, and Jones DT. (2004) Prediction and functional analysis of native disorder in proteins from the three kingdoms of life. J Mol Biol 337:635-45.

Ward WH, Holdgate GA, Rowsell S, McLean EG, Pauptit RA, Clayton E, Nichols WW, Colls JG, Minshull CA, Jude DA, Mistry A, Timms D, Camble R, Hales NJ, Britton CJ, and Taylor IW. (1999) Kinetic and structural characteristics of the inhibition of enoyl (acyl carrier protein) reductase by triclosan. Biochemistry 38:12514-25.

Watson WT, Minogue TD, Val DL, von Bodman SB, and Churchill MEA. (2002) Structural basis and specificity of acyl-homoserine lactone signal production in bacterial quorum sensing. Mol Cell 9:685-94.

Weber T and Marahiel MA. (2001) Exploring the domain structure of modular nonribosomal peptide synthetases. Structure 9:R3-9.

Weber T, Baumgartner R, Renner C, Marahiel MA, and Holak TA. (2000) Solution structure of PCP, a prototype for the peptidyl carrier domains of modular peptide synthetases. Struct Fold Des 8:407-18.

Weissborn AC and Kennedy EP. (1984) Biosynthesis of membrane derived oligosaccharides. Novel glucosyltransferase system from *Escherichia coli* for the elongation of beta 1->2-linked polyglucose chains. J Biol Chem 259:12644–51.

Weissman KJ, Hong H, Popovic B, and Meersman F. (2006) Evidence for a protein-protein interaction motif on an acyl carrier protein domain from a modular polyketide synthase. Chem Biol 13:625-36.

West J, Tompkins CK, Balantac N, Nudelman E, Meengs B, White T, Bursten S, Coleman J, Kumar A, Singer JW, and Leung DW. (1997) Cloning and expression of two human lysophosphatidic acid acyltransferase cDNAs that enhance cytokine-induced signaling responses in cells. DNA Cell Biol 16:691-701.

White SW, Zheng J, Zhang YM, and Rock CO. (2005) The structural biology of type II fatty acid biosynthesis. Annu Rev Biochem 74:791-831.

Wickramasinghe SR, Inglis KA, Urch JE, Muller S, Van Aalten DM, and Fairlamb AH. (2006) Kinetic, inhibition and structural studies on 3-oxoacyl-ACP reductase from *Plasmodium falciparum*, a key enzyme in fatty acid biosynthesis. Biochem J. 393:447-57.

Wilkison WO and Bell RM. (1997) sn-Glycerol-3-phosphate acyltransferase from *Escherichia coli*. Biochim Biophys Acta 1348:3-9.

Williams AH, Immormino RM, Gewirth DT, and Raetz CR. (2006) Structure of UDP-N-acetylglucosamine acyltransferase with a bound antibacterial pentadecapeptide. Proc Natl Acad Sci U S A 103:10877-82.

Witkowski A, Naggert J, Mikkelsen J, and Smith S. (1987) Molecular cloning and sequencing of a cDNA encoding the acyl carrier protein and its flanking domains in the mammalian fatty acid synthetase. Eur J Biochem 165:601-6.

Witkowski A, Joshi AK, and Smith S. (1997) Characterization of the interthiol acyltransferase reaction catalyzed by the beta-ketoacyl synthase domain of the animal fatty acid synthase. Biochemistry 36:16338-44.

Witkowski A, Ghosal A, Joshi AK, Witkowska HE, Asturias FJ, and Smith S. (2004) Head-to-head coiled arrangement of the subunits of the animal fatty acid synthase. Chem Biol 11:1667-76.

Wong HC, Liu G, Zhang YM, Rock CO, and Zheng J. (2002) The solution structure of acyl carrier protein from *Mycobacterium tuberculosis*. J Biol Chem 277:15874-80.

Worsham LMS, Earls L, Jolly C, Langston KG, Trent MS, and Ernst-Fonberg ML. (2003) Amino acid residues of *Escherichia coli* acyl carrier protein involved in heterologous protein interactions. Biochemistry 42:167-76.

Wright PE and Dyson HJ. (1999) Intrinsically unstructured proteins: re-assessing the protein structure-function paradigm. J Mol Biol 293:321-31.

Wyckoff TJO and Raetz CRH. (1999) The active site of *Escherichia coli* UDP-N-acetylglucosamine acyltransferase. Chemical modification and site-directed mutagenesis. J Biol Chem 274:27047-55.

Wyckoff TJ, Lin S, Cotter RJ, Dotson GD, and Raetz CR. (1998) Hydrocarbon rulers in UDP-N-acetylglucosamine acyltransferases. J Biol Chem 273:32369-72.

Xu D, Lin SL, and Nussinov R. (1997) Protein binding versus protein folding: the role of hydrophilic bridges in protein associations. J Mol Biol 265:68-84.

Xu GY, Tam A, Lin L, Hixon J, Fritz CC, and Powers R. (2001) Solution structure of *B. subtilis* acyl carrier protein. Structure (Camb) 9:277-87.

Zhang L, Joshi AK, Hofmann J, Schweizer E, and Smith S. (2005) Cloning, expression, and characterization of the human mitochondrial beta-ketoacyl synthase. Complementation of the yeast CEM1 knock-out strain. J Biol Chem 280:12422-9.

Zhang YM and Rock CO. (2004) Evaluation of epigallocatechin gallate and related plant polyphenols as inhibitors of the FabG and FabI reductases of bacterial type II fatty-acid synthase. J Biol Chem 279:30994-1001.

Zhang YM, Rao MS, Heath RJ, Price AC, Olson AJ, Rock CO, and White SW. (2001) Identification and analysis of the acyl carrier protein (ACP) docking site on beta-ketoacyl-ACP synthase III. J Biol Chem 276:8231-8.

Zhang YM, Marrakchi H, White SW, and Rock CO. (2003a) The application of computational methods to explore the diversity and structure of bacterial fatty acid synthase. J Lipid Res 44:1-10.

Zhang YM, Wu B, Zheng J, and Rock CO. (2003b) Key residues responsible for acyl carrier protein (ACP) and beta-ketoacyl-acyl carrier protein reductase (FabG) interaction. J Biol Chem 278:52935-43.

Zhang YM, Frank MW, Virga KG, Lee RE, Rock CO, and Jackowski S. (2004) Acyl carrier protein is a cellular target for the antibacterial action of the pantothenamide class of pantothenate antimetabolites. J Biol Chem 279:50969-75.

Zornetzer GA, Fox BG, and Markley JL. (2006) Solution structures of spinach acyl carrier protein with decanoate and stearate. Biochemistry 45:5217-27.